BOSTON UNIVERSITY

COLLEGE OF ENGINEERING

Dissertation

A NONLINEAR MULTICOMPARTMENTAL COCHLEAR MODEL

by

SHAN LU

M.S., Virginia Commonwealth University, 2002

Submitted in partial fulfillment of the

requirements for the degree of

Doctor of Philosophy

2009

UMI Number: 3334549

INFORMATION TO USERS

The quality of this reproduction is dependent upon the quality of the copy
submitted. Broken or indistinct print, colored or poor quality illustrations and
photographs, print bleed-through, substandard margins, and improper
alignment can adversely affect reproduction.
    In the unlikely event that the author did not send a complete manuscript
and there are missing pages, these will be noted. Also, if unauthorized
copyright material had to be removed, a note will indicate the deletion.
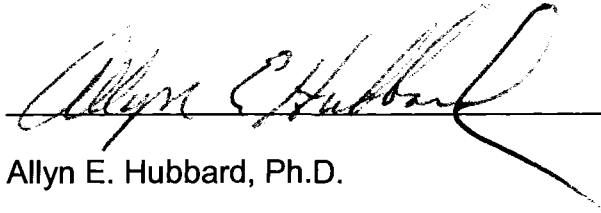
UMI®

UMI Microform 3334549
Copyright 2008 by ProQuest LLC.
All rights reserved. This microform edition is protected against
unauthorized copying under Title 17, United States Code.

ProQuest LLC
789 E. Eisenhower Parkway
PO Box 1346
Ann Arbor, MI 48106-1346

Approved by

First Reader

Allyn E. Hubbard, Ph.D.

Professor of Electrical and Computer Engineering

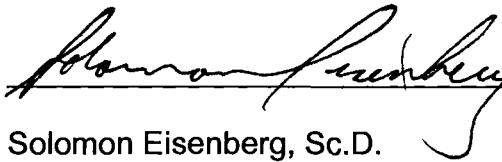Second Reader

David C. Mountain, Ph.D.

Professor of Biomedical Engineering

Third Reader

Solomon Eisenberg, Sc.D.

Chairman ad interim, Biomedical Engineering

Professor of Electrical and Computer Engineering

Fourth Reader

H. Steve Colburn, Ph.D.

Professor of Biomedical Engineering

To my wife Jian Shen and our unborn baby "xiongbaobao"

Acknowledgements

First of all, I would like to express my deepest sense of gratitude to my major advisor and mentor Dr. Allyn E. Hubbard for his patient guidance, encouragement and excellent advice throughout the entire study. He has wide knowledge and always provides unique viewpoints to my research. He not only gave me advices in my academic study, but also gave me a great help in other area. I feel lucky to have worked with him for six years.

A special thank goes to my co-advisor, Dr. David C. Mountain, who is the primary investigator of the project I worked on. His logical way of thinking has been of great value for me. He also has a wide knowledge in science. No matter what type of question I have in my research, he can always provide a valuable advice. To me, he is "the final answer".

Besides my advisors, I would like to thank the rest of my thesis committee members: Dr. Solomon Eisenberg, Dr. H. Steve Colburn and Dr. Roscoe Giles. They asked me good questions and gave insightful comments and reviewed my work on a very short notice.

I would also like to thank all the current and previous members in VLSI and Neural Network System Lab and Cochlear Biophysics Lab who gave me

A NONLINEAR MULTICOMPARTMENTAL COCHLEAR MODEL

ABSTRACT

An active process known as the "cochlear amplifier (CA)" boosts mammalian hearing sensitivity by a hundredfold. This amplification is thought to be due to the outer hair cells (OHCs) electromotility, but the underlying mechanism is still obscure. We studied a new hypothesis that could explain how the CA works, based on results obtained from a nonlinear multicompartment model of the cochlea with OHC piezoelectrical feedback. Unlike the traditional cochlear model, this model includes an additional transmission line: the organ of Corti (OC) fluid flow. The OHC electroanatomical circuit senses the motion of the RL-stereocilia, and feeds back an active force to the hydromechanical system via a piezoelectric element. Therefore, the mechanical loading of the OHC couples bi-directionally with the electrical impedance of the OHC. We also include in the model the fast adaptation of the tension gated channel due to the hair bundle motility.

The results from this study show that, the CA function is a consequence of a combination of forces on the reticular lamina (RL) and the basilar membrane

(BM) coming from both local OHCs and a pressure wave that propagates in the fluid-filled spaces of OC. It suggests that the OC flow observed experimentally is essential to the cochlear active response. We also found that the OHC hair bundle fast adaptation moderates the phase of the active force generated by the OHC, while the OHC somatic motility controls the gain of the active force. The simulation results demonstrate that a piezoelectric OHC can at least partially compensate the OHC low-pass filtering due to the cell wall capacitance, which is a long standing issue in the hearing research area.

Distortion product (DP) otoacoustic emissions (DPOAE) are sounds generated by the inner ear when stimulated with two primary tones. How DPs propagate from the generation site to the stapes has been a major topic in recent years. The model results support the theory that the DPOAE are transmitted back to the stapes via a reverse traveling wave, which starts to dominate from a place that is basal to the f2 place, not from the DP place.

TABLE OF CONTENTS

LIST OF TABLES

LIST OF FIGURES

Chapter 1

Multicompartmental Cochlear Model with Longitudinal Fluid Flow in the Organ of Corti

1.1 Introduction

von Békésy demonstrated that acoustic stimulation produces traveling waves that propagate down the basilar membrane and stimulate the hair cells (von Békésy 1960). Depending on the frequency of tonal excitation, these waves travel to different locations down the spiral, which means that the response of a single location is like a bandpass filter, with each location tuned to a different frequency called the characteristic frequency (CF). von Békésy's data, taken from dead animals, implied that the system was poorly tuned. This differed from auditory nerve tuning, which was highly tuned (Kiang et al. 1967). Then, in 1971, Rhode discovered that the basilar membrane itself was much more frequency selective and sensitive than earlier data had implied (Rhode 1971). Moreover, the tuning was sensitive to the physiological condition of the cochlea. In 1978, Kemp found that normal ears can produce sounds (otoacoustic emissions), while damaged ears cannot (Kemp 1978). Hence, investigators hypothesized the cochlea to be "active". This active process is believed to be mediated by the motor molecule, prestin (Liberman et al. 2002), which is found in outer hair cells (OHC). Most previous theories of cochlear function assume OHC somatic motility are the fundamental engines of the cochlear amplifier (CA) (Geisler 1986;

Neely and Kim 1986; Geisler 1991; Geisler 1993; Neely 1993; Geisler and Sang 1995; Cohen and Furst 2004), and although some evidence suggests hair bundle motility could also contribute to cochlear amplification (Hudspeth 1997). In all these models, OHC force generation is assumed to couple into pressure difference between scala vestibuli (SV) and scala tympani (ST).

But how can cochlear OHCs produce pressure difference and what is the problem? A fundamental problem is that modelers can propose and solve systems of equations that do not correspond to physical systems. For instance, the widely accepted model presented by Neely and Kim (Neely and Kim 1983) assumes that OHCs create the pressure difference. Since the model is based on a classical model formulation, only the pressure difference acts on the basilar membrane (BM). However, the attempt to find a physical realization for that model is difficult, because it appears that the force creating the pressure difference coming from "nowhere".

In an attempt to resolve what may be called a "force-balance riddle" in the cochlea, or in other words "what do the OHCs push against?", de Boer assumed that the OHC stood between the RL and the BM, pushing equally and oppositely on each other. The chambers were the SV, ST, and the OC (de Boer 1990). Unfortunately, simplifying assumptions led de Boer to the conclusion that there

2

was no way such a model could work in an energy-efficient, natural world. de Boer also explored a cylindrical version of the sandwich model and rejected it (de Boer 1990). A model in which waves propagated down the spiral sulcus, also failed to explain cochlear amplification (de Boer 1993). Nor did any of these models well match experimental data, which normally can be regarded as a validation step after a mechanism has been hypothesized. Quite to the contrary, matching experimental data was what a multicompartment model, called the traveling-wave amplifier model (TWAMP), did well (Hubbard 1993). It replicated quite well the high and not narrow peaks, characteristic of the BM motion scaled by stapes motion found experimentally, as well as the corresponding phase angle data. Although the TWAMP was a multicompartment model, the model's additional compartment could not be unambiguously identified as an anatomical compartment in the cochlea, and thus it did not explain how the CA worked. Moreover, there was no obvious structure in the cochlea that seemed reasonably to relate to the model.

Starting with simplifications of structures existing in the cochlea, and satisfying force-balance equations from the outset, Chadwick et al. (1996) explored a model that divided the cochlear partition into three subpartitions: BM, RL and the tectorial membrane (TM). They could produce a BM/stapes velocity gain of around 35 dB using forces on the order of 1 nN per OHC. These numbers were

3

realistic but the model was not compared directly with physiological data of BM motion. Hubbard et al. (Hubbard et al. 2000; Hubbard et al. 2003) also presented a multicompartment model based on force-balance equations. The model could match BM velocity magnitude and phase data. The model also predicted organ of Corti fluid flow, which has been observed experimentally (Karavitaki and Mountain 2007). How that model works has never been elaborated in any published work, and the version whose parameters have been matched as well as possible to dimensions and physical properties of the gerbil cochlea has not been previously vetted in peer-reviewed literature. Lu et al. (2006) presented a multicompartment model based on Hubbard et al. 's work (2000). The model gave an explanation of how OHCs might work in the high frequency range by using a negative feedback system.

Our model is a 1-D model. The pressure in SV and ST does not change with the distance in the direction perpendicular to the BM. This does not allow direct comparison with measurement data from Olson's work(Olson 1998; Olson 1999) since their pressure measurements are at various distances away from BM. However we do compare our model results with Olson's pressure data measured in the more central range of distance from BM.
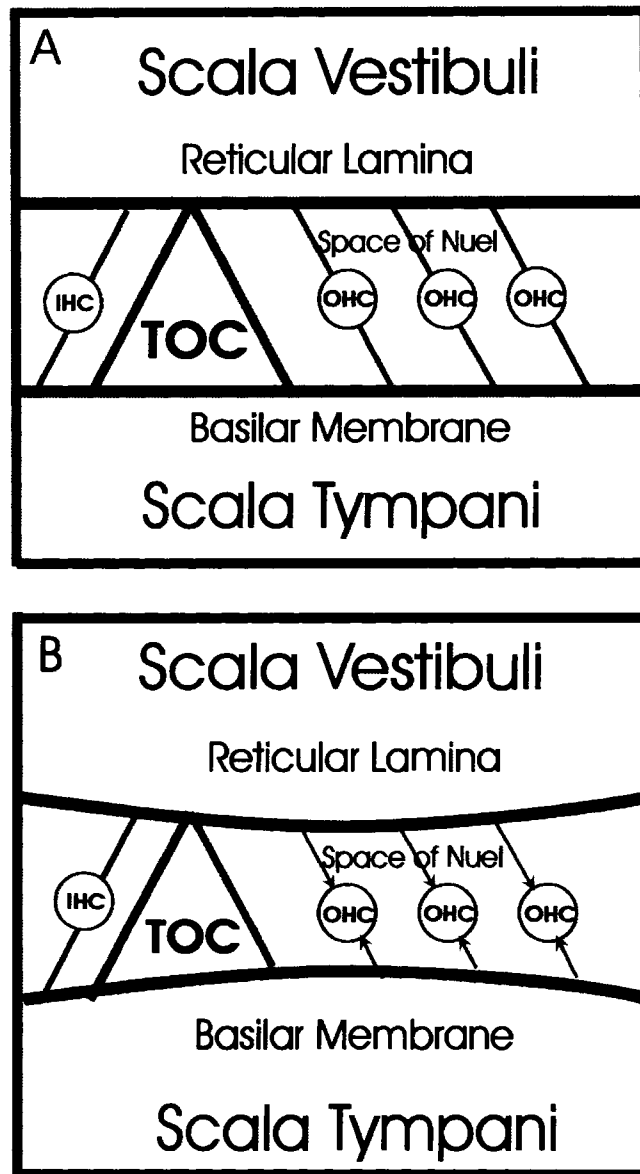
Figure 1- 1 Schematic drawing of a cochlear partition derived from a previous publication (Mountain et al. 2000). The anatomy is simplified for modeling purposes. Panel A: in a conventional model of the cochlea, pressure difference between the scala vestibuli and scala tympani drives the entire space between

5

the RL and the BM, and they move together. Panel B: However, OHCs sit in between the RL and the BM. The tunnel of Corti and space of Nuel are also fluid filled. Thus, when OHCs change length, they should push the RL and the BM apart or pull them together. Therefore, the RL and the BM can move separately. This will also squeeze the fluid inside the OC and produce flow in longitudinal direction.

1.2 Methods

Our interpretation of the anatomy for modeling purposes differs from the actrual anatomy. The following are the assumptions: The OC contains the tunnel of Corti (ToC) located within the bounds of the triangular area formed by the inner and outer pillar cells (See Figure 1-1 Panel A). We did not include the inner spiral sulcus. The fluid of the ToC is continuous with that in the spaces of Nuel, which surround the OHCs. The upper surface of the OC is the RL, which is made up of the apical surfaces of the hair cells and pillar cells. The tops of the OHCs contain hair bundles. The motion of the RL with respect to the TM displaces OHC hair bundles, causing a conductance change, therefore a transduction current was introduced in the OHCs (Davis 1958). This, in turn, results in a change in OHC transmembrane voltage. Prestin changes its conformation with transmembrane voltage changes, causing the cell body to produce axial force on a cycle-by-cycle basis. This OHC force acted on both the RL and BM, and could deform them separately (see Figure 1B), causing a relative movement between the RL and the BM. We propose that this relative movement could have a significant impact on the pressure and longitudinal fluid flow within the OC and that it may play an important role in cochlear amplification.

1.2.1 Model Formulation

The model consists of three fluid-filled compartments: SV, ST and the OC. The pressures inside these compartments are: P_{SV}, P_{ST} and P_{OC} respectively (see Figure 1-2). Their cross-sectional areas vary as a function of longitudinal position. The fluids are assumed to have viscosity and density equal to that of water. The RL and BM are modeled as resonant spring-mass-dashpot structures. The RL separates the OC compartment from the SV compartment, while the BM separates the OC compartment from the ST compartment. The middle section of the circuit is the OC. Part of it is the OHC force generator. The impedance of OC consists of fluid mass L_{OC} and viscosity R_{OC}. Because the space of Nuel, from a hydrodynamic standpoint, must have relatively large viscosity owing to the small size of the space in which the fluid exists, most of the longitudinal fluid flow is assumed to be inside the ToC. Our formulation does not include sufficient fine structure to differentiate the ToC and the spaces of Nuel. The TM is treated as a hinged plate, so, the OHC's stereocilia movement can be considered proportional to RL displacement. We do not consider flow in the subtectorial space that may stimulate the inner hair cells since there is no sub-tectorial space in our model. The helicotrema connects the SV and ST. It is modeled as an acoustic impedance. The ST at the basal end terminates at the round window which was modeled as a volume compliance. The volume compliance of round window is much greater than the BM volume compliance at the apical end of the BM. We assume the ToC terminates with an extremely large acoustic resistance at the

8

basal end, but this is just a ploy to keep the simulator functional, rather than an anatomical fact. At the apical end, the ToC is a closed tube without connecting to other compartments.
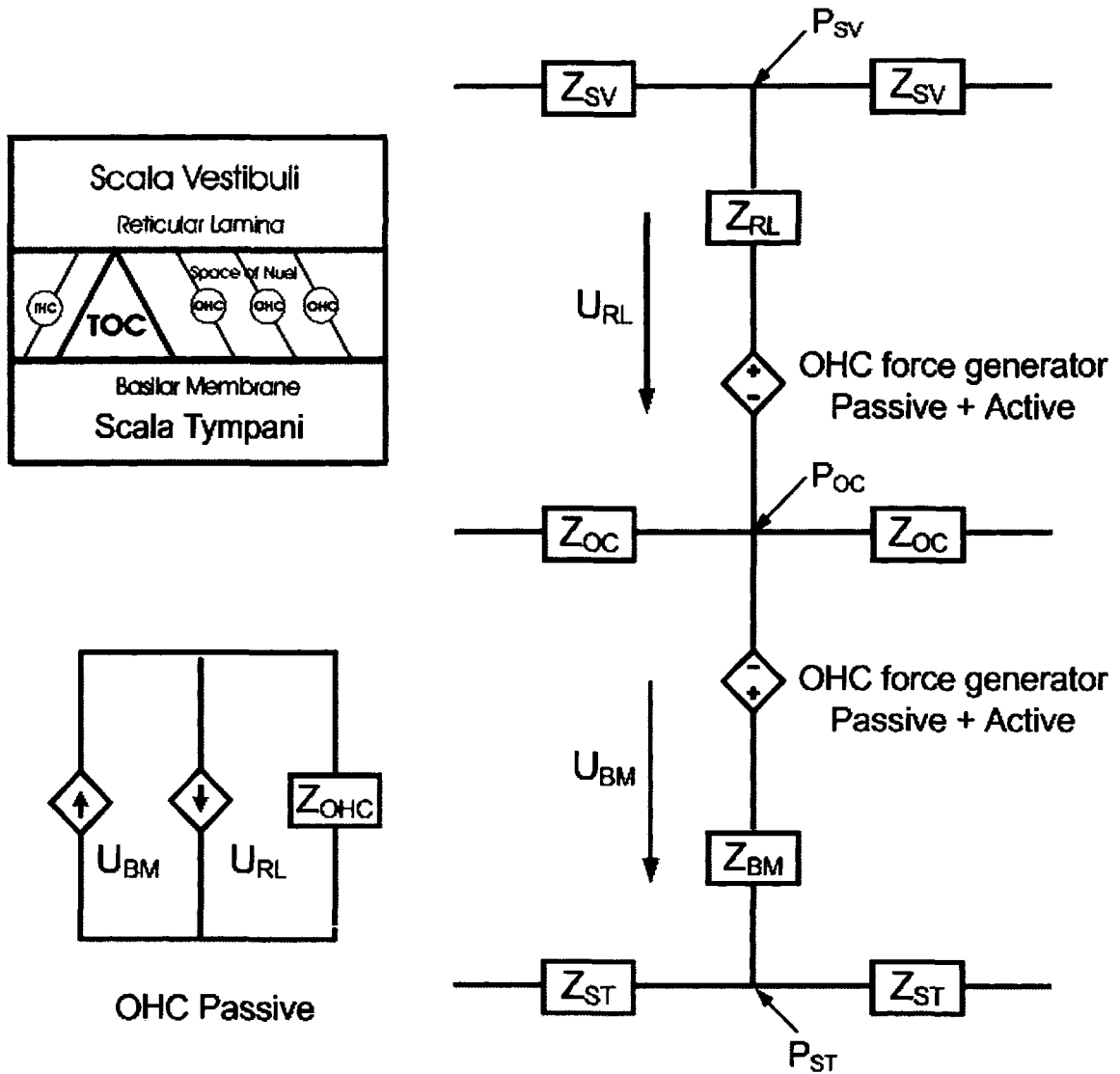
Figure 1- 2 The schematic structure of one section of the model. The entire cochlea is divided into 400 discrete sections in the longitudinal direction from the base to the apex. There are three fluid compartments: SV, ST and OC. The impedance of RL separates the SV and the OC. The impedance of BM separates the OC and ST. The P_{SV}, P_{ST} and P_{OC} are the pressure inside SV, ST and OC respectively. U_{RL} and U_{BM} are the volume velocity of RL and BM respectively.

The OHC force generators represent both passive force and active force generated by OHCs. The passive force is a result of different velocities between RL and BM. It can be calculated by the helper circuit "OHC Passive". Z_{OHC} represents the acoustic impedance of the OHC. The OHC active force is directly proportional to the RL displacement.

We assume the pressure wave in the scalae is planar. Therefore the model is one-dimensional and that dimension is the longitudinal position along the length of the cochlea. If we set the U_{BM} and U_{RL} as the volume velocity of BM and RL respectively, the pressure variables depicted in Figure 1-2 are related to the volume velocity of the RL and the BM by equations 1-3.

$$\frac{d^2 P_{SV}}{dx^2} = k_{LV} \frac{U_{RL}}{dx} \tag{1}$$

$$\frac{d^2 P_{ST}}{dx^2} = -k_{LT} \frac{U_{BM}}{dx} \tag{2}$$

$$\frac{d^2 P_m}{dx^2} = k_{LOC} \left(\frac{U_{RL}}{dx} - \frac{U_{BM}}{dx} \right) \tag{3}$$

11

$$k_{LV} = \rho \frac{1}{A_{SV}} \tag{4}$$

$$k_{LT} = \rho \frac{1}{A_{ST}} \tag{5}$$

$$k_{LOC} = \rho \frac{1}{A_{OC}} \tag{6}$$

K_{LV}, K_{LT} and K_{LOC} are unit length impedance in SV, ST and OC respectively. A_{SV}, A_{ST} and A_{OC} are the cross section area of SV, ST and OC respectively.

The OHCs in one section of the model were modeled as a force source that consists of two parts: An active force generator (P_{OHC_active}) and a passive force generator ($P_{OHC\_passive}$). These force generators are treated as pressures because the forces in the model act over a defined area. The passive force is the result of OHC resisting the stretching and compressing caused by the relative velocity of RL and BM. So if the RL and BM have the same velocity, there is no passive force generated by OHC. The value of OHC passive force was determined by the helper circuit called "OHC Passive". In this helper circuit, OHC

12

was modeled as a spring-mass-dashpot structure. Its impedance was defined by:

$$Z_{OHC} = R_{OHC} + \frac{1}{j\omega C_{OHC}} + j\omega L_{OHC} \qquad (7)$$

The L$_{OHC}$ is chosen to be negligible, so that any OHC resonances are far above the audio range (see table 1-1). The active force is a direct result of OHC electromotility. We assumed that the OHCs sense RL motion and produce an active force proportional to RL displacement. The amount of force produced per nm of RL displacement was adjusted to match BM responses measured experimentally.

The pressure differences between the large scalae (SV and ST) and the OC are given by equations 4 and 5, respectively:

$$P_{SV} - P_{OC} = P_{OHC\_active} + P_{OHC\_passive} + Z_{RL}U_{RL} \qquad (8)$$

$$P_{OC} - P_{ST} = -P_{OHC\_active} - P_{OHC\_passive} + Z_{BM}U_{BM} \qquad (9)$$

where the BM impedance and the RL impedance can be determined by:

13

$$Z_{BM} = j\omega \cdot L_{BM} + R_{BM} + \frac{1}{j\omega \cdot C_{BM}} \qquad (10)$$

$$Z_{RL} = j\omega \cdot L_{RL} + R_{RL} + \frac{1}{j\omega \cdot C_{RL}} \qquad (11)$$

Where Z_{BM} is the BM impedance per unit length and Z_{RL} is the RL impedance per unit length. The OHC force is referenced to an incremental area of the RL and BM, thereby allowing representation as a pressure. Z_{OHC} is the impedance of the OHC per unit length along the cochlea.

$$P_{OHC\_passive} = Z_{HC} \cdot (U_{RL} - U_{BM}) \qquad (12)$$

The active force generator P_{OHC_active} is assumed to be proportional to the displacement of the RL, which is the integral of the volume velocity after compensating for scale factors. Thus,

$$P_{OHC\_active} = G_{OHC} \cdot \int U_{RL} dt \qquad (13)$$

$$G_{OHC} = OHCgain \cdot e^{\frac{-kx}{L}} \qquad (14)$$

Where x is the longitudinal distance from the base. OHCgain is a constant related to the amount of force that an OHC can generate. k is a constant that determines the G_{OHC} changes along the length of the cochlea. L is the total

14

length of the gerbil cochlea, 1.3 cm.

1.2.2 Assignment of the Parameters in the Model

The parameters used in the analog circuit simulation, which computes the model's responses, are calculated based on the gerbil's physiological data. 400 sections are used from base to apex in the model. Therefore, the spatial quantization in the discrete model is $\Delta x = \dfrac{L}{400}$. There are about 3000-4000 OHCs in gerbil's cochlea. So each section contains about 10 OHCs. The OHC compliance, mass and viscosity in the OHC helper circuit are the combination of all the OHCs in one section.

The area of the stapes footplate in the gerbil is 0.62 mm^2 (Lay 1972). This area factor is needed to translate volume velocity in the model to linear velocity of the stapes, which is typically measured (Ren and Nuttall 2001).

The acoustic mass and viscosity of the three compartments depend on the length of each section, cross-sectional areas and the fluid properties. For the current model, we used the scalae cross-sectional areas measured in the gerbil by Plassman et al. (1987). Because the space of Nuel has relatively large viscosity, we only consider ToC area when calculating the cross section area of OC. The cross-sectional area of ToC was estimated based on the structure of unfixed cochlea (Edge et al. 1998).

16

To determine the CF of the BM for each section, we used a Greenwood map (Muller 1996) designed to fit gerbil data, where the CF of the ith section is specified by:

$$CF_i = 398 \cdot \left[10^{2.2(L-x_i)/L} - 0.631 \right]$$

(15)

Where L is the length of the cochlea (1.3 cm), and x_i is the location of the ith section.

The volume compliance of the BM is calculated based on experimental data. We derived volume compliance of the BM using the point stiffness *versus* distance measurements of Naidu and Mountain (1998), by treating radial strips of the BM as a beam (Olson and Mountain 1991). The width of these strips was assumed to be equal to the measurement probe diameter (10 μm) plus two times the longitudinal coupling space constant measured by Naidu and Mountain (2001). Given the CF and the volume compliance of the BM for a certain section, the acoustic mass of the BM and the viscosity corresponding to a particular choice of Q in that section can be calculated as

$$L_{BM} = \frac{1}{C_{BM} \cdot (2\pi \cdot CF)^2}$$

(16)

$$R_{BM} = \frac{\sqrt{L_{BM} / C_{BM}}}{Q} \tag{17}$$

Q is the quality factor of a second-order system. In this model we chose a fixed value of Q for all the sections to simplify the model. The proper Q (Both in RL and in BM compartment) was chosen so that the model's passive BM vibration match the passive experimental data (Ren and Nuttall 2001). In this model we chose the Q of BM to be six for gerbil. And Q of RL was chosen to be about twice of that of BM.

The RL compliance is presumably five times that of the BM, based on data from Mammano and Ashmore (1993). Mammano and Ashmore also observed that the resonant frequency of the RL was approximately 1/2 that of the BM. Thus we further scaled the mass of the RL by a factor of 0.66 so that the RL resonance in this model was on the order of 0.55 times the resonance frequency of BM.

Because our own experimental work suggests the compliance is comparable to that of the RL (Naidu and Mountain 2001), the OHC compliance in one section in the model was set to be 0.2 of the corresponding BM parameter. This means that ten OHCs are about as compliant as the RL. The OHC resistance was also set to be 0.2 of the BM's value. Logically, we think it is not reasonable to use a higher

18

compliance than the RL, or in a "thought experiment", pushing on the RL would not move the BM. On the other hand, if the OHCs have very low compliance then RL and BM are essentially connected, and the "sandwich" aspect of the model disappears. In addition, if the OHC compliance was considerably lower than the BM and/or the RL, its force would all be wasted trying to stretch itself. The OHC mass was set to be 1/500 of the corresponding BM values. Thus the impedance of the OHC was principally a compliance at audio frequencies. Moreover, to dispel the criticism that the helper circuit is a tuned system, its natural frequency is about 30 times higher than the CF of the BM at every BM location. Thus the OHC circuit is basically an RC circuit, and by choosing its RC time constant to be equal to that of the RL would make the OHC passive impedance the same as the RL's impedance, if the RL was not resonant.

Name	Meaning	Value	Unit
N	Section number	400	
x	Distance from the base along the BM	0-1.3	cm
L	Total length of the BM	1.3	cm
CFi	Characteristic Frequency	$CF_i = 398 \cdot \left[10^{2.2(L-x_i)/L} - 0.631 \right]$	Hz

Q_{BM}	Quality Factor	6	
C_{BM}	Volume compliance of the BM	$$C_{BM} = 100 \cdot e^{(-309 + 4.04x)}$$	cm^5/dyne
L_{BM}	Effective acoustic mass of the BM	$$L_{BM} = \frac{1}{C_{BM} \cdot (2\pi * CF_i)^2}$$	dyne*s^2/cm^5
R_{BM}	Viscosity of the BM	$$R_{BM} = \frac{\sqrt{L_{BM} / C_{BM}}}{Q}$$	dyne*s/cm^5
C_{RL}	Volume compliance of the RL	$5*C_{BM}$	cm^5/dyne
L_{RL}	Effective acoustic mass of the RL	$L_{RL} = 0.66 L_{BM}$	dyne*s^2/cm^5
R_{RL}	Viscosity of the RL	$0.2*R_{BM}$	dyne*s/cm^5
C_{OHC}	Volume compliance of OHCs in one section	$0.2*C_{BM}$	cm^5/dyne
R_{OHC}	*Viscosity of the OHCs in one section*	$0.002*R_{BM}$	*dyne*s/cm^5*
OHCgain	OHC gain	$$OHCgain = 13 \times 10^{-3}$$	N/m^5

Table 1- 1 Parameters used in the hydromechanical cochlear model.

To obtain the correct OHC active force, OHCgain was increased gradually until the simulation results fit the experimental data (Ren and Nuttall 2001). We found that $OHCgain = 13 \times 10^{-3}$ N/m^5 produced the best fit for the active cochlea data from the gerbil at the 14 kHz place. This value of OHCgain cannot be used throughout the model, because the OHC sizes increase along the cochlea. Using k=2 in Equation 14 counts for this change, and also keeps the model's apical sections stable. These parameter choices correspond to a single OHC gain of 0.67 nN of force generated per nm of RL deflection in the base, down to a gain of 0.09 nN per nm in the apex. These values are comparable to the values reported previously (Iwasa and Chadwick 1992; Mountain and Hubbard 1994; Frank et al. 1999).

In general, as compared for example, with the TWAMP model (Hubbard 1993), both that model and the present model are fairly insensitive to changes in parameter values. Given a "reasonable" set of parameters that may differ by perhaps a factor of two, one can find gain settings for which the model will show amplification and comparisons with data that are "reasonable". What will change almost surely are the loci of CFs, and that is a metric with which we have rarely been concerned, although our frequency-place maps for the data we seek to match are very accurate. Put simply, however, the present model is not one that just barely works for some narrow choice of parameter values

We embodied the model equations as an electrical impedance analog circuit, and calculated the circuit responses using either TSpice™ (Tanner) or a Cadence analog simulator, Spectre™.

1.3 Results
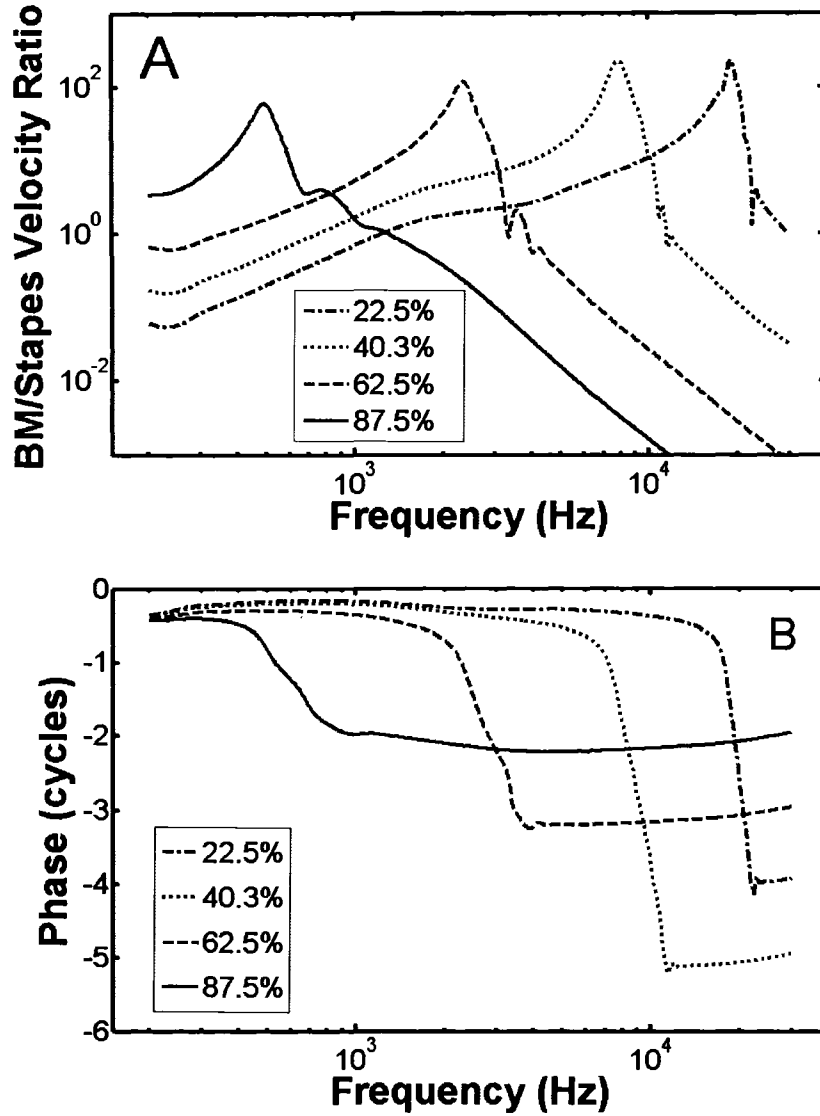
Figure 1- 3 Frequency response of BM/stapes velocity ratio at 22.5%, 40.3%, 62.5% and 87.5% of the total cochlear length from the base. Upper panel: magnitude. Lower panel: phase. The input stimulus is 74 dB SPL pure tone at the stapes.

Figure 1-3 shows the model's BM/stapes velocity ratio frequency response at four different locations along the cochlea. The distances from the base are: 2.925mm (22.5%), 5.239mm (40.3%), 8.125mm (62.5%) and 11.37mm (87.5%). The CFs of these locations are: 18.9 kHz, 16 kHz, 7.89 kHz, 2.34 kHz and 0.49 kHz respectively. The response at the base has a relatively bigger peak magnitude and more phase lag than at the apex. The magnitude response curve from the base, which has a high CF, has a narrow peak compared with the curve from the apex, which has a low CF. This trend can also be found in the frequency tuning of auditory nerve fibers (Muller 1996).

Figure 1-4 is the comparison of Greenwood frequency place map and our model results for active response. Four of six points in the model results are the data from Figure 1-3. The extra two points in Figure 1-4 are at CF=14 kHz and CF=30 kHz. The distance from the base is 3.42 mm and 1.80 mm respectively. The Greenwood map is generated from Equation 15. It is an active map for sensitive gerbil cochlea (Muller 1996). It is clearly shown in the Figure 1-4 that our model results of tuning map fit the experimental data well.
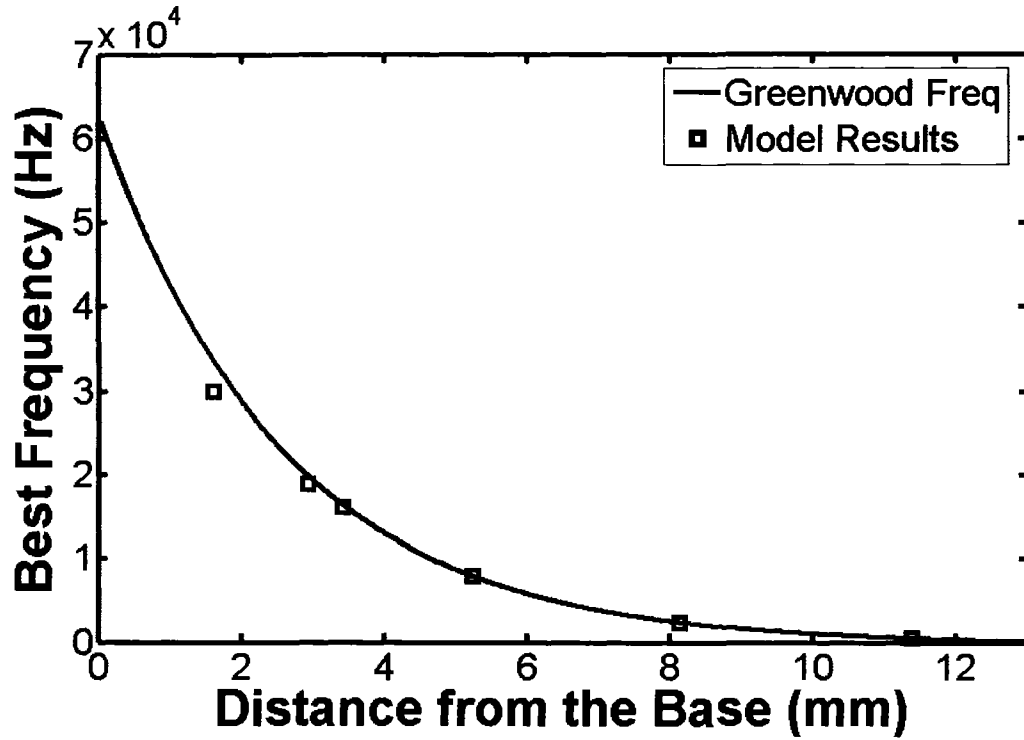
Figure 1- 4 Frequency tuning map along the cochlea for gerbil. The solid line was calculated from Greenwood map. The squares are model results.
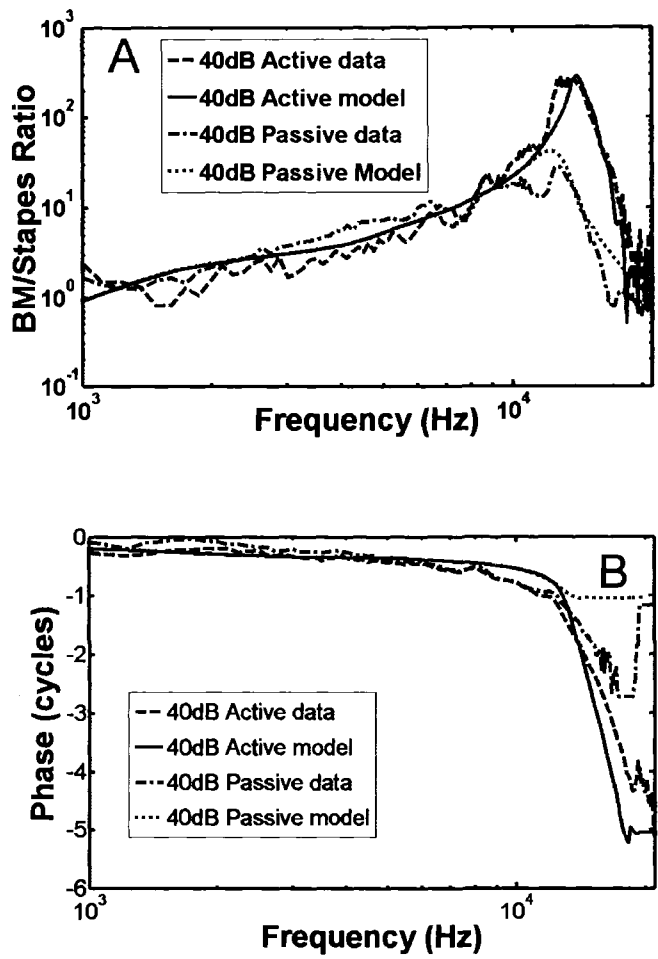
Figure 1- 5 Frequency response of BM/stapes velocity ratio from a cochlear location where CF is about 14 kHz. The dashed lines are the experimental data from gerbil (Ren and Nuttall 2001). The blue dashed line is the measurement for active cochlea at 40 dB SPL input. The green dashed line is for a passive cochlea. The solid lines are the result from the model. Red is active response and pink is passive response at 40 dB SPL input. For the model, we set OHCgain as 0.001 when we calculate passive results.

The model's basilar membrane transfer function, defined as the ratio of the velocity measured at a point on the basilar membrane to the velocity of the stapes, compares well with experimental data from the gerbil (Ren and Nuttall 2001) shown in Figure 1-5. The experimental stimulus level is a tone at 40 dB SPL in the ear canal. Its frequency is swept from about 1 kHz to 20 kHz. The predicted active transfer function magnitude closely fits the experimental data in the CF region (14 kHz). It rises about 45 dB from 1 kHz to the peak at 14 kHz. The model's passive transfer function magnitude also fits the experimental data well. To mimic low CA gain, we set the model's OHC gain to near zero. Both the model and experimental data show that the peaks shift to low frequency when the cochlear changed from active to passive.

The lower panel of Figure 1-5 is the comparison of phase data. The active model phase data are similar to the experimental data. At CF, the phase angles are nearly equal. The main difference between the phase curves is that the slope for the model is less than the slope for the experimental data below CF and greater than the slope of the experimental data above CF. The passive phase lag in the model is less than seen in the data. The model phase data end up one cycle short of where the experimental data end up. This is somewhat interesting in that many contemporary models show far too much phase lag as compared with experimental data. Moreover, the experimental data are shown to "return" to one

27

cycle lag at higher frequencies, and this apparently strange phenomenon may all be an artifact of the phase unwrapping methods used.
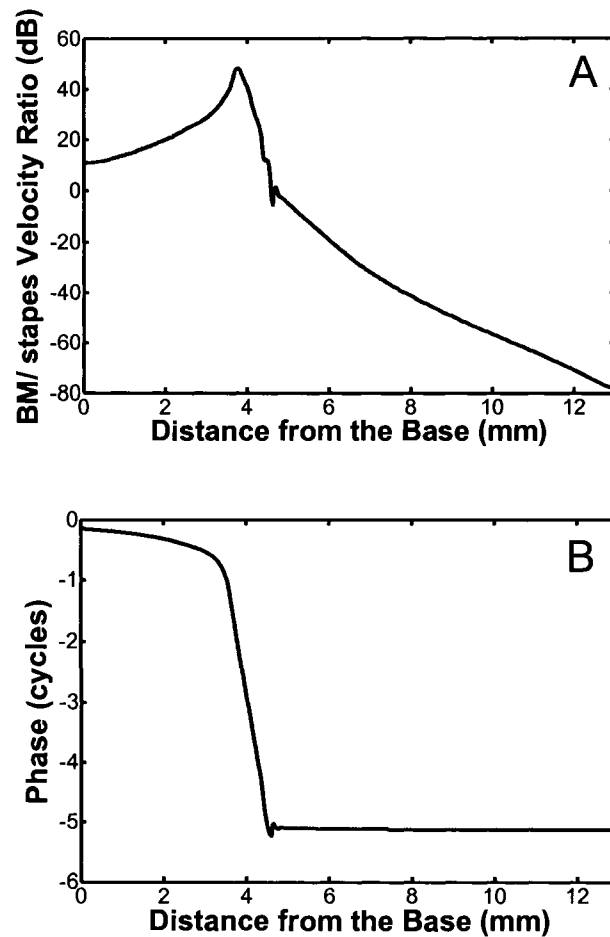
Figure 1- 6 BM/stapes velocity ratio from the base to the apex along the cochlea. The input stimulus is a 14 kHz sinusoid. This is the so-called "panoramic" view, which may become more and more relevant as better measurements are made along the length of the cochlea.

Figure 1-6 shows the longitudinal change in the BM/stapes velocity ratio responses of the model when stimulated with a sinusoid at 14 kHz. The data are plotted versus longitudinal distance along the cochlea. Starting from the base (0 mm), the response grows exponentially with longitudinal distance at a rate of 10 dB per mini meter. Near the best place, the response grows more rapidly, approaching a growth rate 50 dB/mm. Spatially, the upper 20 dB of the response occupies a region that is 0.6 mm in length. Past the peak, the wave attenuates rapidly over about 1mm. Beyond this region, the attenuation per unit length is significantly less. Starting from the base, the phase angle lags about one cycle approaching the region of rapid growth of the magnitude response. The phase curve shows that the wave travels rapidly as it leaves the base, because the faster a wave travels, the fewer number of cycles that occur over the distance that it travels. Approaching the place of maximum amplitude, the wave slows down and many cycles of phase lag occur. This so-called "panoramic" view cannot actually be measured in the cochlea over large distances along the cochlea, and thus we show model predictions in anticipation of such experimental measurements being carried out in the future.
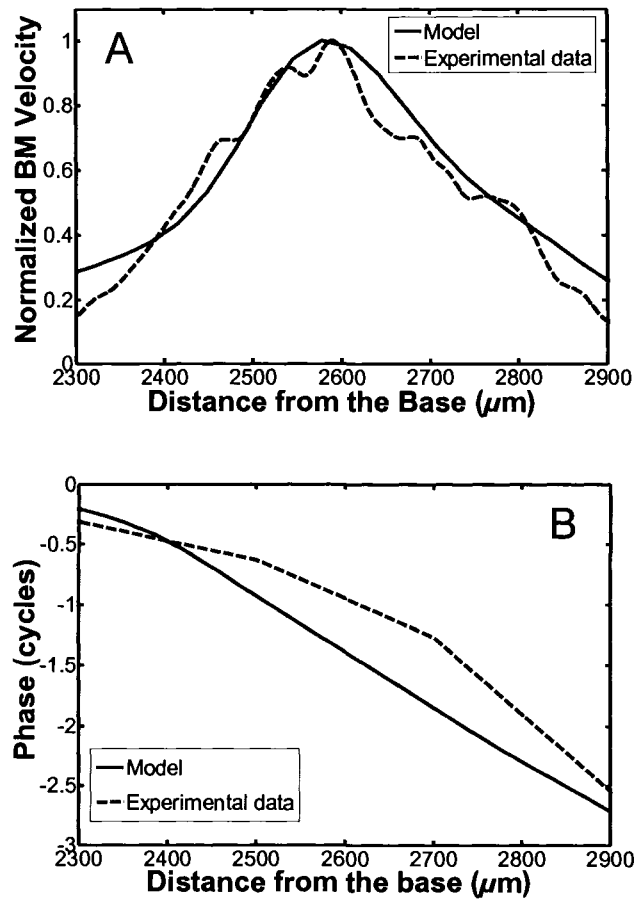
Figure 1- 7 Longitudinal BM velocity profiles. The left panel is normalized magnitude. The right panel is phase. The input stimulus is a 50 dB SPL sinusoid at 16 kHz. The dashed line is experimental data from the gerbil. It is recorded from location 2.1 mm to 3.0 mm from the base. The solid line is the simulation result of our model, shifted 1 mm toward the base.

Figure 1-7 compares the longitudinal velocity pattern obtained from the model with experimental data obtained from the gerbil (Ren 2002) measured over only about 600 um length along the BM. The input is 50 dB SPL in the ear canal. The left panel shows the normalized BM velocity at various longitudinal locations. The data shown for each curve were normalized to their maximum value. The reason we use the normalized comparison is because the experimental data used in Figure 1-5 and the experimental data used in Figure 1-7 are from different experiments on different animals, whose measured BM velocities differ considerably in magnitude. We cannot use the same set of model parameters to mimic the experimental from both animals, so we chose to use absolute units as per Figure 1-5 and then use normalized data in Figure 1-7. The right panel is the comparison of the phase data. The phase angles are referred to BM vibration in the basal end of the measured region at 90 dB SPL. The best frequency location of 16 kHz is about 3.6 mm from the base in our model. In Ren's experimental measurement the corresponding location is approximately 2.6 mm from the base. We think this is because the total cochlear length depends on the starting point where one begins measuring (Naidu and Mountain 1998).
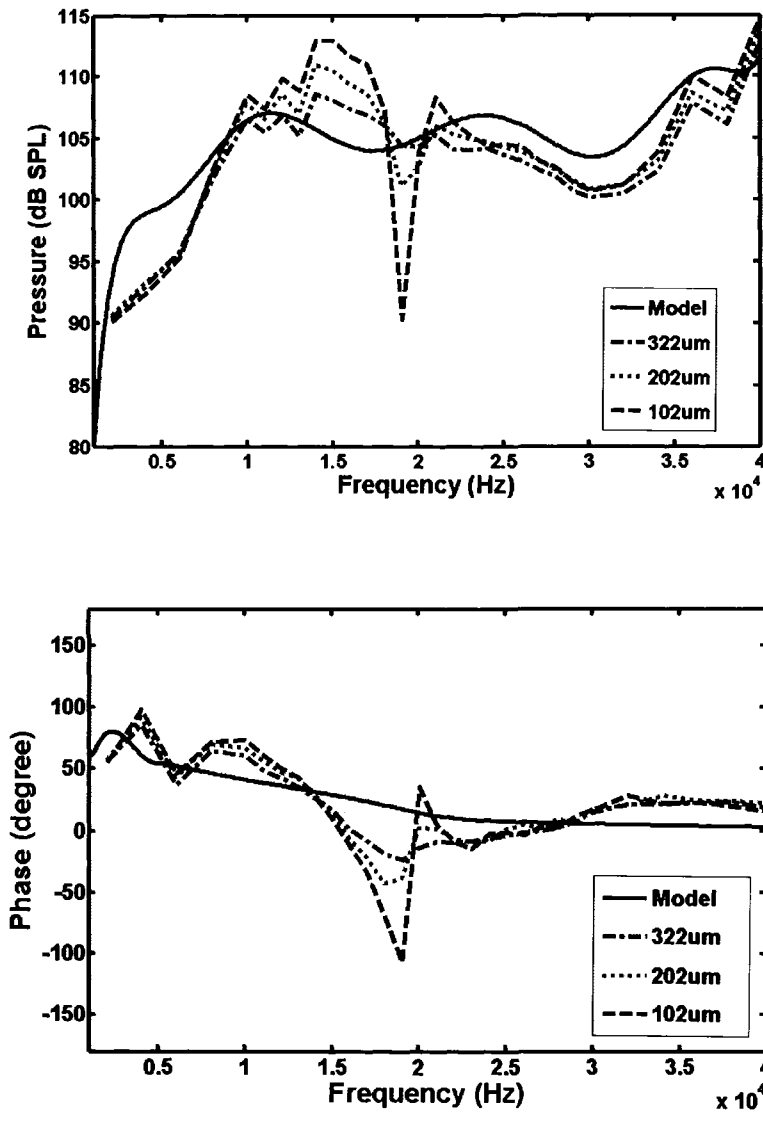
Figure 1- 8 Comparison of pressure in ST in the frequency domain. The upper panel is the magnitude comparison. The lower panel is the phase comparison. The input stimuli are 80 dB SPL pure tones in the ear canal. The dashed lines are the experimental data from the gerbil at different distances from the BM. The solid line is the simulation result of our model.

Figure 1-8 is the comparison of model results with pressure versus frequency measurements (Olson 1998; Olson 1999) in the cochlea. Bear in mind that this model is an one-dimensional model, and cannot mimic the gradients in pressure that occur as one moves away from the BM. Note also that the model input is sound level in SV at the stapes, so to get back to Olson's reference of pressure in SV near the stapes, we need to use her input pressure in SV (constant level at the eardrum, but not at all constant just inside SV because of the middle ear transfer function) for our model's input. We obtained the data from Olson and used it to generate our model's input pressure signal inside the stapes. The measurement is at a location that has a CF about 30 kHz. And the input sound pressure level is 80 dB SPL in the ear canal. The vertical positions of the dashed lines in the figure are 322 μm, 202 μm and 102 μm from the BM. Both the magnitudes and the phase angles from the model compare favorably, especially when considered that this particular one-dimensional model was never intended to replicate data measured in a dimension that the model represents as a single lumped element.
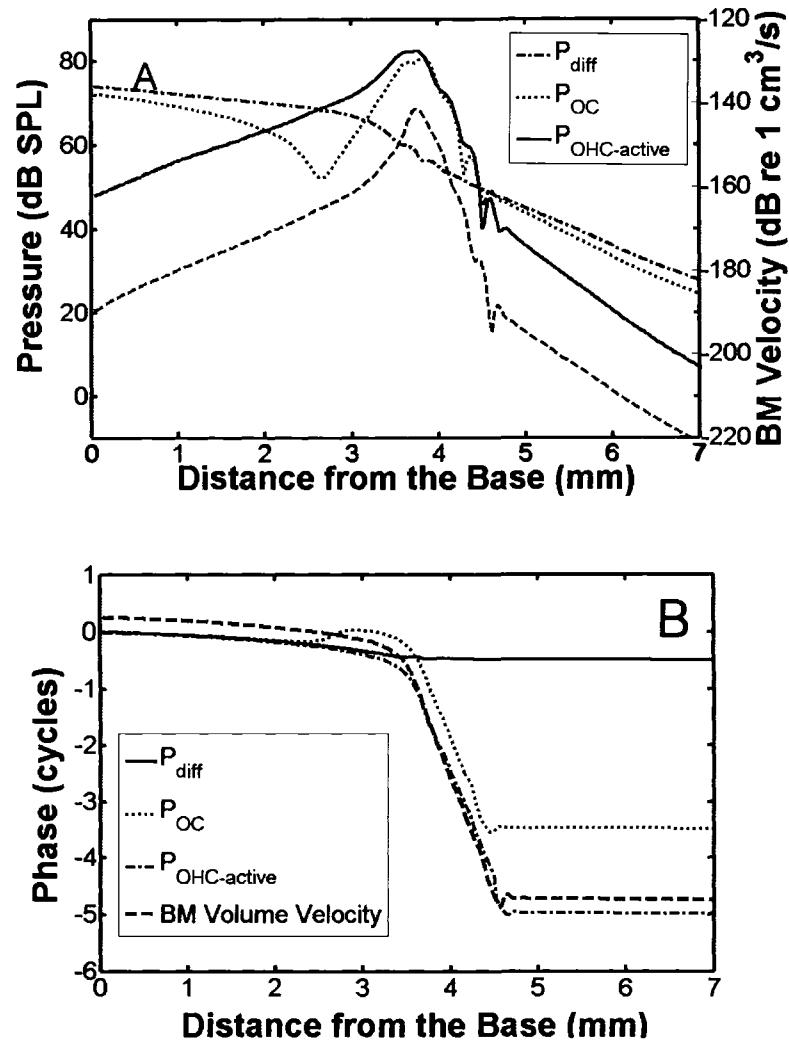
Figure 1- 9 The pressures response (solid lines) and BM velocity response (dashed line) along the cochlea. The input stimulus is a 74 dB SPL, 14 kHz sinusoid at the stapes. Left panel: magnitude. Right panel: phase. The pressures shown here are: 1. P_{diff} : the classical pressure difference wave (Peterson and Bogert 1950; Zwislocki 1950). P_{diff} equals to P_{SV}-P_{ST} in the classical models. 2. P_{OC} : the OC pressure wave (P_{OC}-P_{ST}). 3. P_{OHC_active} : the mechanical active force generated by OHC converted to the pressure.

Figure 1-9 show the magnitudes and phase angles of the pressures in the model as well as the volume velocity of BM. The same input pressure of 74 dB SPL at stapes produced all model responses. The OHC gain was set to be the same as that used to generate the results in Figure 1-5. At this setting the cochlea is considered to be active. P_{diff}, which is almost equal to P_{SV} at the input (since the P_{ST} is very low due to a compliant round window), is about 74 dB SPL at the stapes. The BM volume velocity, not the BM/stapes ratio is plotted on the right ordinate, while the pressures are in dB SPL.

In the far basal regions relative to the best place, the classical pressure difference wave is dominant. The pressure-difference wave is relatively fast-traveling, and loses only about half a cycle of phase approaching the best place. This "relatively-fast" wave (P_{SV}-P_{ST}) should not be confused with the classical P+ wave (the average of P_{SV} and P_{ST}) which travels at the velocity of sound in water (about 1500 m/s). In this model as well as in previous models (Hubbard et al. 2000; Hubbard et al. 2003; Lu et al. 2006), the P_{SV} and P_{ST} waves are assumed to be incompressible. It makes almost no difference at the frequencies involved whether the velocity of sound is around 1500 m/s or infinite, because the "relatively slow" wave has a velocity below 100 m/s.

The location where the effect of the P_{OC} wave acting on cochlear structures exceeds the action of the P_{diff} wave corresponds to the same location where the slope of the BM magnitude curve begins to change dramatically. Near the best place, the P_{OC} and P_{OHC_active} (local OHC force applied to an area) dominate. Both the active OHC forces and the OC pressure drive the BM almost equally, and this action is continued on the apical side of the peak. If one looks at the spatial extent of the OHC force, it is also wave-like, and could be thought of or mathematically expressed as a traveling force wave, which is strictly mechanical in nature. In any case, these are very slow waves, and many cycles of delay occur as they pass through the peak region. In the peak region, P_{OHC_active}, P_{OC} and BM velocity have similar spatial profile. After the peak, both P_{OHC} and P_{OC} drop in a similar fashion, and their magnitudes are similar, while their phase angles differ. This produces ripples (cancellations) in the BM velocity magnitude, because one and then the other driving force slightly dominates, and thus the phase of the BM velocity, when unwrapped, undergoes more lag than either P_{OC} or P_{OHC} due to the way the unwrapping algorithm works. The "classical" pressure difference wave contributes $1/20^{th}$ of the force acting on the BM in the amplification region. So the pressure difference between SV and ST does not drive the BM at the peak region. This conclusion is reasonable, giving the size and complexity of the organ of Corti, and the BM is the bottom portion of the organ of Corti.

In the more apical region relative to the best place, the location at which the OC pressure wave becomes less than the pressure difference wave corresponds to the location where the slope of the basilar membrane velocity also changes dramatically: the magnitude falls off much less quickly. In this region, the RL and BM move in phase. When the pressure difference wave again dominates, a "plateau" in phase falloff occurs. The value of the total lag of the BM velocity is resolved at some integer number of cycles away from the phase of P_{diff}. Here the BM velocity (not the BM/stapes) lags about 90 degrees relative to P_{diff}, as expected, because it is an acoustic mass driven by a pressure difference. Near the stapes, where the cochlear partition impedance is stiffness dominated, BM velocity leads P_{diff} by about ¼ cycles.

Calculations based on our new theory show that the force produced by cochlear OHCs couples back to SV and ST, because a nonlinear version of the model generates DPOAE comparable to experimental data. The OHC is the only nonlinear component in the model. So the OHC force must coupled back to the fluid channels. But OHC force does not cause much change in the pressure difference (P_{SV}-P_{ST}) (see the small bump in Figure 1-9 near CF). Near CF, pressure difference contributes almost nothing to CA. Although some other models could do an arguably good job of matching experimental data, they failed to explain how pressure difference (P_{SV} -P_{ST}) could be created by OHCs.

1.4 Discussion

How can a multicompartment model, in which the OHCs seemingly have nothing to push against, work (de Boer 1990)? Part of the answer is that the RL and BM are not in phase when the CA shows highest gain (Hubbard et al. 2000; Hubbard et al. 2003). Thus RL and BM are essentially pushed toward or pull away from each other by the OHC force and the OC pressure, and these equal and opposite forces face different impedances in a dynamic sense. Thus, RL and BM are not in phase, and they move with different magnitudes; and therefore there must be longitudinal OC fluid flow. Concomitantly, there is also a traveling pressure wave in the OC, in addition to the pressure waves in SV, and ST. The force acting on the BM comes from the difference between the OC and ST pressure plus the active force produced by the OHCs (see Figure 1-9).

The model offers a novel explanation of a number of standing experimental results. The high-frequency plateau, observed experimentally, (Figure 1-5 both the magnitude and the phase), and first thought possibly to be anomalous, has never before been interpreted as a shift in drive from the OC and OHC modes to the pressure difference mode. Other models can also show such a plateau, but it has never been explained as a mode shift.

38

This model also offers two separate accounts for why BM tuning "looks" like auditory nerve tuning. One explanation involves the RL as an intermediary component, as follows: The model predicts RL motion that is similar to but not identical to BM motion. Under the assumption that RL motion beneath a fixed TM would produce subtectorial flows, this might predict inner hair cell (IHC) excitation similar to RL motion, which is similar to BM motion. Nowotny and Gummer (Nowotny and Gummer 2006) showed that OHC electromotility can stimuli IHC directly via fluid in the sub-tectorial space up to 3 kHz. We cannot verify this because we did not consider IHC, TM and sub-tectorial space in our current model. Another potential explanation is that OC pressure moves IHCs from the underside. This would not be possible unless OC pressure peaked as it does in the model, again, similar in profile but not identical to the velocity of the BM.

The explanation of the working of this model describes a completely new theory of how the mammalian CA might work. Work based on this theory (Hubbard et al. 2000; Hubbard et al. 2003; Lu et al. 2006) all show a fairly good match to experimental data. Lu's model (Lu et al. 2006) explains little about the CA from a physiological point of view, because it is a transfer-function model, not a first-principle, finite-difference model as ours is. Our work shows that the driving forces in the peak region are the OC pressure wave and the force generated by the OHCs. They contribute almost equally to the CA in the peak region.

39

Concomitant with the OC pressure wave is the longitudinal fluid flow within the

OC, which has been recently observed (Karavitaki and Mountain 2007).

1.5 References

Brownell, W. E., C. R. Bader, et al. (1985). "Evoked mechanical responses of isolated cochlear outer hair cells." Science 227(4683): 194-6.

Chadwick, R. S., E. K. Dimitriadis, et al. (1996). "Active control of waves in a cochlear model with subpartitions." Proc Natl Acad Sci U S A 93(6): 2564-9.

Cohen, A. and M. Furst (2004). "Integration of outer hair cell activity in a one-dimensional cochlear model." J Acoust Soc Am 115(5 Pt 1): 2185-92.

Davis, H. (1958). "A mechano-electrical theory of cochlear action." Trans Am Otol Soc 46: 180-96.

Davis, H. (1983). "An active process in cochlear mechanics." Hear Res 9(1): 79-90.

Davis, H. (1984). "New insights in the evaluation of cochlear impairment." Ann Otol Rhinol Laryngol Suppl 112: 74-5.

de Boer, E. (1990). "Can shape deformations of the organ of Corti influence the travelling wave in the cochlea?" Hear Res 44(1): 83-92.

de Boer, E. (1990). Wave-propagation modes and boundary conditions for the ulfendahl-flock-khanna preparation. The Mechanics and Biophysics of Hearing Proceedings. P. Dallos. Berlin, Springer-Verlag: 333-339.

de Boer, E. (1993). "The sulcus connection. On a mode of participation of outer hair cells in cochlear mechanics." J Acoust Soc Am 93(5): 2845-59.

Edge, R. M., B. N. Evans, et al. (1998). "Morphology of the unfixed cochlea." Hear Res 124(1-2): 1-16.

Frank, G., W. Hemmert, et al. (1999). "Limiting dynamics of high-frequency electromechanical transduction of outer hair cells." Proc Natl Acad Sci U S A 96(8): 4420-5.

Geisler, C. D. (1986). "A model of the effect of outer hair cell motility on cochlear vibrations." Hear Res 24(2): 125-31.

41

Geisler, C. D. (1991). "A cochlear model using feedback from motile outer hair cells." Hear Res **54**(1): 105-17.

Geisler, C. D. (1993). "A realizable cochlear model using feedback from motile outer hair cells." Hear Res **68**(2): 253-62.

Geisler, C. D. and C. Sang (1995). "A cochlear model using feed-forward outer-hair-cell forces." Hear Res **86**(1-2): 132-46.

Hubbard, A. (1993). "A traveling-wave amplifier model of the cochlea." Science **259**(5091): 68-71.

Hubbard, A. E., D. C. Mountain, et al. (2003). Time-domain responses from a nonlinear sandwich model of the cochlea. Biophysics of the Cochlea: From Molecules to Models. A. W. Gummer. New Jersey, London, Singapore, Hong Kong., World Scientific: 351-358.

Hubbard, A. E., Z. Yang, et al. (2000). Multi-mode Cochlear models. Recent Developments in Auditory Mechanics. H. Wada. Singapore, New Jersey, London, Hong Kong, World Scientific: 167-173.

Hudspeth, A. (1997). "Mechanical amplification of stimuli by hair cells." Curr Opin Neurobiol **7**(4): 480-6.

Iwasa, K. H. and R. S. Chadwick (1992). "Elasticity and active force generation of cochlear outer hair cells." J Acoust Soc Am **92**(6): 3169-73.

Karavitaki, K. D. and D. C. Mountain (2007). "Evidence for oscillatory fluid flow in the tunnel of Corti." Biophys J.

Kemp, D. T. (1978). "Stimulated acoustic emissions from within the human auditory system." J Acoust Soc Am **64**(5): 1386-91.

Kiang, N. Y., M. B. Sachs, et al. (1967). "Shapes of tuning curves for single auditory-nerve fibers." J Acoust Soc Am **42**(6): 1341-2.

Lay, D. M. (1972). "The anatomy, physiology, functional significance and evolution of specialized hearing organs of gerbilline rodents." J Morphol **138**(1): 41-120.

Liberman, M. C., J. Gao, et al. (2002). "Prestin is required for electromotility of the outer hair cell and for the cochlear amplifier." Nature **419**(6904): 300-4.

Lu, T. K., S. Zhak, et al. (2006). "Fast cochlear amplification with slow outer hair cells." Hear Res 214(1-2): 45-67.

Mammano, F. and J. F. Ashmore (1993). "Reverse transduction measured in the isolated cochlea by laser Michelson interferometry." Nature 365(6449): 838-41.

Mountain, D. C. and A. E. Hubbard (1994). "A piezoelectric model of outer hair cell function." J Acoust Soc Am 95(1): 350-4.

Mountain, D. C., H. H. Nakajima, et al. (2000). Forward and Reverse Traveling Waves in the Gerbil Cochlea. Recent Developments in Auditory Mechanics. H. Wada. Singapore, New Jersey, London, Hong Kong, World Scientific: 102-108.

Muller, M. (1996). "The cochlear place-frequency map of the adult and developing Mongolian gerbil." Hear Res 94(1-2): 148-56.

Naidu, R. C. (2001). Mechanical properties of the organ of Corti and their significance in cochlea mechanics. Unpublished doctoral dissertation, Boston University.

Naidu, R. C. and D. C. Mountain (1998). "Measurements of the stiffness map challenge a basic tenet of cochlear theories." Hear Res 124(1-2): 124-31.

Naidu, R. C. and D. C. Mountain (2001). "Longitudinal coupling in the basilar membrane." J Assoc Res Otolaryngol 2(3): 257-67.

Neely, S. T. (1993). "A model of cochlear mechanics with outer hair cell motility." J Acoust Soc Am 94(1): 137-46.

Neely, S. T. and D. O. Kim (1983). "An active cochlear model showing sharp tuning and high sensitivity." Hear Res 9(2): 123-30.

Neely, S. T. and D. O. Kim (1986). "A model for active elements in cochlear biomechanics." J Acoust Soc Am 79(5): 1472-80.

Nowotny, M. and A. W. Gummer (2006). "Nanomechanics of the subtectorial space caused by electromechanics of cochlear outer hair cells." Proc Natl Acad Sci U S A 103(7): 2120-5.

Olson, E. S. (1998). "Observing middle and inner ear mechanics with novel intracochlear pressure sensors." J Acoust Soc Am 103(6): 3445-63.

43

Olson, E. S. (1999). "Direct measurement of intra-cochlear pressure waves." Nature **402**(6761): 526-9.

Olson, E. S. and D. C. Mountain (1991). "In vivo measurement of basilar membrane stiffness." J Acoust Soc Am **89**(3): 1262-75.

Peterson, L. C. and B. P. Bogert (1950). "A Dynamical Theory of Cochlea." J Acoust Soc Am **22**(3): 369-381.

Plassmann, W., W. Peetz, et al. (1987). "The cochlea in gerbilline rodents." Brain Behav Evol **30**(1-2): 82-101.

Ren, T. (2002). "Longitudinal pattern of basilar membrane vibration in the sensitive cochlea." Proc Natl Acad Sci U S A **99**(26): 17101-6.

Ren, T. and A. L. Nuttall (2001). "Basilar membrane vibration in the basal turn of the sensitive gerbil cochlea." Hear Res **151**(1-2): 48-60.

Rhode, W. S. (1971). "Observations of the vibration of the basilar membrane in squirrel monkeys using the Mossbauer technique." J Acoust Soc Am **49**(4): Suppl 2:1218+.

von Békésy, G. (1960). Experiments in hearing. New York,, McGraw-Hill.

Zwislocki, J. J. (1950). "Theory of the Acoustical Action of the Cochlea." J Acoust Soc Am **22**(6): 778-784.

Chapter 2

A Physiologically Based Nonlinear Multicompartment Cochlear Model with a Piezoelectric OHC Feedback System

2.1 Introduction

More than 50 years ago, a one dimensional (1-D) cochlear model was proposed to describe traveling wave propagation inside the cochlea (Peterson and Bogert 1950; Zwislocki 1950). In the classical 1-D cochlear model, which is basically a non-uniform, passive transmission line (Viergever and de Boer 1987), the cochlear partition is driven by pressure difference between the scala vestibuli (SV) and scala tympani (ST). After nonlinear cochlear amplification (CA) was observed (Rhode 1971), several models were introduced to represent the active processing in the cochlea (Hubbard and Geisler 1972; de Boer 1983; Neely and Kim 1983). These models could achieve some sort of "active" response, but lacked physiological explanation for the source of the active force. In fact, at the time, it was unclear whether the physically observed phenomenon was due to an active force or to a "nonlinear damping" mechanism involved. Since outer hair cell (OHC) somatic electromotility was discovered (Brownell et al. 1985), it is largely accepted that OHC voltage-dependent length changes observed *in vitro* form the basis for the CA *in vivo*, although there is evidence suggesting that hair bundle motility may also contribute to the CA (Hudspeth 1997; Martin and Hudspeth 1999; Chan and Hudspeth 2005).

45

The discovery of OHC electromotility gave rise to a new era of active research in cochlear modeling. OHC electromotility has been utilized by many models to achieve CA (Geisler 1986; Neely and Kim 1986; Zwicker 1986; Kolston et al. 1990; Geisler 1991; Geisler 1993; Hubbard 1993; Kanis and de Boer 1993; Neely 1993; Geisler and Sang 1995; Chadwick 1998; Spector 1999; Cohen and Furst 2004). A downside for these models is that they all lacked a realistic OHC electroanatomical circuit, which describes the mechanoelectrical and electromechanical processes in detail. Without a proper OHC circuit model, it is not possible from an electroanatomical standpoint to realistically model hair bundle motion and active force generation. But, modelers can side-step the problematic details by way of a simplifying assumption relating, for example, reticular lamina (RL) motion to OHC force generation.

A frequently-mentioned drawback of the conventional OHC circuit model is that, when the frequency is high, the voltage across the OHC's basal-lateral wall drops due to the low-pass filtering of the basal-lateral wall capacitance. Hence, the CA is reduced severely. Because experimental data showed that the OHC electromotility works well in the high frequency range (Frank et al. 1999; Grosh et al. 2004; Scherer and Gummer 2004), there must exist some mechanism to overcome the OHC low-pass filtering problem. Many theories have been developed to model the potential mechanisms (Dallos and Evans 1995; Spector

46

et al. 2003; Liao et al. 2005; Liao et al. 2005; Spector et al. 2005; Lu et al. 2006). Among them, the piezoelectric-like OHC has been an area of great interest for more than ten years (Mountain and Hubbard 1994; Spector et al. 2003; Rabbitt et al. 2005; Lim and Li 2006; Spector et al. 2006). Piezoelectric effects imply a bi-directional coupling between the mechanical and electrical system (Mountain and Hubbard 1994). The length of the OHC changes when the transmembrane voltage changes. This somatic change of OHC, in turn, will alter the surface area of the cell body and cause the change of electrical impedance of the cell itself. This local feedback mechanism works like a piezoelectric system (Mountain and Hubbard 1994; Tolomeo and Steele 1995; Iwasa 2001; Dong et al. 2002). Current research suggests that this piezoelectric feedback system may at least partially cancel the voltage drop across the cell wall and sustain the CA in the high frequency range (Weitzel et al. 2003; Spector and Jean 2004).

Another research area inspired by the discovery of OHC motility is multimode cochlear modeling. The OHC contractions would be expected to pull the RL and basilar membrane (BM) together. Therefore, The BM and RL may move separately. This concept suggests that there may be more than one propagation mode inside the cochlea. Regarding this, de Boer presented a sandwich model that allowed the organ of Corti (OC) to transfer energy along the cochlea (de Boer 1990; de Boer 1990). Markin and Hudspth (1995) published a model with

47

BM and RL vibrating in different modes. In their model BM and RL are coupled by an intermediate spring (the OHC). Chadwick et al and Cai et al also presented a series of multi-compartment models, which included a more realistic embodiment of OHC force production and tectorial membrane motion (Chadwick et al. 1996; Chadwick 1998; Cai et al. 2004). These models can produce BM responses comparable to experimental data.

In a multicompartment model, the OHC voltage-dependent length change pushes the RL and BM away or pulls them together. This would squeeze the fluid inside the OC, produce flow in the longitudinal direction. Based on this hypothesis, Hubbard et al (Hubbard et al. 2000; Hubbard et al. 2003) developed a multi-compartment model simulation that allowed traveling wave propagation inside the OC. The model included OHC active force generation that was directly proportional to the displacement of RL. The model, with its parameters based on physiological cochlear data, can replicate the BM response well. The model predicts that the pressure inside the OC and the force generated by OHC are the driving forces of CA in the peak region. This hypothesis is supported by the recent finding of the presence of the fluid motion inside the tunnel of Corti (ToC) when the cochlea is stimulated (Karavitaki and Mountain 2007).

48

In this paper we present a new, nonlinear, multicompartment model with a piezoelectric OHC feedback system. Unlike our previous models, this model incorporates an OHC electroanatomical circuit and a piezoelectric feedback from the OHC circuit to the hydromechanical system. By adopting an OHC circuit model and piezoelectric feedback system, this model enables us to explore the cochlear mechanical responses and the electrical potential changes in the OC simultaneously. There are two feedback loops in this model. One loop is BM and RL motion causing OHC depolarization and voltage-dependent length change, which generates active force that enhances BM and RL motion. The other loop is a local piezoelectric feedback system. In this local feedback loop, OHC electrical impedance couples with the mechanical load of the OHC directly. Simulation results show that this multi-loop model can largely overcome the OHC low-pass filtering problem, and can replicate cochlear responses at both low and high frequencies.

In the following parts of the paper, we will discuss the structure of the model and how the parameters in the model were determined. We will also discuss how to perform the simulations. The simulation results from the model will be compared with the cochlear microphonic input/output response curves for our own laboratory, BM velocity ratio data (Ren and Nuttall 2001) and longitudinal patterns of BM velocity (Ren 2002).

49

2.2 Methods

In this section, we explain the structure of the model and how to determine the parameters in the model. Then we discuss how to set up the simulations and the key issues in the simulations. In this work, the gerbil was chosen as the target animal. Therefore gerbil's physiological data were used to determine the parameters in the model.

2.2.1 Structure of the Model

In our model the entire cochlea is divided into 400 discrete sections in the longitudinal direction from the base to the apex. The fluid in the model is considered as incompressible. The walls of the tubes are considered rigid. Figure 2-1 shows the schematic structure of one section of the model.
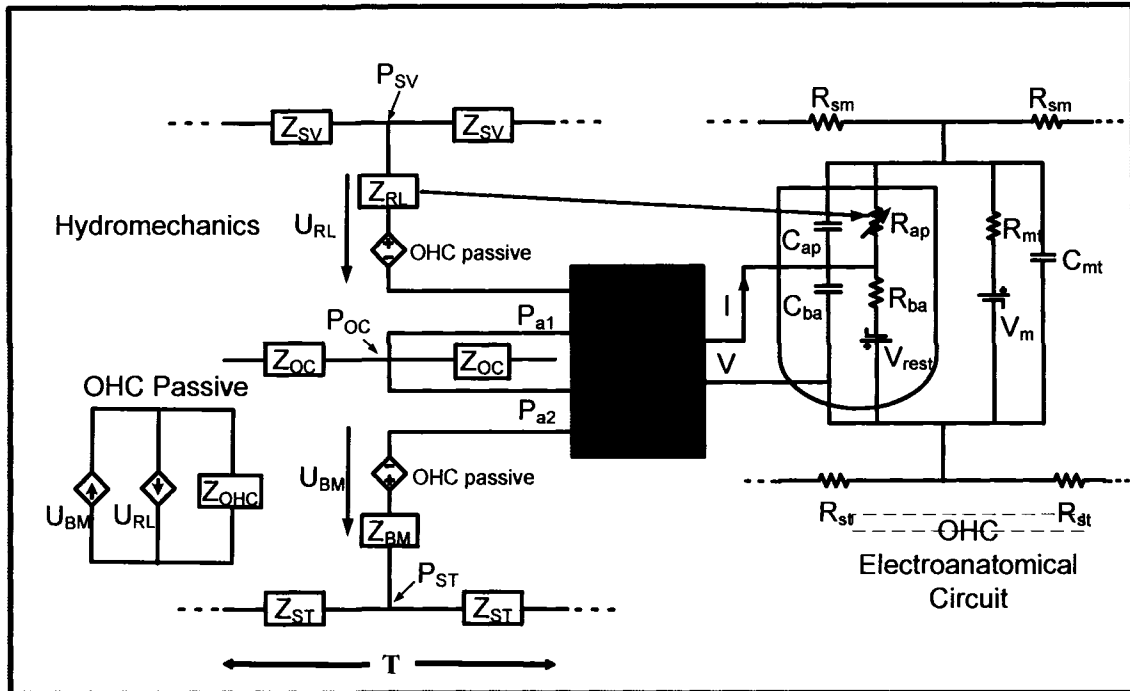
Figure 2-1 The schematic drawing of one section of the model. The left portion is the hydromechanical part of the model. The right portion is the OHC anatomical circuit. A bi-directional piezoelectric feedback system connects the mechanical part and the electrical part. The adjacent sections of OHC model are coupled by resistors in both SM and ST.

2.2.1.1 Hydromechanical Portion of the Model

The left part of Figure 2-1 is the hydromechanical model as described partially in previous publications (Hubbard et al. 2000; Hubbard et al. 2003; Lu et al. Submitted). The formulation of this model includes SV, ST and OC fluid compartments. The BM and RL impedances separate these compartments

vertically. The three transmission lines (SV, ST and OC fluid) in the hydrodynamic model are governed by the following equations respectively:

$$\frac{d^2 P_{SV}}{dx^2} = k_{LV}\,\frac{U_{RL}}{dx}$$

$$\frac{d^2 P_{ST}}{dx^2} = -k_{LT}\,\frac{U_{BM}}{dx} \qquad (1)$$

$$\frac{d^2 P_{OC}}{dx^2} = k_{LOC}\left(\frac{U_{RL}}{dx} - \frac{U_{BM}}{dx}\right)$$

Where P_{SV}, P_{ST} and P_{OC} are the pressures inside SV, ST and OC; K_{LV}, K_{LT} and K_{LOC} are per unit length impedance in SV, ST and OC respectively. U_{RL} and U_{BM} are the volume velocity of the RL and BM. The OHC force generators represent both the passive and the active forces generated by the OHCs. The OHC passive force is the result of differential velocities of the RL and BM stretching and compressing the OHC. The force is computed using the helper circuit called "OHC Passive". The active force is proportional to the output of the OHC piezoelectric feedback system. The OHC forces couple back to the fluid channels via Z_{RL} and Z_{BM}.

52

2.2.1.2 Hydromechanical Parameters Estimation

The dimensional parameters used in this model, including the BM width and the cross-sectional areas of SV, ST, and scala media (SM), were calculated from measured data (Plassmann et al. 1987). The ToC dimensional data (Edge et al. 1998) were also used to calculate the parameters of the hydromechanical model. SV and SM were considered together as one tube in the model. Thus, the cross-sectional area of the upper fluid channel in this model was actually the summation of measured SV and SM areas. BM volume compliance data were calculated from point stiffness measurements under the assumption that the BM consists of a series of beams that were clamped at each end (Olson and Mountain 1991; Naidu and Mountain 1998).

The acoustic mass (L) and the viscosity (R) of one section in each tube were calculated by:

$$L = T\frac{\rho}{A} \tag{2}$$

$$R = \frac{8\pi\mu T}{A^2} \tag{3}$$

Where T is the length of one section of the tube, A is the cross- section area of the tube, ρ= 1 g/cm^3 is the density of the fluid and μ=0.02 g/ (cm*s) is the viscosity factor.

The CF at each location along the BM was calculated from the Greenwood function (Greenwood 1990):

$$CF = A \left(10^{\,ax/L} - K\right) \qquad\qquad (4)$$

where A=398, a=2.2 and K=0.631 (Muller 1996). x is the distance from the base. L is the length of the cochlear. For gerbil, L= 13 mm was used in our model.

The RL parameters were calculated based on scaling the BM parameters. The details have been reported in our previous publications (Hubbard et al. 2000; Hubbard et al. 2003; Lu et al. Submitted).

2.2.1.3 OHC Electroanatomical Circuit Model

The right part of Figure 2-1 depicts one section of the OHC electro-anatomical model. The adjacent sections are coupled by resistors in both SM and ST along the length of the cochlea. Since the model has 400 sections and there are about 4000 OHCs in the gerbil's cochlea, each section has roughly 10 OHCs. We scaled these 10 OHCs into one lumped OHC, as shown in the Figure 2-1. The resistors in the lumped OHC are one tenth the corresponding resistors in a single OHC. The capacitors in the lumped OHC are ten times larger than the corresponding capacitors in a single OHC. Thus the RC constants remain the same after the scaling. The parameters in the OHC electroanatomical model were calculated based on previous publications with minor adjustments to match experimental cochlear microphonic (CM) data from our own laboratory.

The resting potential (V_{rest}) of the OHC was set to be -70 mV (Dallos 1986). The electrical potential in SM was determined by the stria vascularis potential data measured in our laboratory. In this model we used V_m=110 mV.

In the apical part of the OHC circuit, the tension-gated conductance changes nonlinearly in response to the stereocilia motion, which is assumed to be proportional to RL motion. When the tension gated channel is opened, current goes into the OHC and depolarizes it. In turn, the potential in the basal-lateral

wall of the OHC changes. This potential change causes OHC length change. Consequently, the mechanical loading of the OHC translates bi-directionally with the electrical impedance of the OHC.

The asymmetrical nonlinearity of tension-gated conductance is usually described by a Boltzmann function (Holton and Hudspeth 1986). In our model an asymmetrical nonlinear Boltzmann curve was used:

$$g_{ap} = \frac{g_{max}}{1+e^{-\delta v/w}(1+e^{-5\delta v/w})} + g_0 \qquad (5)$$

Where δv is the motion of stereocilia, w is the saturation constant, g_0 is the constant representing the minimum conductance of the channel, and g_{max} is the maximum conductance of the stereocilia tension gated channel ($g_0 \ll g_{max}$).

The single OHC input resistance can be calculated as $R_{ap} \| R_{ba}$. In this model we used 12 MΩ (Dallos 1985) as the OHC input resistance. Because R_{ap} is much larger than R_{ba} and $R_{ap} \| R_{ba}$ equal to 12 MΩ, R_{ba} is approximately 12 MΩ for one OHC. Since there are 10 OHCs in one section, the final value of R_{ba} we used in this model is 1.2 MΩ. Because the peak-to-peak membrane potential is about 20 mV (Cheatham and Dallos 1994), the maximum current can be calculated as i =

(20 mV/12 MΩ)=1.67 nA. The value of maximum apical conductance of one OHC can be calculated as:

$$g_{max} = \frac{i}{(V_m - V_{rest})} \qquad (6)$$

From equation 6 we calculated the maximum conductance in the apical part of the OHC as being about 11 nS. So the minimum value of R_{ap} for a single OHC is about 91 MΩ. This is consistent with $R_{ap} \gg R_{ba}$. For a section with 10 OHCs, we use value g_{max} =110 nS.

The total capacitance of a single OHC (C_{ohc}) is the combination of apical capacitance (C_{ap}) and basal capacitance (C_{ba}). The value C_{ohc} was set as 23 pF (Santos-Sacchi 1989). The size of OHC changes from base to apex and the ratio of C_{ap}/C_{ba} varies from 0.156 (turn 1) to 0.064 (turn 3) (Dallos 1983). To simplify the model, we used 0.1 as C_{ap}/C_{ba}, which is the average value of measured C_{ap}/C_{ba} along the cochlea. Since the total capacitance is 23 pF and the C_{ap}/C_{ba} is approximate 0.1, C_{ap} and C_{ba} in a single OHC can be calculated as C_{ap}=2.1 pF and C_{ba}=20.9 pF. For 10 OHCs, we use 21 pF for the apical capacitance and 209 pF for the basal capacitance.

The electrical behavior of the SM is determined by the resistance of the SM fluid

57

(R_{sm}), the resistance between SM and ST (R_{mt}) and the capacitance between SM and ST (C_{mt}). R_{sm} can be calculated from SM fluid resistivity R_f (Salt and Konishi 1986), the cross-sectional area (A_{sm}) and the length of every section of the SM (T). Here in this model, we chose R_f= 46 Ω*cm. R_{sm} can be calculated as:

$$R_{sm} = R_f \ \frac{T}{A_{sm}} \qquad (7)$$

R_{mt} is estimated from the space constant (λ_{sm}) of SM. The space constant is the distance in which voltage drops to 1/e of the initial value. Experiments indicated that this space constant of SM was about 0.11 cm (Misrahy et al. 1958). R_{mt} can be determined by:

$$R_{mt} = R_{sm} \ \left(\frac{\lambda_{sm}}{T} \right)^2 \qquad (8)$$

C_{mt} is determined by the time constant (t_{am}) of SM, t_{am} is the time in which the voltage rises to (1-1/e) of its steady state value when the input is a step current, and C_{mt} can be calculated by t_{sm}/R_{mt}.

Name	Meaning	Value	Unit
V_{rest}	OHC Resting potential	-70	mV
Vm	Stria vascularis battery	110	mV
g_{max}	Max conductance of OHC tension gated channel	110	nS
g_0	Apical leakage conductance	11	nS
w	Saturation constant in OHC tension gated channel	70	um/s
R_{ap}	OHC Apical resistance	$1/g_{ap}$	Ω
C_{ap}	OHC Apical capacitance	21	pF
R_{ba}	OHC Basal resistance	1.2e6	Ω
C_{ba}	OHC Basal capacitance	209	pF
R_{sm}	Fluid resistance in SM	$R_{sm} = R_f \dfrac{T}{A_{sm}}$	Ω
C_{mt}	Capacitance between SM and ST	383.3	pF
R_{mt}	Source resistance of stria vascularis battery	2e5	Ω

Table 2- 1 Parameter used in the OHC electroanatomical circuit.

2.2.2 Piezoelectric OHC Feedback System

Between the hydromechanical part and the OHC circuit is the piezoelectric feedback system. Directed towards the hydromechanical part of the model, the output of the feedback system functions as a force generator. To the OHC electrical model, the transformer reflects the mechanical load of the hydromechanical system as an electrical load. Here we assume there is no energy loss in the transaction, i.e., the piezoelectric feedback system works like an ideal transformer. Therefore, we can describe the function of this transformer as:

$$V*I = P_{a1}*U_{RL} + P_{a2}*U_{BM} \tag{9}$$

$$P_{a1} = - P_{a2} \tag{10}$$

where V and I are the voltage and current going into the transformer at the OHC side, P_{a1} and P_{a2} are the active pressures that are commonly referred to as active forces, assuming the pressure is applied to a particular area of the model. U_{RL} and U_{BM} are the volume velocity of RL and BM. Although energy can flow in either direction of the transformer, the piezoelectric feedback system (the transformer) itself does not produce power. The gain of the piezoelectric feedback system is controlled by the transformer ratio N. Increasing N means increasing the pressure/voltage gain of the feedback system. In our model N is set to be about 30000 in the basal part of the cochlea when the cochlea is active. The force generated is about 2nN per OHC per mV change in the OHC basal

lateral transmembrane potential. N is larger in the apical part of the cochlea than it is in the basal part, to count in the OHC size influence.

2.2.3 Simulation Setup and Procedure

In this work we used an analogous electrical circuit to mimic the hydromechanical system. According to the acoustic- electrical analogy, the inductors, capacitors and resistors represent the acoustic mass, acoustic compliance and acoustic viscosity. Based on these definitions, the fluid inside the channels is modeled by a series of inductors, which represent the inertia of the fluid. Both the RL and the BM are modeled as series circuits comprised of an inductor, a capacitor and a resistor. The pressures generated by the OHC are modeled by dependent voltages sources. The currents represent volume velocities. P_{SV}, P_{ST} and P_{OC} are the pressures in SV, ST and OC. We use Tspice^{TM} (Tanner EDA) to run the simulations. All the simulations were done in the time domain because the model is nonlinear and the signal levels are not small. The inputs are sinusoidal pressures signals at different intensities and different frequencies. The stapes velocity and BM velocity at certain locations are recorded to demonstrate the BM/stapes velocity ratio. The pressures in the hydromechanical part were also recorded. In the OHC circuit, the voltage differences between the SM and the ST were recorded to calculate the CM produced by the model.

2.3 Results

2.3.1 Cochlear Microphonic Data Comparison
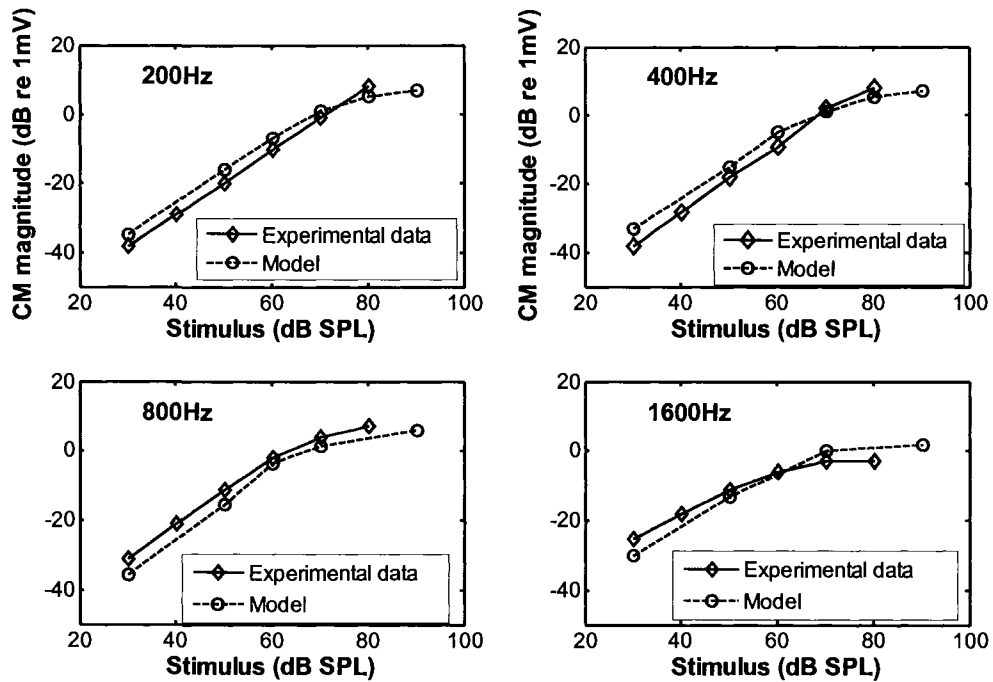
Figure 2- 2   Comparison of cochlear microphonic results. The solid lines are experimental data from gerbil from our laboratory. They are recorded from a location where the CF is about 2.5 kHz. The input frequencies are: 200 Hz, 400 Hz, 800 Hz and 1600 Hz. The dashed lines are the simulation results of our model at the same cochlear location.

CM is the AC potential generated by the hair cells in response to acoustic stimulation. It is an important indicator of OHC function. It can be used to

characterize the mechanoelectrical transduction process in the OHC. We use CM

data to calibrate the OHC circuit in our model. Figure 2-2 compares CM

input/output responses of the model with experimental data at low frequencies.

The experimental CM data were recorded from a second-turn location in the

gerbil cochlea where the CF is around 2.5 kHz (Nakajima et al. 1994). The model

results came from same place (CF = 2.5 kHz). Because the CM potentials are

nonlinear, we compared the fundamentals of Fourier components of the CM

response waveforms. The qualitative comparison of the two sets of data shows a

good fit. In all four panels, the input/output responses for both the model and the

experimental data are nearly linear when the input level is below 60 dB SPL.

Both the model and experimental data enter saturation at about 60 dB SPL.

2.3.2 BM Velocity Ratio Comparisons
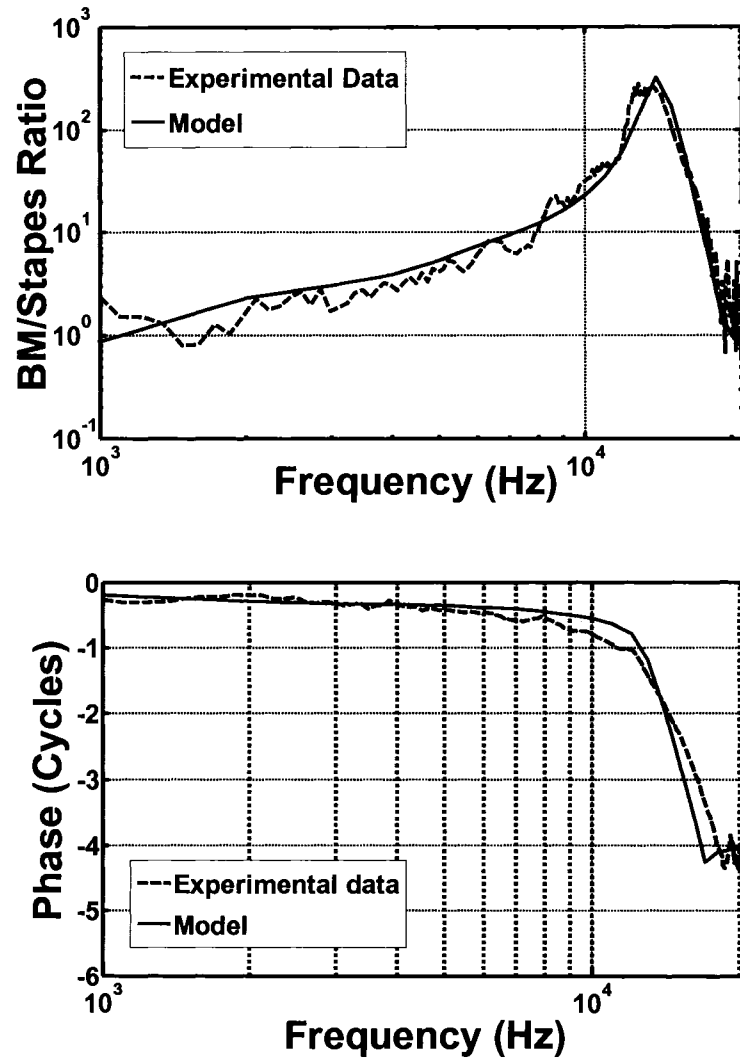
Figure 2- 3   BM velocity ratio (BM/stapes) comparison. The upper panel is magnitude. The lower panel is phase. The dashed line is experimental data for gerbil. It is recorded from a location where CF is about 14 kHz. The solid line is the simulation result of our mode.

Figure 2-3 shows the BM velocity ratio (BM velocity versus velocity at the stapes) comparison with experimental data (Ren and Nuttall 2001), which were obtained from a sensitive gerbil cochlea. The data were recorded at the location where CF is about 14 kHz. The frequency range is from 1 kHz to 21 kHz. The figure shows the BM velocity ratio when the input was 40 dB SPL in the ear canal. The magnitude of BM velocity ratio (upper panel of Figure 2-3) from the model agrees well with the experimental results over the entire range of comparison. The lower panel of Figure 2-3 compares the phase angle of the BM velocity ratio of the model with the phase angle of the experimental data. The model phase response is similar to the experimental data but with a slightly steeper phase slope near the CF.

2.3.3 BM Longitudinal Vibration Pattern
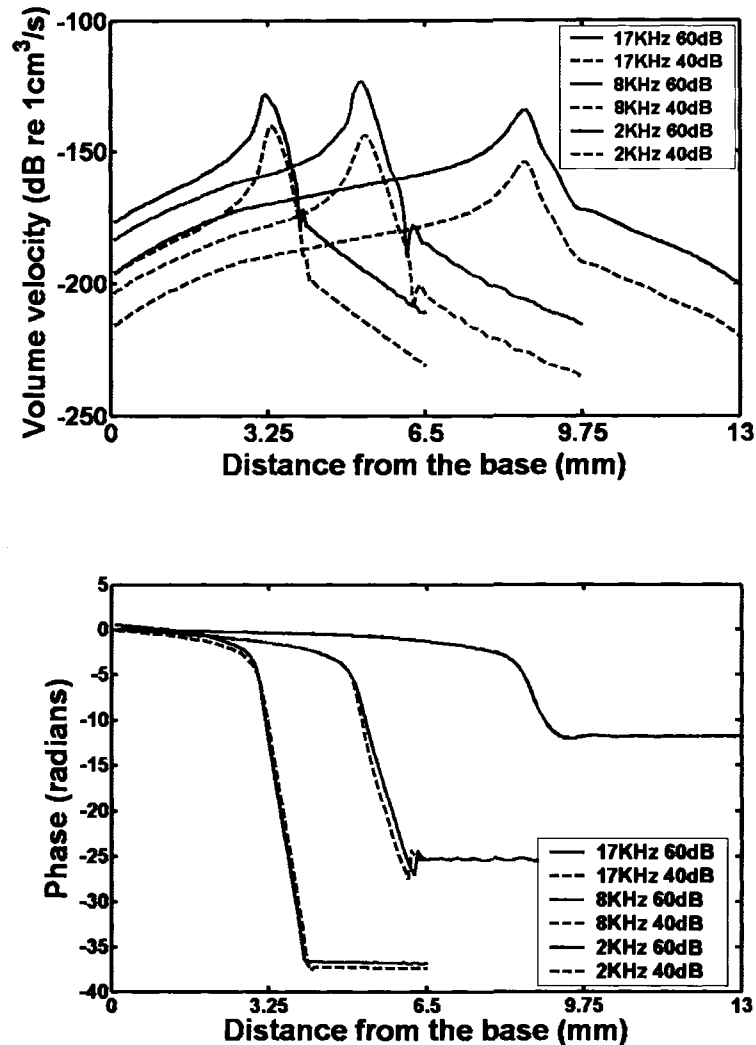
Figure 2- 4   Longitudinal BM vibration pattern at different places. The upper panel is magnitude. The lower panel is phase. The blue lines are generated by 17 kHz tone input. The red lines are generated by 8 kHz tone input. The green lines are generated by 2 kHz tone. The dashed lines are results from 40 dB SPL input. The solid lines are results from 60 dB SPL input.

Figure 2-4 shows the longitudinal profile of BM volume velocity at different single

tone inputs. The peaks are at 3.25 mm (17 kHz), 5.3 mm (8 kHz) and 8.5 mm (2

kHz). From the phase panel we can find that, the high frequency tone generate

largest phase lag. The phase total phase lag for 17 kHz tone is about 6 cycles,

while the total lag for 2 kHz tone is only 2 cycles.

2.3.4 Comparisons of the Longitudinal Pattern of BM Velocity
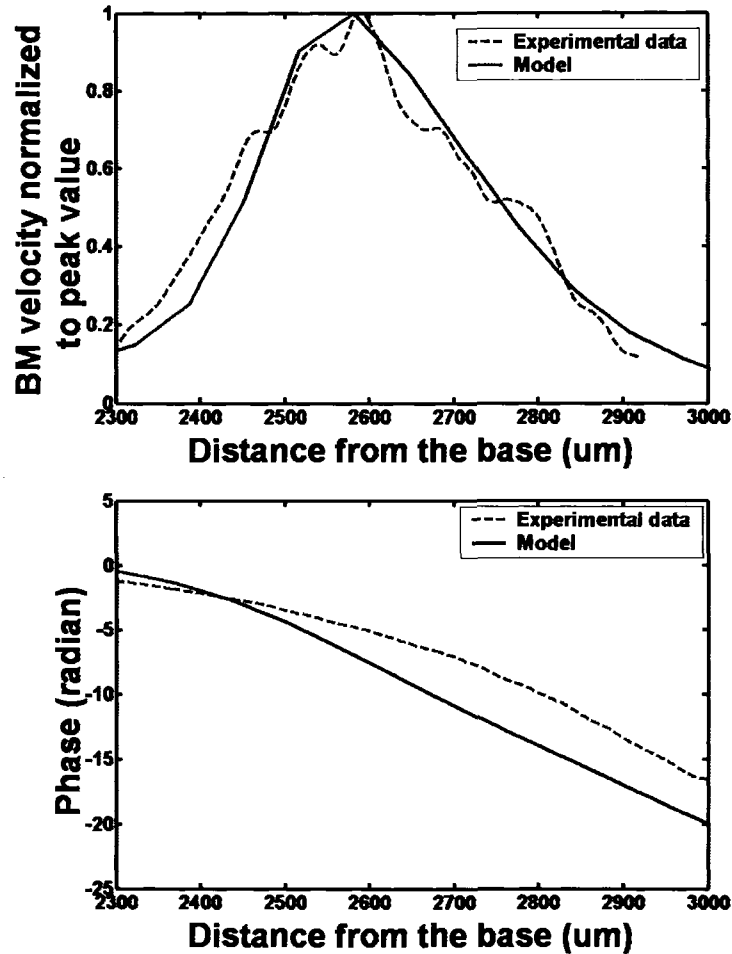
Figure 2- 5 Longitudinal BM velocity profiles. The left panel is magnitude. The right panel is phase. The phases are referred to BM vibration at the basal end of the measured region at 90 dB SPL stimulus level. The solid line is experimental data from the gerbil. It is recorded from a location where CF is about 16 kHz. The dashed line is the simulation result from our model.

Figure 2-5 compares the longitudinal velocity pattern of the model with experimental data obtained from the gerbil in a region where the CF is about 16 kHz (Ren 2002). The input stimulus is 50 dB SPL in ear canal. The recording range is from 2.3 mm to 2.9 mm. The left panel shows the normalized BM velocity magnitude. The magnitude data is normalized to the peak value. Therefore the maximum value for the curves is always one. For the longitudinal study, we only care about the velocity pattern along the cochlea, because the absolute velocity value varies from the experiments due to animal difference, preparation difference and calibration. The right panel is the comparison of the phase data. The phase angles are referred to BM vibration in the basal end of the measured region at 90 dB SPL. Both the model and experimental data show that there is about three cycles of phase delay in the peak region.

2.3.5 Comparison of the OHC Output with Piezoelectrical Feedback to the Output without Piezoelectrical Feedback
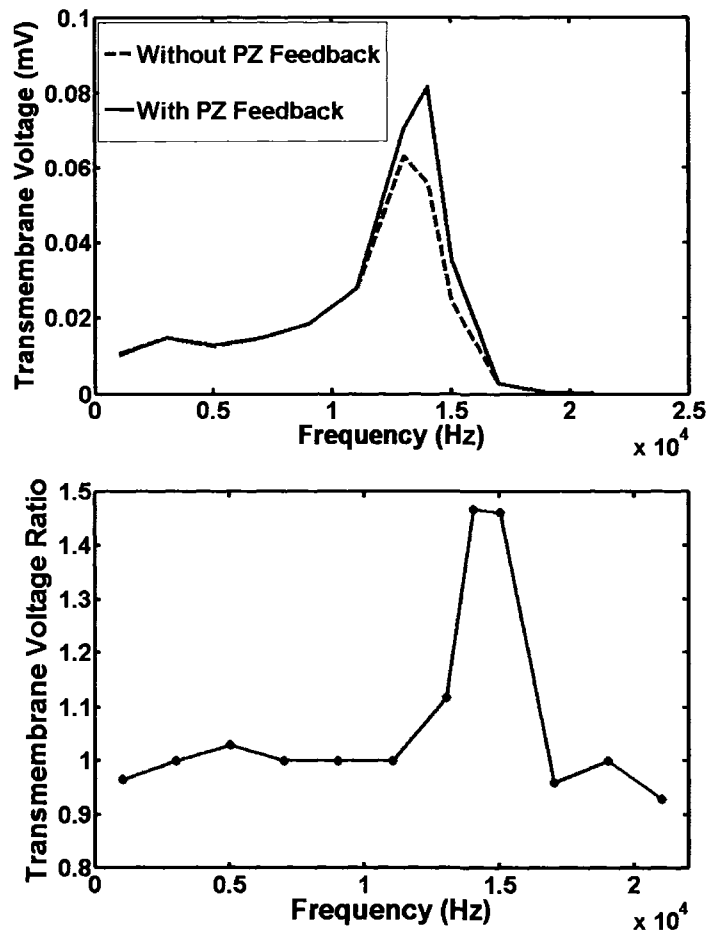
Figure 2- 6 Transmembrane voltages in the models with and without piezoelectric feedback. The input stimulus is a 45 dB SPL sinusoid at the ear canal. The frequencies sweep from 1 kHz to 21 kHz. The upper panel is absolute results. The lower panel is the ratio.

The upper panel of Figure 2-6 compares the OHC transmembrane voltages in the model with and without piezoelectric feedback. The lower panel is the ratio of transmembrane voltage of the models with piezoelectric feedback, to the model without piezoelectric feedback. The data was from a place whose CF is about 14 kHz. In the peak region, the model with piezoelectric feedback has about 50% voltage increase. Therefore, the model with piezoelectrical feedback generates more active force compared to the model without piezoelectrical feedback. Other places along the cochlea also show a similar pattern in our model simulation. Table 2-2 shows the value of transmembrane voltage ratio (with piezoelectric feedback versus without piezoelectric feedback) at different locations. The input stimuli are from 20 kHz to 500 Hz. The transmembrane voltages are measured at the CF places relative to the input tones.

Position (mm)	2.925	3.80	5.2	8.125	11.375
CF (Hz)	20k	14k	8k	2.4k	0.500
Vmpz/Vm	1.34	1.46	1.19	1.01	1.04

Table 2- 2 Transmembrane voltage changes in different locations along the cochlea. Position is the distance from base. Vmpz is the OHC transmembrane voltage from a model with piezoelectric feedback. Vm is from the exact same model but without piezoelectric feedback.

71

2.3.6 RL and BM Time Domain Impulse Response
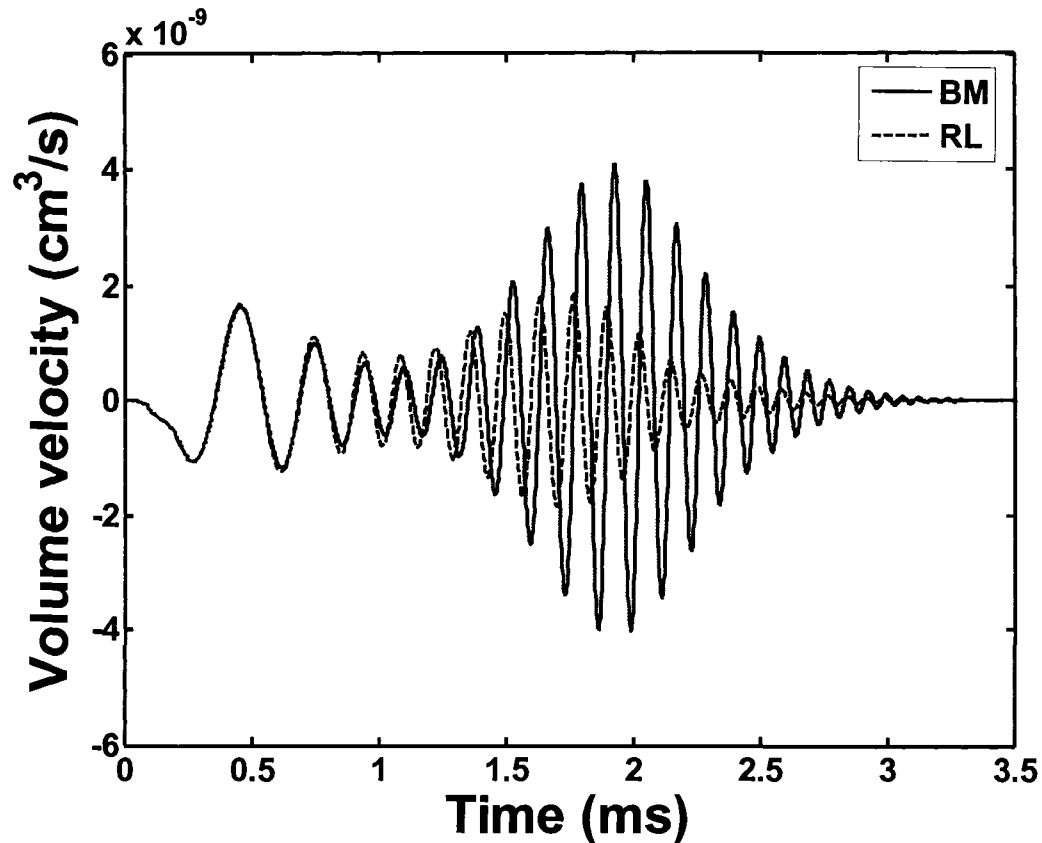
Figure 2- 7 Time domain impulse response of the RL and BM.

Figure 2-7 shows the time domain impulse response of the RL and BM in a place located 3.77mm from the base. The results show that the lower frequency components reach the recording place faster than the higher frequency components. The RL reached its peak at about 1.6 ms, earlier than the BM (1.9 ms), because the RL's CF at this location is set to be about half of that of the BM. The vibrations of the RL and BM are in-phase for frequencies not close to their CFs. They are out-of-phase for frequencies close to their CFs.

2.3.7 Active and Passive Time Domain Impulse Response
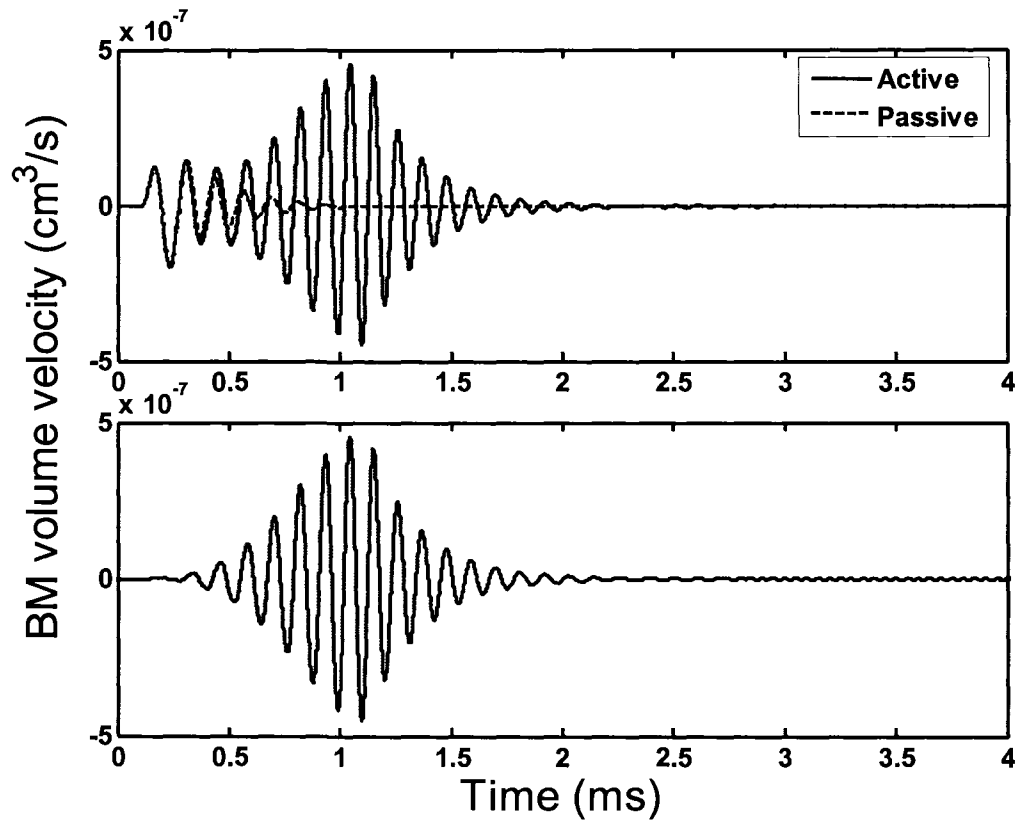
Figure 2- 8 Time domain impulse response of active and passive model.

Figure 2-8 compares the active and passive impulse responses. It is recorded at the place 4.9 mm from the base. The upper panel is the passive and the active response. The blue curve is the active response. The read curve is the passive response. The lower panel is the results of subtracting the passive response from the active response. The results show that the passive response is smaller than the active response. It reaches its peak earlier than the active response. The first

part of the active response (before 0.3 ms) is exactly the same as the passive

response. We think the curve in the lower panel shows the contribution of the

OHC active force.

2.4. Discussion

2.4.1 Comparison of This Model with Its Previous Versions and Another Piezoelectrical Cochlear Model

Previous hydromechanical multicompartment models (Hubbard et al. 2000; Hubbard et al. 2003; Lu et al. Submitted) of the cochlea with OHC force generation were able to mimic the physiologically measured responses of the BM, but lacked a realistic OHC circuit model to represent mechanoelectrical transduction and electromechanical transduction. An improved model that included nonlinear OHC electroanatomical model was able to mimic CM data at low frequencies, but could not achieve high frequency CA due to the OHC low pass filtering problem (Lu et al. 2006). By adopting piezoelectric OHC feedback and using RL velocity to drive the tension gated channel of OHC, the model presented here has enough gain at high frequencies, and can replicate the CM data at low frequencies, and the BM response data at both low and high frequencies.

This model enables us to explore the hydromechanical responses of the cochlea and the electrical potential changes in the OHC simultaneously. Ramamoorthy et al also present a model with similar solution (Ramamoorthy et al. 2007). Unlike the model presented in this paper, their mechano-electro-acoustical model does not include the fluid flow inside the OC. The model includes a linear OHC

electroanatomical model with longitudinal electrical coupling in SV, SM and ST. The mechanical part and the electrical part were coupled via a piezoelectric model of OHC electromotility. The model does not include a stria vascularis battery. It also does not include the SM to ST resistor and capacitor, which in our model is principally responsible for OHC transmembrane voltage drop in the high frequency range.

2.4.2 Velocity Drives the Tension-gated Channels in the Hair Bundle

The active force generated by the OHC plays a key role in CA and it is one of the critical components that we explored. To achieve cycle-by-cycle amplification at high frequencies, the active force must have the correct magnitude as well as phase. If the phase is not correct, the active force will not inject power into the hydromechanical system (Markin and Hudspeth 1995).

One of our previous models with RL-stereocilia displacement driving the OHC tension-gated channel could not produce sufficient CA to match the experimental data, due to incorrect phase delay between the motion sensing and the force generation. When we added the piezoelectric component to that model, increasing transducer sensitivity, similarly, did not help because the phase angle of the somatic force was still wrong. The problem is that the OHC membrane

76

voltage at the high frequencies introduces approximately 90 degrees extra phase shift. We knew from the earliest model (Hubbard et al. 2000) that had no electroanatomical circuit that the OHC active force proportional to the RL displacement (OHC active force is in phase with the RL displacement) produced good fit to the experimental data.

Existing experimental results suggest that the mechanoelectrical channel is fast-adaptive (Ricci et al. 2000; Kennedy et al. 2003; Strassmaier and Gillespie 2003). This fast adaptive channel may be approximately described as being related to the derivative of displacement, which is velocity. So in this work, we used RL velocity to drive the conductance change of the OHC tension gated channel, instead of using RL displacement. Compared with the displacement drive, this fast-adaptive velocity drive has a 90 degrees phase lead. The system performed well using velocity drive. It can match the experimental data, and remained stable even for a very high gain, higher in fact than needed to match the BM/stapes velocity ratio data we used in Figure 2-3.

The results from our model suggest that the stereocilia fast adaptation may play an important role in OHC-mediated cochlear active amplification. Current research shows that the tension gated OHC current exhibits a fast adaptation in response to stereocilia motion and this fast adaptation causes a 90-degree

phase leading (Rabbitt et al. 2005). Such an adaptation process, at least for inward current, resembles a high pass filter or a derivative of the stereocilia displacement. Since velocity is the derivative of the displacement, fast adaptation may underlie the reason that, velocity driven apical conductance, rather than displacement, works well in our model.

The results from our model suggest that both hair bundle fast adaptation and somatic motility are essential to the active response of the cochlea. The hair bundle fast adaptation moderates the phase between RL-stereocilia motion and active force generated by the OHC (mechno-electro transduction), while somatic motility decides the magnitude of the active force (reverse transduction).

2.4.3 Piezoelectric OHC and Low-pass Filtering of Basal-lateral Wall Capacitance

In the traditional OHC model (refer to the left part of the Figure 2-1), when the frequency is high, more current goes from SM through C_{mt} to the ST due to the low-pass filtering. Therefore, less current goes into the OHC from the stria vascularis battery. Dallos has proposed that currents from adjacent regions of the cochlea add to boost OHC current in the peak region, thereby increasing OHC receptor potential. For this to happen in the model, we would note the increased

current flow through the longitudinal scala media resistor (R_{sm}) near the peak region. We checked the current through the R_{sm} in every section in the model, and did not observe the current increasing in the peak region. Current from the neighbor cochlear regions does not compensate the OHC transmembrane voltage drop in the peak region.

The OHC circuit is somewhat like a voltage divider between the apical part and the basal part of the OHC. In high frequency range, the impedances of capacitors are small. So the ratio of this divider is determined by the ratio of C_{ap} and C_{ba}. To the OHC circuit, the piezoelectric feedback system is also an impedance, which reflects the load of the hydromechanical system. This impedance will change the divider ratio of the OHC, and hence change the transmembrane voltage. After introducing the piezoelectrical feedback, we found the OHC transmembrane voltages increase up to 46% in the high frequency range, while they do not change significantly in the low frequency range. This fits with the concept that OHCs do not need help at low frequency to overcome the low-pass shunt effect. The transmembrane voltage increase caused by piezoelectric feedback system can at least partially cancel the voltage drop due to OHC basal-lateral wall low pass filtering.

2.5 References

Brownell, W. E., C. R. Bader, D. Bertrand and Y. de Ribaupierre (1985). "Evoked mechanical responses of isolated cochlear outer hair cells." Science 227(4683): 194-6.

Cai, H., B. Shoelson and R. S. Chadwick (2004). "Evidence of tectorial membrane radial motion in a propagating mode of a complex cochlear model." Proc Natl Acad Sci U S A 101(16): 6243-8.

Chadwick, R. S. (1998). "Compression, gain, and nonlinear distortion in an active cochlear model with subpartitions." Proc Natl Acad Sci U S A 95(25): 14594-9.

Chadwick, R. S., E. K. Dimitriadis and K. H. Iwasa (1996). "Active control of waves in a cochlear model with subpartitions." Proc Natl Acad Sci U S A 93(6): 2564-9.

Chan, D. K. and A. J. Hudspeth (2005). "Mechanical responses of the organ of corti to acoustic and electrical stimulation in vitro." Biophys J 89(6): 4382-95.

Cheatham, M. A. and P. Dallos (1994). "Stimulus biasing: a comparison between cochlear hair cell and organ of Corti response patterns." Hear Res 75(1-2): 103-13.

Cohen, A. and M. Furst (2004). "Integration of outer hair cell activity in a one-dimensional cochlear model." J Acoust Soc Am 115(5 Pt 1): 2185-92.

Dallos, P. (1983). "Some electrical circuit properties of the organ of Corti. I. Analysis without reactive elements." Hear Res 12(1): 89-119.

Dallos, P. (1985). "Response characteristics of mammalian cochlear hair cells." J Neurosci 5(6): 1591-608.

Dallos, P. (1986). "Neurobiology of cochlear inner and outer hair cells: intracellular recordings." Hear Res 22: 185-98.

Dallos, P. and B. N. Evans (1995). "High-frequency motility of outer hair cells and the cochlear amplifier." Science 267(5206): 2006-9.

de Boer, E. (1983). "Power amplification in an active model of the cochlea--short-wave case." J Acoust Soc Am 73(2): 577-9.

de Boer, E. (1990). "Can shape deformations of the organ of Corti influence the travelling wave in the cochlea?" Hear Res **44**(1): 83-92.

de Boer, E. (1990). Wave-propagation modes and boundary conditions for the ulfendahl-flock-khanna preparation. The Mechanics and Biophysics of Hearing Proceedings. P. Dallos. Berlin, Springer-Verlag: 333-339.

Dong, X. X., M. Ospeck and K. H. Iwasa (2002). "Piezoelectric reciprocal relationship of the membrane motor in the cochlear outer hair cell." Biophys J **82**(3): 1254-9.

Edge, R. M., B. N. Evans, M. Pearce, C. P. Richter, X. Hu and P. Dallos (1998). "Morphology of the unfixed cochlea." Hear Res **124**(1-2): 1-16.

Fettiplace, R. (2006). "Active hair bundle movements in auditory hair cells." J Physiol **576**(Pt 1): 29-36.

Fettiplace, R. and A. J. Ricci (2003). "Adaptation in auditory hair cells." Curr Opin Neurobiol **13**(4): 446-51.

Frank, G., W. Hemmert and A. W. Gummer (1999). "Limiting dynamics of high-frequency electromechanical transduction of outer hair cells." Proc Natl Acad Sci U S A **96**(8): 4420-5.

Geisler, C. D. (1986). "A model of the effect of outer hair cell motility on cochlear vibrations." Hear Res **24**(2): 125-31.

Geisler, C. D. (1991). "A cochlear model using feedback from motile outer hair cells." Hear Res **54**(1): 105-17.

Geisler, C. D. (1993). "A realizable cochlear model using feedback from motile outer hair cells." Hear Res **68**(2): 253-62.

Geisler, C. D. and C. Sang (1995). "A cochlear model using feed-forward outer-hair-cell forces." Hear Res **86**(1-2): 132-46.

Greenwood, D. D. (1990). "A cochlear frequency-position function for several species--29 years later." J Acoust Soc Am **87**(6): 2592-605.

Grosh, K., J. Zheng, Y. Zou, E. de Boer and A. L. Nuttall (2004). "High-frequency electromotile responses in the cochlea." J Acoust Soc Am **115**(5 Pt 1): 2178-84.

Holton, T. and A. J. Hudspeth (1986). "The transduction channel of hair cells from the bull-frog characterized by noise analysis." J Physiol **375**: 195-227.

Hubbard, A. (1993). "A traveling-wave amplifier model of the cochlea." Science **259**(5091): 68-71.

Hubbard, A. E. and C. D. Geisler (1972). "A hybrid-computer model of the cochlear partition." J Acoust Soc Am **51**(6): 1895-903.

Hubbard, A. E., D. C. Mountain and F. Chen (2003). Time-domain responses from a nonlinear sandwich model of the cochlea. Biophysics of the Cochlea: From Molecules to Models. A. W. Gummer. New Jersey, London, Singapore, Hong Kong., World Scientific: 351-358.

Hubbard, A. E., Z. Yang, L. Shatz and D. C. Mountain (2000). Multi-mode Cochlear models. Recent Developments in Auditory Mechanics. H. Wada. Singapore, New Jersey, London, Hong Kong, World Scientific: 167-173.

Hudspeth, A. (1997). "Mechanical amplification of stimuli by hair cells." Curr Opin Neurobiol **7**(4): 480-6.

Iwasa, K. H. (2001). "A two-state piezoelectric model for outer hair cell motility." Biophys J **81**(5): 2495-506.

Kanis, L. J. and E. de Boer (1993). "Self-suppression in a locally active nonlinear model of the cochlea: a quasilinear approach." J Acoust Soc Am **94**(6): 3199-206.

Karavitaki, K. D. and D. C. Mountain (2007). "Evidence for oscillatory fluid flow in the tunnel of Corti." Biophys J.

Kennedy, H. J., M. G. Evans, A. C. Crawford and R. Fettiplace (2003). "Fast adaptation of mechanoelectrical transducer channels in mammalian cochlear hair cells." Nat Neurosci **6**(8): 832-6.

Kennedy, H. J., M. G. Evans, A. C. Crawford and R. Fettiplace (2006). "Depolarization of cochlear outer hair cells evokes active hair bundle motion by two mechanisms." J Neurosci **26**(10): 2757-66.

Kolston, P. J., E. de Boer, M. A. Viergever and G. F. Smoorenburg (1990). "What type of force does the cochlear amplifier produce?" J Acoust Soc Am **88**(4): 1794-801.

Liao, Z., A. S. Popel, W. E. Brownell and A. A. Spector (2005). "High-frequency force generation in the constrained cochlear outer hair cell: a model study." J Assoc Res Otolaryngol 6(4): 378-89.

Liao, Z., A. S. Popel, W. E. Brownell and A. A. Spector (2005). "Modeling high-frequency electromotility of cochlear outer hair cell in microchamber experiment." J Acoust Soc Am 117(4 Pt 1): 2147-57.

Lim, K. M. and H. Li (2006). "A two-layer outer hair cell model with orthotropic piezoelectric properties: Correlation of cell resonant frequencies with tuning in the cochlea." J Biomech.

Lu, S., F. Chen, D. C. Mountain and A. E. Hubbard (Submitted). "Is Longitudinal Fluid Flow in The Organ of Corti Fundamental to Cochlear Function?" Submitted.

Lu, S., J. Spisak, D. C. Mountain and A. E. Hubbard (2006). A New Multicompartments Model of Cochlea. Auditory Mechanics: Processes and Models. A. L. Nuttall, T. Ren, P. Gillespice, K. Grosh and E. De Boer. New jersey, London, Singapore, Beijing, Shanghai, Hong Kong, Taibei, Chennai, World Scientific: 508-509.

Lu, T. K., S. Zhak, P. Dallos and R. Sarpeshkar (2006). "Fast cochlear amplification with slow outer hair cells." Hear Res 214(1-2): 45-67.

Markin, V. S. and A. J. Hudspeth (1995). "Modeling the active process of the cochlea: phase relations, amplification, and spontaneous oscillation." Biophys J 69(1): 138-47.

Martin, P. and A. J. Hudspeth (1999). "Active hair-bundle movements can amplify a hair cell's response to oscillatory mechanical stimuli." Proc Natl Acad Sci U S A 96(25): 14306-11.

Misrahy, G. A., K. M. Hildreth, E. W. Shinabarger and W. J. Gannon (1958). "Electrical properties of wall of endolymphatic space of the cochlea (guinea pig)." Am J Physiol 194(2): 396-402.

Mountain, D. C. and A. E. Hubbard (1994). "A piezoelectric model of outer hair cell function." J Acoust Soc Am 95(1): 350-4.

Muller, M. (1996). "The cochlear place-frequency map of the adult and developing Mongolian gerbil." Hear Res 94(1-2): 148-56.

83

Naidu, R. C. and D. C. Mountain (1998). "Measurements of the stiffness map challenge a basic tenet of cochlear theories." Hear Res 124(1-2): 124-31.

Nakajima, H. H., E. S. Olson, D. C. Mountain and A. E. Hubbard (1994). "Electrically evoked otoacoustic emissions from the apical turns of the gerbil cochlea." J Acoust Soc Am 96(2 Pt 1): 786-94.

Neely, S. T. (1993). "A model of cochlear mechanics with outer hair cell motility." J Acoust Soc Am 94(1): 137-46.

Neely, S. T. and D. O. Kim (1983). "An active cochlear model showing sharp tuning and high sensitivity." Hear Res 9(2): 123-30.

Neely, S. T. and D. O. Kim (1986). "A model for active elements in cochlear biomechanics." J Acoust Soc Am 79(5): 1472-80.

Olson, E. S. and D. C. Mountain (1991). "In vivo measurement of basilar membrane stiffness." J Acoust Soc Am 89(3): 1262-75.

Peterson, L. C. and B. P. Bogert (1950). "A Dynamical Theory of Cochlea." J Acoust Soc Am 22(3): 369-381.

Plassmann, W., W. Peetz and M. Schmidt (1987). "The cochlea in gerbilline rodents." Brain Behav Evol 30(1-2): 82-101.

Rabbitt, R. D., H. E. Ayliffe, D. Christensen, K. Pamarthy, C. Durney, S. Clifford and W. E. Brownell (2005). "Evidence of piezoelectric resonance in isolated outer hair cells." Biophys J 88(3): 2257-65.

Ramamoorthy, S., N. V. Deo and K. Grosh (2007). "A mechano-electro-acoustical model for the cochlea: response to acoustic stimuli." J Acoust Soc Am 121(5 Pt1): 2758-73.

Ren, T. (2002). "Longitudinal pattern of basilar membrane vibration in the sensitive cochlea." Proc Natl Acad Sci U S A 99(26): 17101-6.

Ren, T. and A. L. Nuttall (2001). "Basilar membrane vibration in the basal turn of the sensitive gerbil cochlea." Hear Res 151(1-2): 48-60.

Rhode, W. S. (1971). "Observations of the vibration of the basilar membrane in squirrel monkeys using the Mossbauer technique." J Acoust Soc Am 49(4): Suppl 2:1218+.

Ricci, A. J., A. C. Crawford and R. Fettiplace (2000). "Active hair bundle motion linked to fast transducer adaptation in auditory hair cells." J Neurosci 20(19): 7131-42.

Salt, A. N. and T. Konishi (1986). The cochlear fluids:perilymph and endolymph. Neurobiology of Hearing: The Cochlea. R. A. Altschuler and R. P. Bobbin. New York, Raven Press: 123-137.

Santos-Sacchi, J. (1989). "Asymmetry in voltage-dependent movements of isolated outer hair cells from the organ of Corti." J Neurosci 9(8): 2954-62.

Scherer, M. P. and A. W. Gummer (2004). "Vibration pattern of the organ of Corti up to 50 kHz: evidence for resonant electromechanical force." Proc Natl Acad Sci U S A 101(51): 17652-7.

Spector, A. A. (1999). "Nonlinear electroelastic model for the composite outer hair cell wall." ORL J Otorhinolaryngol Relat Spec 61(5): 287-93.

Spector, A. A., W. E. Brownell and A. S. Popel (2003). "Effect of outer hair cell piezoelectricity on high-frequency receptor potentials." J Acoust Soc Am 113(1): 453-61.

Spector, A. A., N. Deo, K. Grosh, J. T. Ratnanather and R. M. Raphael (2006). "Electromechanical models of the outer hair cell composite membrane." J Membr Biol 209(2-3): 135-52.

Spector, A. A. and R. P. Jean (2004). "Modes and balance of energy in the piezoelectric cochlear outer hair cell wall." J Biomech Eng 126(1): 17-25.

Spector, A. A., A. S. Popel, R. A. Eatock and W. E. Brownell (2005). "Mechanosensitive channels in the lateral wall can enhance the cochlear outer hair cell frequency response." Ann Biomed Eng 33(8): 991-1002.

Strassmaier, M. and P. G. Gillespie (2003). "Fast adaptation in the mammalian cochlea: a conserved mechanism for cochlear amplification." Nat Neurosci 6(8): 790-1.

Tolomeo, J. A. and C. R. Steele (1995). "Orthotropic piezoelectric properties of the cochlear outer hair cell wall." J Acoust Soc Am 97(5 Pt 1): 3006-11.

Viergever, M. A. and E. de Boer (1987). "Matching impedance of a nonuniform transmission line: application to cochlear modeling." J Acoust Soc Am 81(1): 184-6.

Weitzel, E. K., R. Tasker and W. E. Brownell (2003). "Outer hair cell piezoelectricity: frequency response enhancement and resonance behavior." J Acoust Soc Am 114(3): 1462-6.

Zwicker, E. (1986). "A hardware cochlear nonlinear preprocessing model with active feedback." J Acoust Soc Am 80(1): 146-53.

Zwislocki, J. J. (1950). "Theory of the Acoustical Action of the Cochlea." J Acoust Soc Am 22(6): 778-784.

Chapter 3

Distortion Product Otoacoustic Emission Generated by the Model

3.1 Introduction

Otoacoustic emissions (OAE) are sounds generated within the inner ear. The existence of OAE was first discovered experimentally by David Kemp (Kemp 1978). Since then, different types of OAE have been explored. Some are generated by inserting electrical stimuli into the inner ear (EEOAE) (Hubbard and Mountain 1983; Mountain and Hubbard 1989; Murata et al. 1991; Nakajima et al. 1994; Ren and Nuttall 1995). Some are generated by placing two primary tone stimuli into the ear canal. These generated sounds are called distortion product OAEs (DPOAE) (Wilson and Johnstone 1973; Kemp 1979). Researchers have found that OAEs will disappear after the inner ear is damaged. So OAEs are often used as a measure of inner ear health (Kemp 2002). They are the basic way to test hearing defects in newborns and babies, who are too young to participate in traditional hearing tests (Stone et al. 2000). OAEs also play an important role in diagnosing higher level hearing losses, such as auditory neuropathy (Hall et al. 1994; Ami et al. 2008).

DPOAEs are evoked by stimulating the ear with two primary tones, whose frequencies are f1 and f2 (f1<f2, f1 and f2 are close). The intensities of these two primaries are usually between 50 - 65 dB SPL in order to generate the largest distortion products. The evoked sound responses from these two stimuli have

frequencies (f_{dp}) mathematically related to the two primary frequencies: f_{dp} = mf1±nf2 (m and n are integers). The most widely studied distortion products (DP) are at the frequencies 2f1 − f2 and 2f2 - f1 (the "cubic" DPs).

A very interesting and long-standing set of questions about DPOAE are: What is the mechanism of DPOAEs generation and where do the DPOAEs come from? Are they generated from one or more places? In the past thirty years, numerous theories have been proposed. Although the interaction of the f1 and f2 tone occurs along the entire basilar membrane (BM), the major contributor to the DP is considered to be at the place near the f2 place (Brown, Kemp 1983). In 1980, Kim's work (Kim et al. 1980) suggested that the lower sideband (f_{dp} < f1) DPOAE was first generated near the f2 site, then it traveled backward to the ear canal, as well as traveled forward to the DP site, which is more apical. Current evidences suggest that the lower sideband DPOAE measured in the ear canal might come from two places: One is from the f2 place by nonlinear distortion of the overlapping primaries ("wave-fixed" or "distortion emission"), the other is a reflection wave from the DP place ("place-fixed" or "reflection emission"), whose characteristic frequency (CF) equals the f_{dp} (Kemp 1978; Kemp et al. 1986; Zweig and Shera 1995; Shera and Guinan 1999; Knight and Kemp 2001; Kemp 2002; Withnell et al. 2003; Wilson and Lutman 2006).

All these hypotheses we have just mentioned assume that the DP travels back to the stapes in the form of a traveling wave (i.e. a reverse traveling wave). The reverse traveling wave theory has been largely accepted and is supported by some indirect evidence (Kimberley et al. 1993; Faulstich and Kossl 2000; Kalluri and Shera 2001; Shera et al. 2004; Shera et al. 2007; Dong and Olson 2008), although direct experimental evidence to support the theory is still absence. One limitation of this theory is that, if the reverse wave carrying DP travels "on" the BM, given the fact that the BM is not connected to the stapes, how does the DP drive the stapes and emit to the ear canal? What drives the stapes and emits from the cochlea is surely some version of the pressure in scala vestibuli (SV), just inside the stapes. In this regard, some researchers argue that the DP may travel back to the stapes in the form of a compression wave in the cochlear fluid (Wilson 1980; Ren 2004; Vetesnik et al. 2006; He et al. 2007; He et al. 2008). Compression wave is a longitudinal wave which is much faster than the reverse traveling wave. The speed of the compression wave is about the speed of sound in the water (about 1500 m/s). If the compression wave theory were true, the reversed compression wave carrying the DP would propagate to the stapes immediately after generated, and would be reflected by stapes and formed a forward traveling wave. Ren measured the velocity of the BM in the longitudinal direction at the DP frequency as well as the stapes velocity. He found the phase change on the BM at the DP frequency to be negative around the DP place, suggesting that a forward traveling wave is dominant. He did not observe the

89

reverse traveling wave on the BM around the DP place (Ren 2004). This result contradicts to the theory that a major part of reverse traveling wave starts at the DP place due to the reflection. Ren also found that, at the DP frequency, the stapes vibrated earlier than the DP place. In other words, stapes vibration leads BM vibration at the DP place. This suggests that the DP wave propagated backward to the stapes before it reached the DP place, implying it traveled back much faster than traveled forward on the BM near the best place. Other experiments conducted recently also observed forward traveling wave at places basal to the DP site (He et al. 2007; He et al. 2008). Ren and his colleagues also found that the group delay of DP vibration at stapes is equal or less than that of DP vibration measured at the DP place (Ren et al. 2006), indicating that the DP measured near the stapes cannot come from a reverse traveling wave starting at the DP site.

Regard the pressure measurement in the fluid channel, Dong and Olson measured the DP inside the scala tympani (ST) (Dong and Olson 2005; Dong and Olson 2008). They found the forward traveling wave near the DP place in the ST and the phase of DPOAE is shallow than the phase of DP in the best frequency place. Again there is no direct SV pressure measurement supporting the reverse traveling wave.

In order to give more insight of the DP generation, the cubic DP (2f1-f2) will be generated from a nonlinear multicompartment model with piezoelectrical OHC feedback. The longitudinal patterns of the BM vibration and the pressure in the SV fluid of the f1 tone, f2 tone and the DP will be present. We found what can be interpreted as a reverse-traveling wave, that appears to be "fast", although not as fast as the speed of sound in water.

3.2 Methods

3.2.1 Introduction to the Model

The model used to generate the DPOAE in this study is a nonlinear multicompartment model with outer hair cell (OHC) piezoelectrical feedback (Hubbard et al. 2006; Lu et al. 2006; Lu et al. Submitted). Unlike the classic cochlear model which only has two fluid compartments, this model has an additional third transmission line: organ of Corti (OC) fluid flow, which has been experimentally observed (Karavitaki and Mountain 2007). The structure of one section of the model is as follows (Figure 3-1). The whole cochlea is simulated using a discrete element model that consists of 400 sections.

The left part of the Figure 3-1 is a traditional multicompartment model, called the sandwich model in some publication (Hubbard et al. 2000; Hubbard et al. 2003; Hubbard et al. 2006; Lu et al. 2006; Lu et al. Submitted). Z_{RL} and Z_{BM} separate the fluid compartments vertically. OHC force is coupled back to the fluid channel by Z_{RL} and Z_{BM}. The right part of Figure 3-1 is the OHC electro-anatomical model. The adjacent sections are coupled by resistors in both SM and ST along the length of the cochlea. The significance of SM and ST circuits is that they bring longitudinal electrical coupling, not a local coupling, into the system. In the apical part of the OHC, the tension gated channel senses the velocity of the RL motion. The conduction changes follow a nonlinear curve. When the channel is ON,

current flows inward, and the OHC is depolarized. This causes a transmembrane voltage change in the basal-lateral portion of the OHC.

Between the hydromechanical portion and the OHC electroanatomical circuit is the piezoelectric feedback system. Towards the hydromechanical part of the model, the output of this feedback system functions as a force generator. Towards the OHC electrical model, the transformer reflects the mechanical load of the hydromechanical system. Hence the impedance of the basal part of the OHC will change according to the mechanical load of the piezoelectrical feedback system. Here we assume there is no energy loss in the transaction itself. Therefore the piezoelectric feedback system works like an ideal transformer. The gain of the feedback system is controlled by the transformer ratio, N.
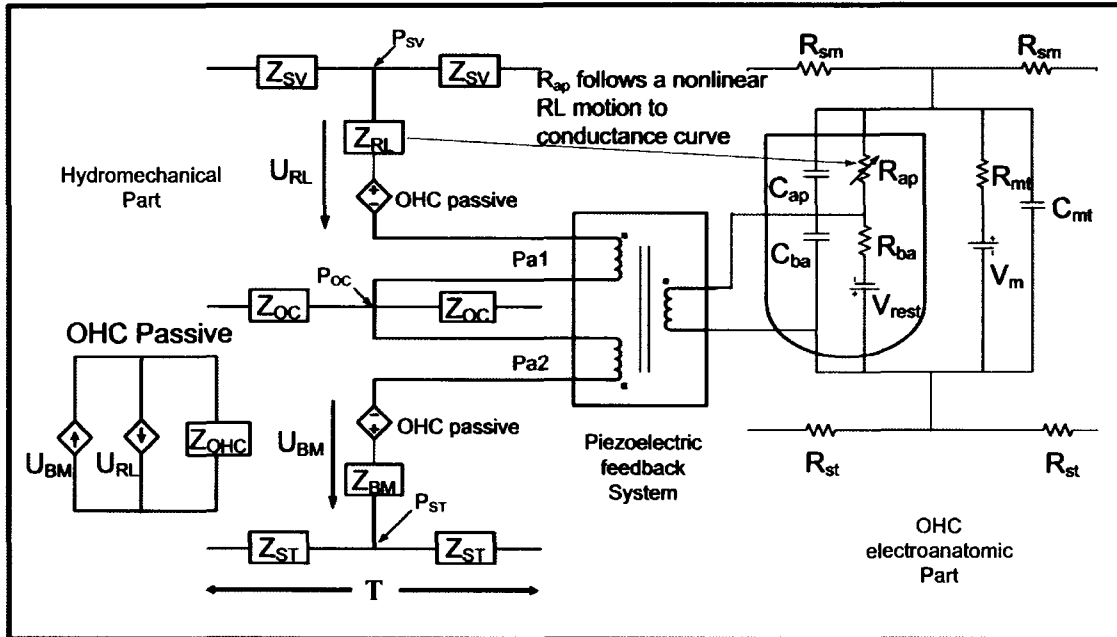
Figure 3- 1 The schematic drawing of one section of the model. The left portion is the hydromechanical model. The right portion is the OHC anatomical circuit. A bi-directional piezoelectric feedback system connects the mechanical part and the electrical part. The adjacent sections of OHC model are coupled by resistors in both SM and ST.

There are two feedback loops in this model. One loop is between BM and RL motion causing OHC depolarization and voltage-dependent length change (OHC electromotility), which generates active force feeding back to the system and enhancing the BM and the RL motion. The other loop is a local piezoelectric feedback system. In this local feedback loop, OHC electrical impedance couples with the mechanical load of the OHC directly, so that any mechanical loading

94

changes in the system will affect the OHC electrical impedance. Simulation results from this model show that this multi-loop model can at least partially overcome the OHC low-pass filtering problem in the high frequency range, and can replicate cochlear responses at both low and high frequencies.

The OHC response is often described as near-linear for low SPL inputs and highly nonlinear for the high SPL inputs. In our model, OHC transduction is the only nonlinearity. Due to both the structural nature of the OHC circuit model and the curve used to describe the tension-gated conductance in the apical part of the OHC, the active force generated by OHC, which is assumed to be proportional to OHC transmembrane potential, is also nonlinear with respect to the model's input pressure at the stapes, regardless the intensity of the input signal. For small signal inputs, the fundamental component of the active force increases nearly linearly with the level increase of the input.

In the previous studies we show that this cochlear model can match BM vibration data and cochlear microphonic data fairly well (Hubbard et al. 2000; Hubbard et al. 2003; Hubbard et al. 2006; Lu et al. 2006; Lu et al. Submitted). In this study we will compare the model's output with some selected DPOAE data. However our comparison is limited by the fact that we do not have detailed gerbil ear canal model and middle ear model.

3.2.2 Experimental Design

Both the DP pressure and the BM-DP vibration pattern are reported in this study. Pressure waveforms are recorded in the stapes as well as other places in the SV along the length of the cochlea in response to acoustic stimuli. Magnitude and phase of the DP pressure are obtained by using a FFT to filter out the components of interest. The BM vibration patterns are also recorded at locations along the cochlea. We are interested in if we observed a forward DP traveling wave (negative phase slope) or a reverse DP traveling wave (positive phase slope) along the length of the cochlea.

The simulations presented are as follows: The first data set we generated from the model is that DPOAE amplitude changes in response to the intensity change of the primary tones. In this simulation the frequencies of two primary tones were fixed. Therefore, the f2/f1 ratio is fixed. The intensity of the f1 tone is swept from 40 dB SPL to 85 dB SPL at the ear canal. The intensity of f2 tone is set to be the same as that of the f1 tone, or is 20 dB lower than that of the f1 tone. The second set of simulation results is the longitudinal BM velocity patterns for both primaries and cubic DP (2f1-f2) near their peak region. The frequencies of the f1 tone and f2 tone are 15.455 kHz and 17 kHz respectively. The intensities of the two primaries are 60 dB SPL at the ear canal. These settings are approximately the same as Ren used in his experiments (Ren 2004). The last results we report

here are the BM vibration pattern and SV pressures for both primaries and DP along the entire length of the cochlea. The frequencies of the primary tones are 2.5 kHz and 3 kHz so that the peaks are in the apical region of the cochlea, contrasted with primaries of 15.5 kHz and 17 kHz used by Ren in his experiments. Those primary frequencies put the two tones and the DP all within a narrow region, quite close to the base of the cochlea. We will show that abbreviated region to be fraught with irregularities, and the picture is much clearer if one works over a broader range of cochlear length. The middle ear was modeled as a linear system (Voss and Shera 2004) in this study. We assume that the middle ear has a fixed gain in the frequency range we are interested in. The gains were derived from existing publications (Olson 1998; Magnan et al. 1999; Ruggero and Temchin 2002; Dong and Olson 2006). The forward gain is set to be 27dB, while the reverse gain of the middle ear is set to be -32 dB.

3.3 Results

3.3.1 Waveform of Distortion Products
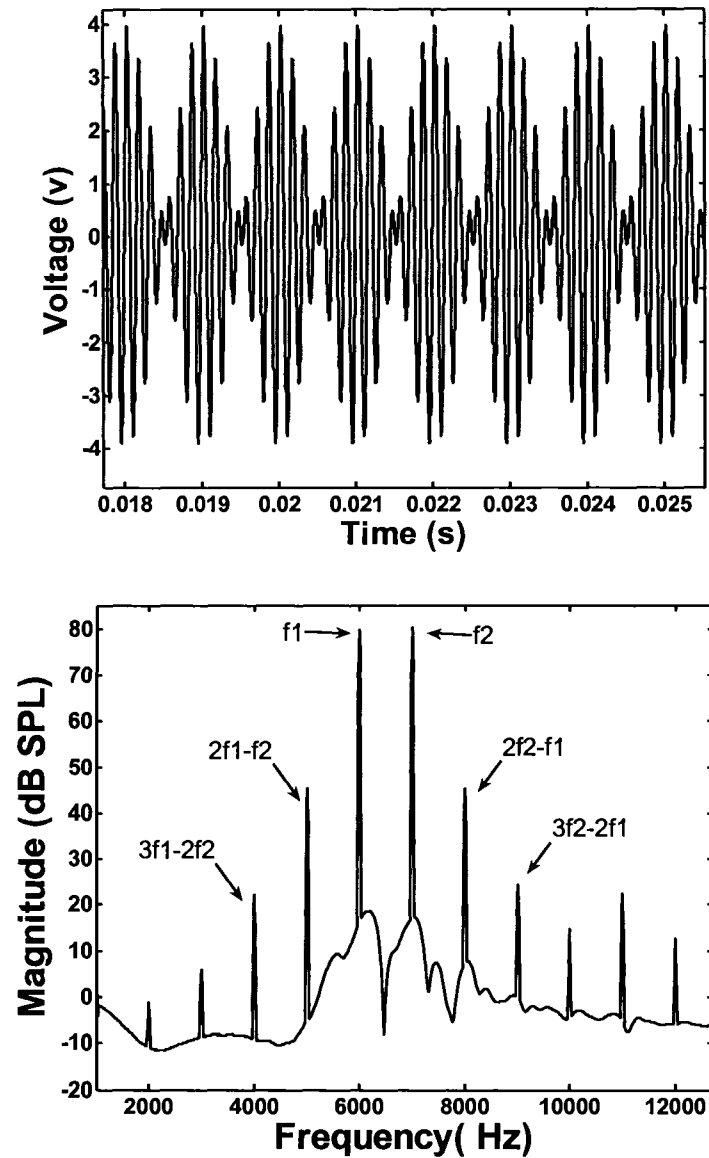
Figure 3- 2 *Upper panel: time domain pressure waveform at the stapes. Lower*

panel: FFT results showing the primaries and DPs.

Figure 3-2 show the time domain pressure waveform at the stapes when two primary tones were present to the cochlea. The frequencies of the two tones are: f1=6 kHz, f2=7 kHz. The intensities are about 80 dB SPL at the stapes. The time domain waveform clearly shows beating. The lower panel shows the DP generated inside the cochlea. The DP frequencies are: 2f1-f2=5 kHz, 2f2-f1=8 kHz, 3f1-2f2=4 kHz, 3f2-2f1=9 kHz, and etc. The results show that the cubic DP (2f1-f2 and 2f2-f1) are the largest DP. They are about 35 dB lower than the primaries.

3.3.2 Changes of DPOAE Intensity in Response to the Intensity Sweep of the Primaries
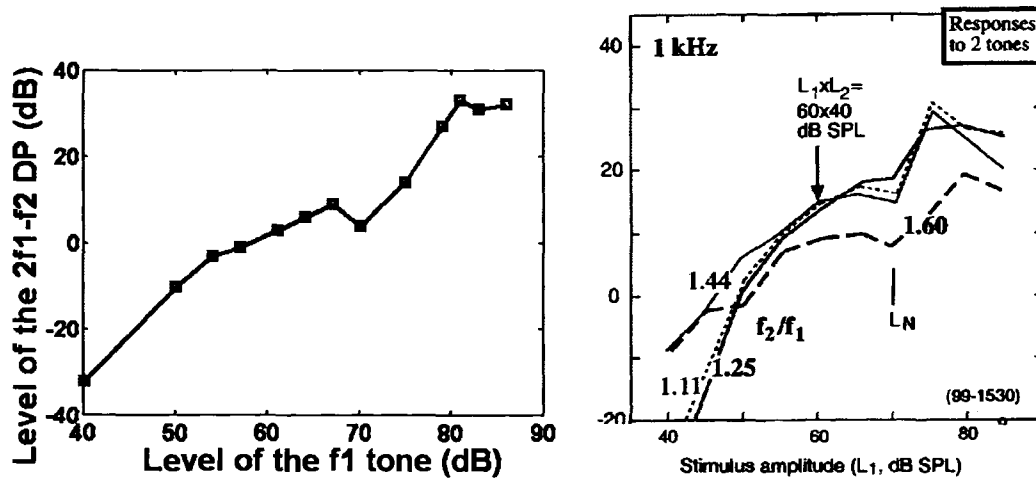
Figure 3- 3 Changes of DPOAE (2f1-f2) intensity in response to intensity sweep of the primaries. Left panel: the DPOAE generated from the Model. Right panel: experimental data (Milles 2000).

Figure 3-3 shows the typical input-output function for the DPOAE. The left panel of Figure 3-3 shows the magnitude of the DPOAE (2f1-f2) pressure in response to the intensity sweeping of the primaries. The frequencies of the f1 and f2 tone are 800 Hz and 1000 Hz, respectively. The f2/f1 ratio is 1.25. They are the same as what was used to generate the curve of f2/f1=1.25 in the right panel. The frequency of cubic DPOAE (2f1-f2) is 600 Hz. The intensity of the f1 tone was swept from 40 dB to 85 dB. The intensity of the f2 tone is set to be always 20 dB

below that of the of f1 tone. The right panel of Figure 3-3 is the experimental result from Mills (Mills 2000). Compared the results of left panel with the experimental results of f2/f1=1.25 in the right panel, both panels show a notch when the level of the f1 tone is near 70 dB SPL. After the dip, the rising slope of the curve is larger compared to the slope of the low level input before the notch. Both the model and the experimental data show the saturation after 80 dB SPL input.

3.3.3 DPOAE Frequency Responses
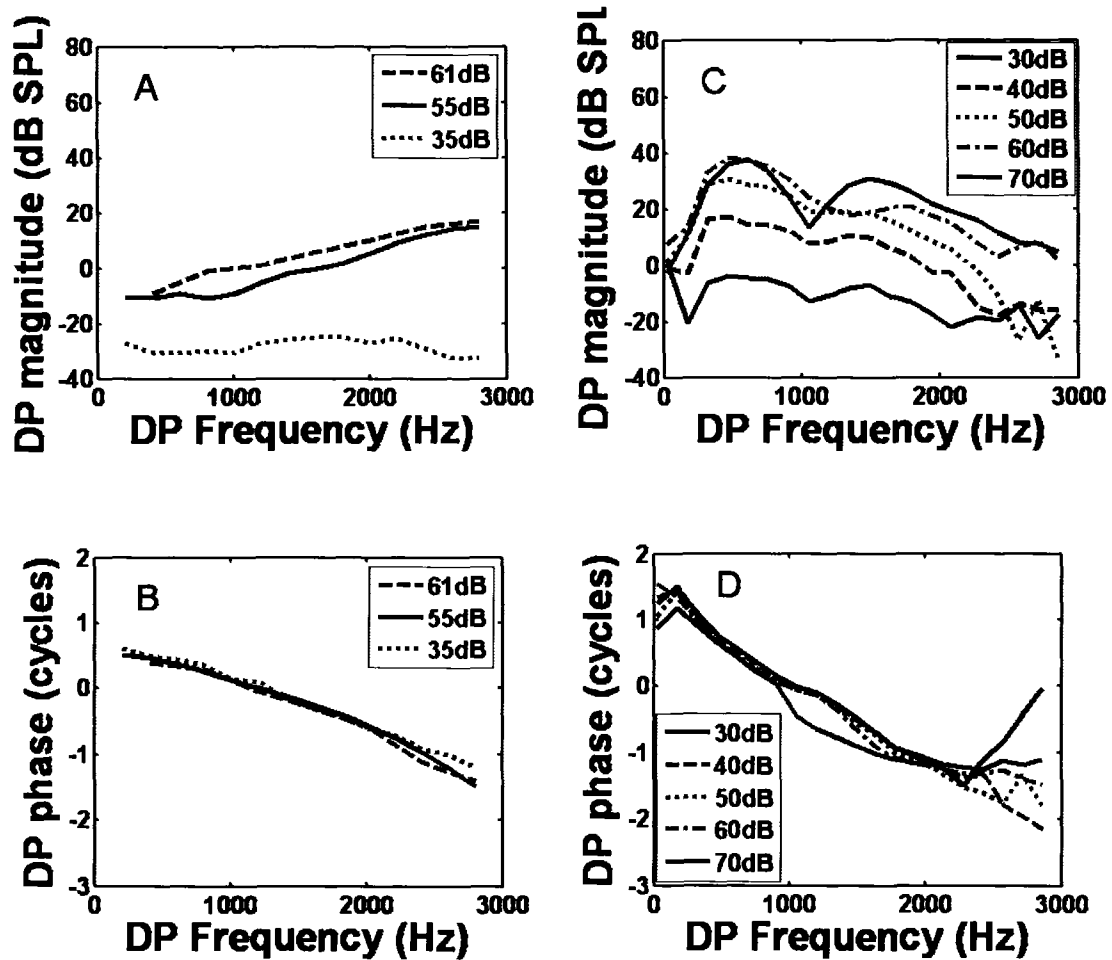
Figure 3- 4 Frequency response of DPOAE at different input levels. The frequency of the f2 tone is fixed at 3 kHz. Panel A and B are the magnitude and phase response from the model. Panel C and D are the experimental data (Mountain et al. 2000). The frequency of the f1 tone is swept from 1.6 kHz to 2.9 kHz. The intensities of the f1 tone and the f2 tone are the same.

Figure 3-4 shows the DPOAE frequency responses from our model and from the experimental data. The model results include the DPOAE magnitudes and phases for input level at 35dB, 55dB and 61dB SPL at ear canal. The input levels of experimental data are from 30dB to 70dB SPL. The trend of magnitude results (Panel A) from the model at 55dB and 61dB SPL are similar. They both increase about 30 dB SPL from 200 Hz to 2800 Hz. But they are different from the model results from 35dB SPL input which is flat in the same frequency range. The phases of model (Panel B) at different input levels are similar. They all drop about two cycles from 200 Hz to 2800 Hz. The trends of the magnitudes results of the model at high level input (55dB and 61dB) are not the same as the experimental data (Panel C). The DPOAE magnitude of the model shows a increase when the frequency goes high while the magnitudes of experimental data show a slight decrease when the frequency goes high. The model has less total phase lag compared with the experimental data. The phase of the experimental data drops about 2.5 cycles in the same range as the model.

3.3.4 Longitudinal BM Vibration Pattern of primaries and cubic DPs in the Basal Part of the Cochlea
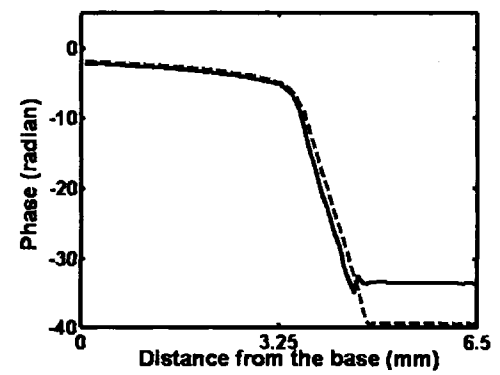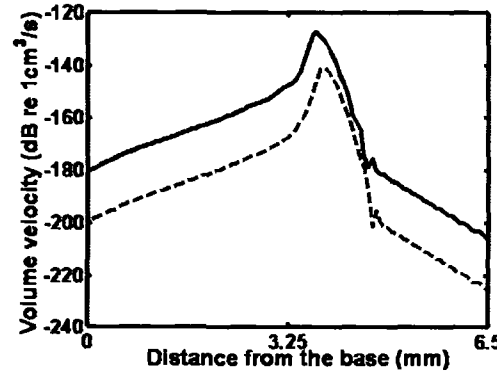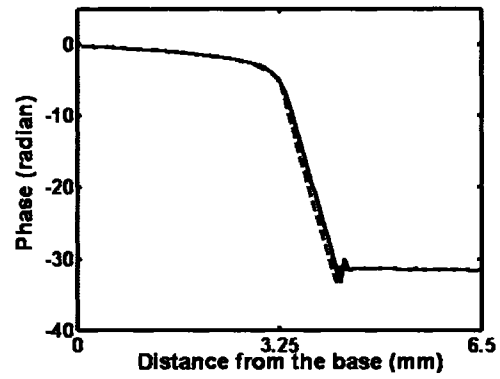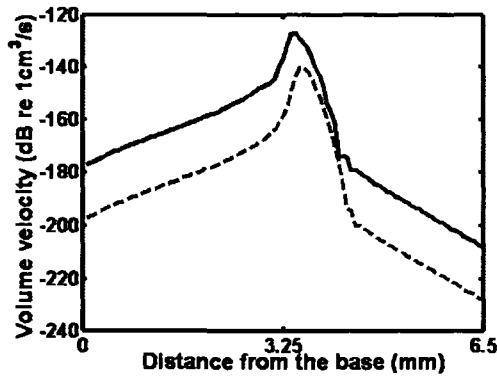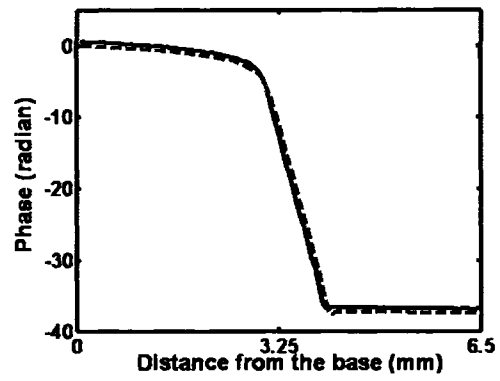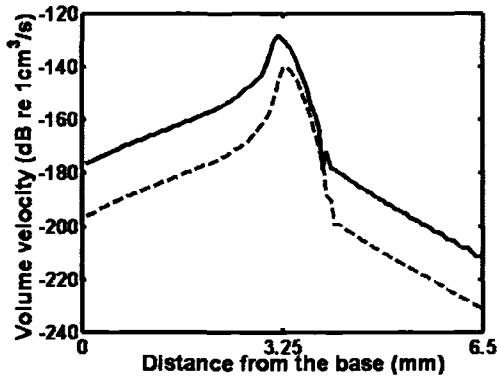
Figure 3- 5 Longitudinal BM velocity pattern for the single tone inputs. The frequencies are 17 kHz (upper two panels), 15.455 kHz (middle two panels) and 13.91 kHz (lower two panels) respectively. For each frequency, the intensities of the input stimuli are at 40 dB SPL (dashed line) and 60 dB SPL (solid line). The left panels are magnitude responses. The right panels are phase responses.

In Figure 3-5, compared with 40 dB results, the 60 dB results clearly show the nonlinear compression in the peak region in all three frequencies. The peaks of 60 dB input also shift to the basal site (shift to high frequency) compared with 40 dB input. There are no significant differences between the phase of the 40 dB tone and 60 dB tone. There are some small ripples after the peak in the magnitude plots. We believe this observation is due to the interaction of the OHC somatic drive and the OC pressure drive (Lu et al. Submitted). The simulation results of the longitudinal BM vibration pattern of signal tone are similar to the experimental data (Ren 2002).
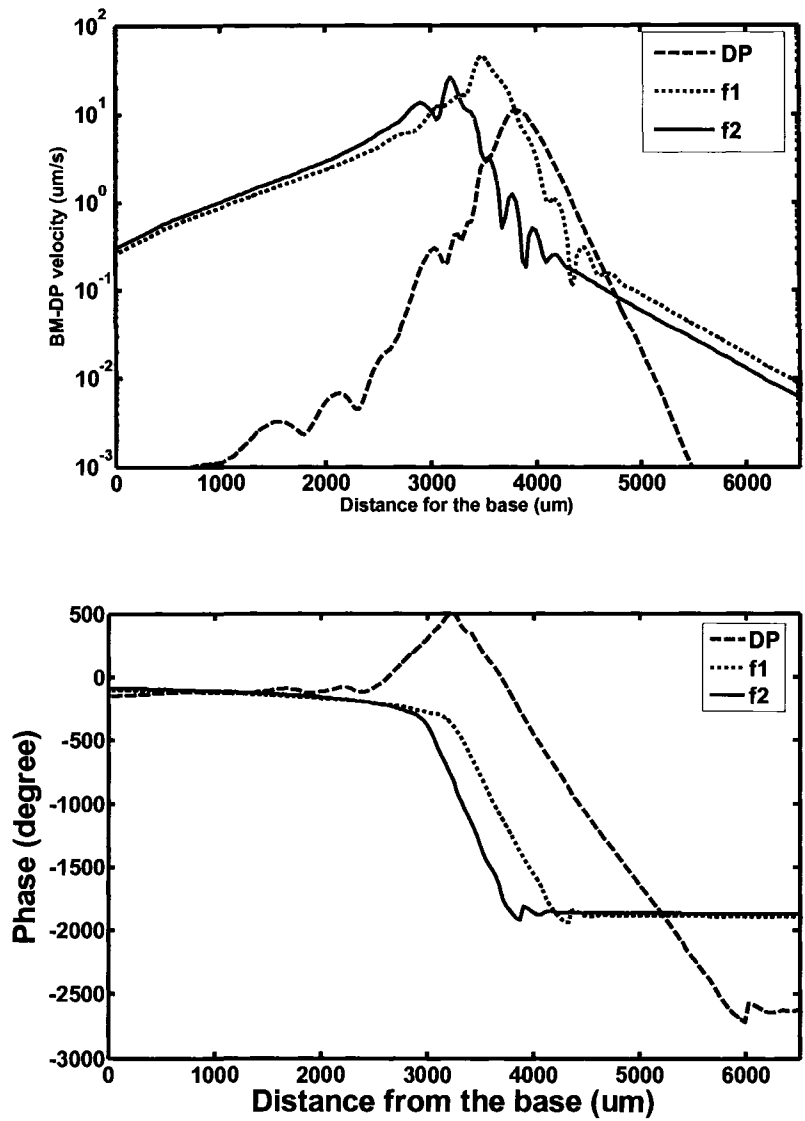
Figure 3- 6 Longitudinal BM velocity pattern for the f2 tone, f1 tone and cubic DP
(2f1-f2) generated by these two primaries. Upper panel is the magnitude while
lower panel is the phase. The frequencies are f2 tone 17 kHz (red solid line), f1
tone 15.455 kHz (green dotted line) and DP 13.91 kHz (blue dashed line)
respectively.

Figure 3-6 shows the longitudinal BM vibration pattern when the cochlea is stimulated by two tones (f1 and f2). The intensities of these two primaries are at 50 dB SPL in the ear canal. Compare with the single tone responses in Figure 3-5, the peaks of the primaries and the peak of the DP have more ripples near the peak region when two tones are present to the cochlea simultaneously. When the DP reaches its peak value, the magnitude of the f2 tone is already 20 dB below. For the DP on the BM, the results show that the DP peak on the BM is at the DP place. The shape of the DP curve is different from the single tone response of the DP frequency. There is only a small bump in the f2 place, no obvious DP peak near the f2 place. The phase panel shows that the DP phase has a negative slope near the DP place, which suggests a forward traveling wave of the DP frequency dominating near the DP place. Basal to the f2 place, the DP phase shows positive slope, indicating a reverse traveling wave is dominant. The reverse traveling wave is symmetric with the forward traveling wave regarding their starting place about 3200μm from the base of the cochlea. The reverse traveling wave is very slow near the f2 place. Then it becomes a very fast traveling wave back to the stapes.

3.3.5 Comparison of the BM Longitudinal Vibration Pattern Generated from the Model with the Experimental Data
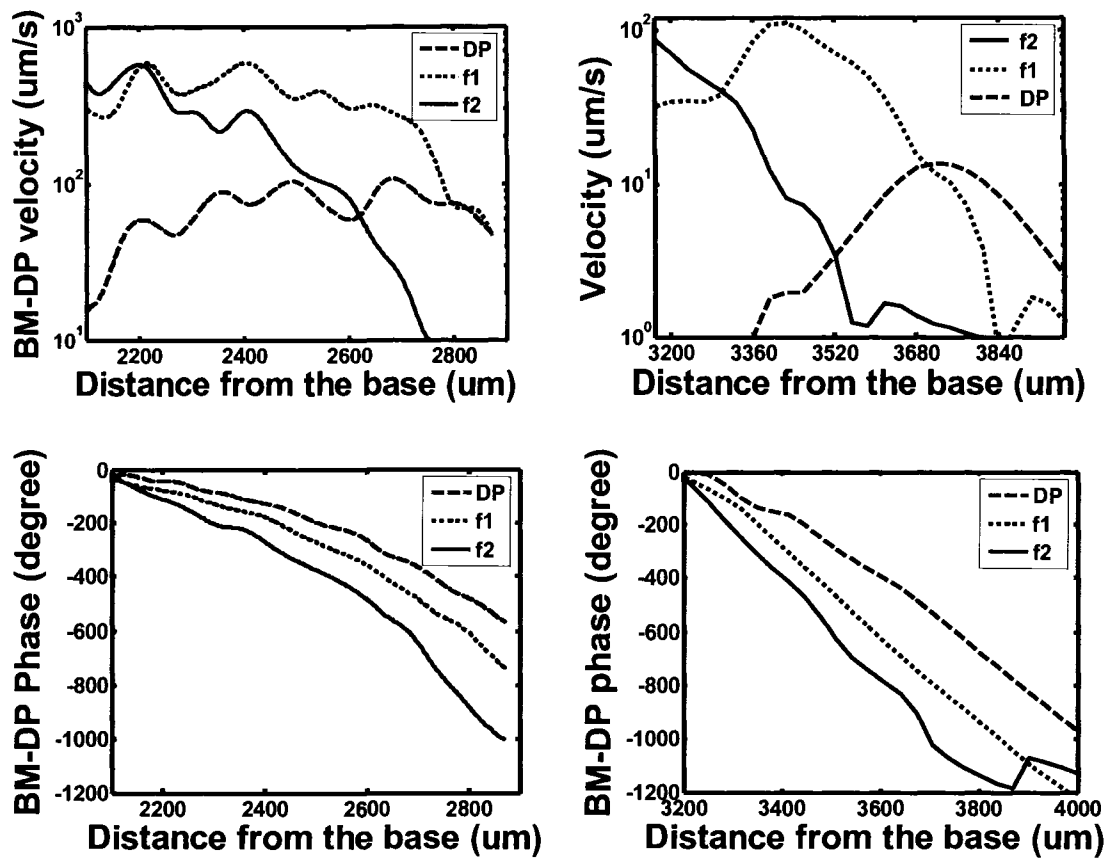
Figure 3- 7 Left panels: BM vibration pattern experimentally recorded from a gerbil (Ren 2004). Right panels: BM vibration pattern from our model. The frequencies of the f1 (green dotted line), f2 (red solid line) and DP (blue dashed line) tone are 15.455 kHz, 17 kHz and 13.9 kHz respectively. The intensity of the primaries are 60 dB SPL at ear canal.

Figure 3-7 shows the BM vibration pattern for the f1 tone, f2 tone and the DP (2f1-f2) in the basal part of the cochlea. The phase panels show the phase delays relative to the starting point of the region. Because the definition of the starting point of the BM in our model is not the same as what Ren used in his measurement, the peak regions have an about 1100 μm shift between our model and the experimental data. The measurement ranges from 2100μm to 2900 μm. The model results ranges from 3200 μm to 4000 μm. Both the f1 tone and f2 tone are 60 dB SPL at the ear canal. The frequencies of the f1 tone and f2 tone are 15.455 kHz and 17 kHz respectively. The model's magnitude responses are similar to the experimental data in several aspects. First, the curves are much irregular compared to the single tone input in Figure 3-5. We have explained in a previous paper that the ripples after the peak is partially caused by the trading off of OHC somatic drive (mechanical) with OC pressure drive (Lu et al. Submitted). In the case of the experimental data, f2 should peak most basal ward, with f1 next, followed by DP. In the model, f2 peaks off the left side of the graph, and the DP peaks at a location that is apical and it is at about the same place as if the tone were presented as an input. In the overlap region of the f1 tone and the f2 tone, the DP velocity is much smaller than the primaries. When the DP reaches its peak, the magnitude of f2 tone is already 20 dB below. The model's absolute velocities are smaller than that measured experimentally. This is because we calibrated our model using the data from another paper (Ren and Nuttall 2001), which has relatively small BM velocity measurements.

109

In the phase domain, there are also similarities between the model's output and the experimental data. The ordering of the lagging curves is the same: DP leads f1, which leads f2. Over 0.8 mm range, the experimental data has a 600-1000 degree phase lag. The model has systematically 200 degrees more lag than the data. Also, in the model the phase curves are straighter, while in the experimental data the slopes of the curves increases with distance.

The similarities are sufficient to agree with a limited number of Ren's conclusions: At the BM-DP's best place, the phase plot shows that the forward traveling wave (negative phase slope) is dominant. Moreover, the rapid phase change of BM-DP at the DP place is interpreted to mean that the wave is slow. The apparent speed is about 3.7 m/second (the DP changes by about 3 cycles in 0.8 mm).

3.3.6 BM Vibration and SV Pressure Pattern along the Cochlea

Figure 3- 8 BM vibration pattern (magnitude and phase) along the length of the cochlea from our model. The frequencies of the f1 tone, f2 tone and the DP (2f1-f2) are 2.5k Hz, 3 kHz and 2 kHz respectively. The green dotted lines are the f1 responses. The red solid lines are the f2 responses. The blue dashed lines are the DP responses.

Figure 3-8 is the simulation result from our model. The place is more apical compared to Ren's measurement. Therefore we can clearly distinguish between a reverse traveling wave and a compression wave. It would be difficult to do that if the DP site is close to the base of the cochlea. The f2 tone (3 kHz) and the f1

tone (2.5 kHz) peak at 7.6mm and 8.0 mm from the base of the cochlea respectively. The cubic DP (2 kHz) peaks at about 8.5mm from the base, which is the DP place if it were presented alone as an input. Like the model's results in the basal region of the cochlea (see Figure 3-6), there is also a very small bump in the DP curve at the f1 tone and f2 tone overlap region. But unlike the results in the basal region of the cochlea, there are no obvious ripples in the peaks of the f1 tone, f2 tone and DP.

From the phase of the DP on the BM, we deduce that the wave is traveling forward at an apparent speed of about 1.6 m/second (DP changes 1.2 cycles in 1mm) from a place 7.8 mm from the base. We also find a dominant reverse traveling wave at the DP frequency that starts at a place near the f2 place (starting from 7.8mm from the base). It does not start from the DP place. Or the reverse traveling wave from the DP place is too weak to be observed. The DP wave on the BM appears to be traveling back towards the stapes at a slow speed first near the f2 place region, then travel at a relatively high speed (DP travels 6.5mm in 0.25 cycles) back to the stapes. The apparent speed is much faster (about 52 m/s) compared to the apparent forward traveling wave speed (about 1.6 m/s) around the DP place. The total phase delay of the reverse traveling wave from the generating place to the stapes is smaller than the phase delay from the generation place to the DP place. Like the simulation results from the

112

basal part of the cochlea (Figure 3-6), the phase of the forward traveling DP wave and the phase of the reverse traveling DP wave are almost symmetric with regard to the starting point.
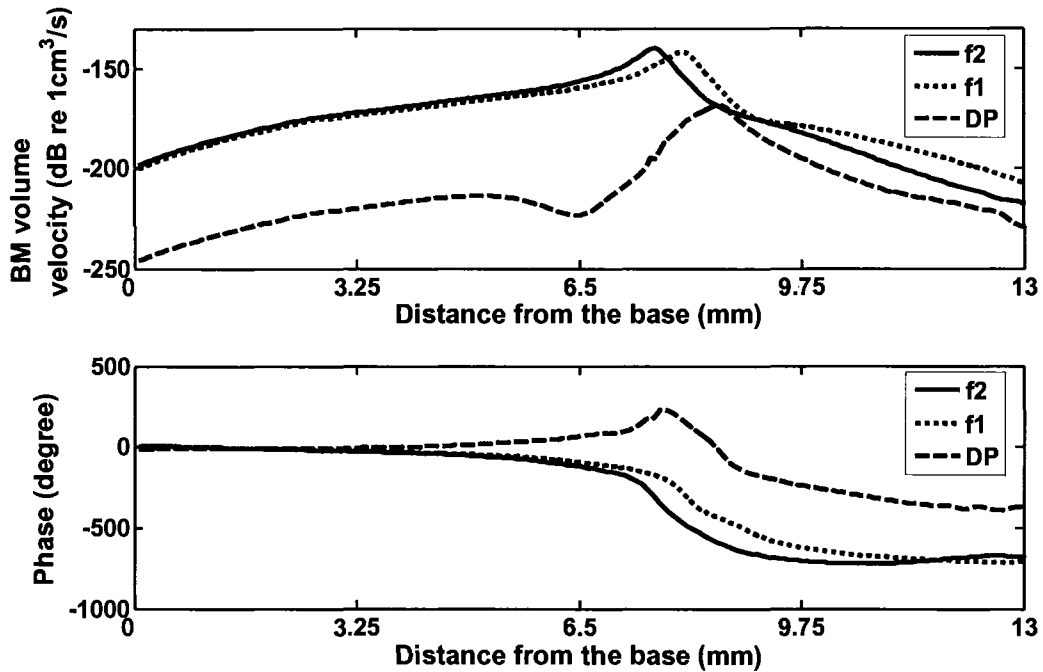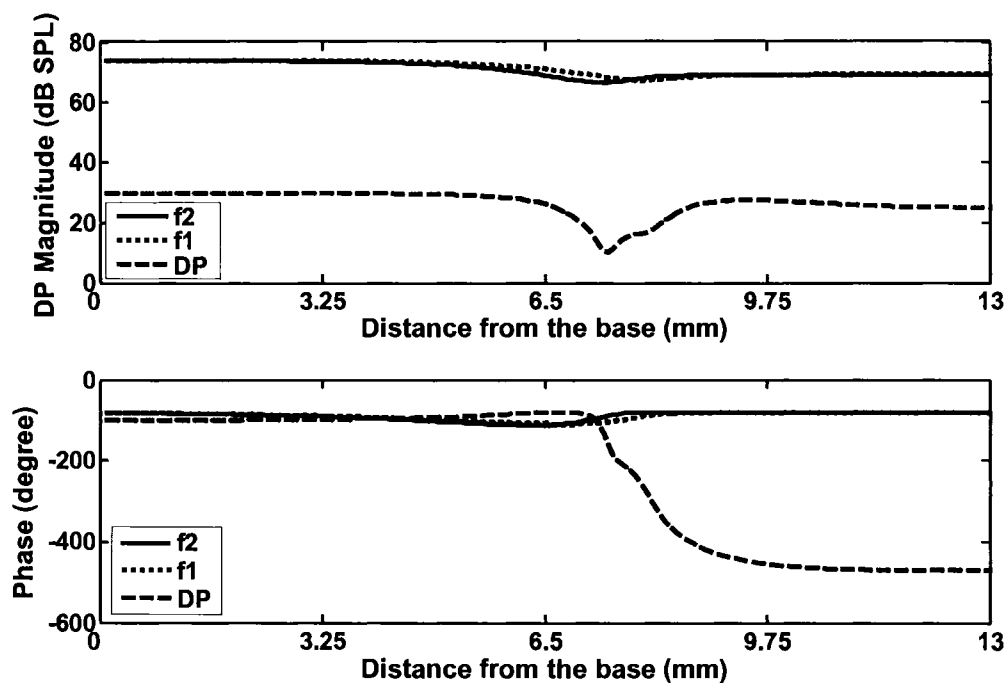

Figure 3- 9 SV pressure pattern (magnitude and phase) along the length of the cochlea from our model. The frequencies of the f1 tone, f2 tone and the DP (2f1-f2) are 2.5k Hz, 3 kHz and 2 kHz respectively. The green dotted lines are the f1 responses. The red solid lines are the f2 responses. The blue dashed lines are the DP responses.

Unlike the measured DP pressure in the ST (Dong and Olson 2008), our model results of SV pressure (Figure 3-9) do not show obvious DP pressure peaks. We have explained before that this is because our model is a 1-D model and the SV pressure here represents the average pressure in the SV (Lu et al. Submitted). The DP pressure in the SV has a big notch in the f1 tone and f2 tone overlap region. The reverse traveling wave of DP pressure also can be observed in the pressure plot. It starts roughly at a place about 6.8mm from the base. It is much basal than the f2 place. The apparent speed of the reverse traveling DP wave in the SV fluid is about 250 m/s (DP changes about 20 degree in 6.8 mm), much faster than the traveling wave on the BM. This suggests that the stapes should vibrate earlier than the DP place, if we agree that the stapes vibration is driven by the SV pressure just inside the stapes.

3.4 Conclusion & Discussion

The comparisons of the DPOAE input/output function (Figure 3-3) are fairly good. The model result has a small dip around 70 dB SPL and saturation after 80 dB, similar to reported experimental data (Mills 2000). The comparisons of the model results with Ren's experimental data (Figure 3-7) are qualitatively satisfying. The shapes of the magnitude curves show peaking of the DP in roughly the same way. Both the model curves and the experimental data are "irregular", not smooth. The phase angles versus distance along the cochlea are similar although the slope of the experimental data slope less at more basal positions, and are concave down, while the model curves are closer to being straight lines. In the comparison of frequency response of model and experimental data, the phase responses are similar (see Panel B and D in Figure 4). But the magnitude of DPOAE from the model in the high level input (55 dB and 61 dB SPL) cannot match the experimental data (see Panel A and C in Figure 3-4). The possible reasons for this difference are: First, there are no fine details of middle ear transfer function (METF) in our model. The gain of METF was set to be a constant for the frequency range we are studying (0 to 3 kHz). Second, the ear canal model is not considered in this study. The DPOAE studies usually require a sealed ear canal which should be modeled as a capacitor plus a resistor in our model. It should have its own gain and cut-off frequency.

"The DP generation site" and "the reverse traveling wave starting point" are two different concepts. It is generally agreed that the majority of the DP is generated by nonlinear distortion in the region where f1 tone and f2 tone have maximum overlap. This means the DP generation site is from a location near the f2 place. After been generated, the DP propagates to both forward and reverse direction, causing reflection of DP along the cochlea (Kim et al. 1980; Shera and Guinan 1999). Therefore the DPOAE measured in the ear canal consists of more than one component. The model predicts the backward DP traveling wave on the BM is not dominant until one is basal from the f2 place. Because the generation zone (f1 and f2 overlapping places) is a relatively large area and the f1 and f2 phases change rapidly in this area (more than two cycles in Figure 3-6 and Figure 3-7), the DP components generated in this area may cancel each other. The evidence of this hypothesis is that there are peaks and valleys in their magnitude and their phase show irregularities at the peak region (see Figure 3-6 and Figure 3-7). This may explain why we observe the reverse traveling wave of DP on the BM in our model starts at a place near to the f2 place.

Does the DP propagate to the stapes via a reverse traveling wave or a compression wave? The first thing we need to know before we give the answer is that, do we refer to the DP pressure wave in the SV fluid, or we refer to the reverse traveling wave on the BM at the DP frequency? The stapes vibration at

116

the DP frequency is driven by the DP pressure in the SV just inside the stapes, not by the BM vibration at the DP frequency in the basal site of the cochlea. The DP pressure wave has not been recorded in the SV longitudinally along the cochlea yet, although it has been recorded in the ST at a fixed point (Dong and Olson 2008). Therefore, it is not easy to directly prove or reject the existence of a reverse DP traveling pressure wave in the SV by experimental data. Our model results show that the reverse traveling waves of both the DP pressures and the BM motion can be found *in* SV fluid and *on* the BM respectively. A dominant reverse traveling wave on the BM at the DP frequency starts at a place near the f2 place, while a forward traveling wave on the BM dominates near the DP place. The reverse traveling wave on the BM is faster compared to the forward traveling wave in the DP place.

Interpreted as a wave, in which the slope versus distance implies directionality, the DP pressure wave in the SV fluid is predominately reverse-traveling at a significantly more basal region than when the BM's DP wave is predominately reverse-traveling (see Figure 3-9). In the region of the DP's velocity peak on the BM, the DP pressure wave in the SV is forward-traveling. The reverse DP pressure traveling wave in the SV fluid is much faster. The longitudinal patterns of both DP pressure in SV and DP on the BM depend on the place of observation. In some region the forward traveling waves dominate, while in other region

117

reverse traveling waves dominate.

Does the stapes vibrate first in relative to the DP site? Notice that the slope of the phase curve of the reverse traveling DP pressure wave in the SV nearly mirrors the slope in the forward-traveling f1 and f2 waves. In other words, over about 6.8 mm of cochlea, it appears that the apparent velocity of the DP pressure wave in SV is around 250 m/s, traveling *backwards*. This number is calculated on the basis of a 20 degree phase change at the DP frequency (read off the DP curve in Figure 3-9). Relative to the same time frame of reference, the DP on the BM has traveled forward about 2mm at an apparent speed of about 3m/second. This velocity is calculated based on 400 degrees lag (Figure 3-8). Since in this case, the pressure sources of DP are near the primary frequencies, the DP pressure in SV drives the stapes, and the load is arguably resistive (it matters little from a numeric standpoint), the stapes velocity at the DP frequency should lead the BM velocity at the DP frequency. In other words, the stapes vibrates first.

3.5 References

Ami, M., A. Abdullah, M. A. Awang, B. Liyab and L. Saim (2008). "Relation of distortion product otoacoustic emission with tinnitus." Laryngoscope 118(4): 712-7.

Dong, W. and E. S. Olson (2005). "Two-tone distortion in intracochlear pressure." J Acoust Soc Am 117(5): 2999-3015.

Dong, W. and E. S. Olson (2006). "Middle ear forward and reverse transmission in gerbil." J Neurophysiol 95(5): 2951-61.

Dong, W. and E. S. Olson (2008). "Supporting evidence for reverse cochlear traveling waves." J Acoust Soc Am 123(1): 222-40.

Faulstich, M. and M. Kossl (2000). "Evidence for multiple DPOAE components based upon group delay of the 2f(1)-f(2) distortion in the gerbil." Hear Res 140(1-2): 99-110.

Hall, J. W., 3rd, J. E. Baer, P. A. Chase and M. K. Schwaber (1994). "Clinical application of otoacoustic emissions: what do we know about factors influencing measurement and analysis?" Otolaryngol Head Neck Surg 110(1): 22-38.

He, W., A. Fridberger, E. Porsov, K. Grosh and T. Ren (2008). "Reverse wave propagation in the cochlea." Proc Natl Acad Sci U S A 105(7): 2729-33.

He, W., A. L. Nuttall and T. Ren (2007). "Two-tone distortion at different longitudinal locations on the basilar membrane." Hear Res 228(1-2): 112-22.

Hubbard, A. E., S. Lu, J. Spisak and D. C. Mountain (2006). The Evolution of Multicompartment Cochlear Model. Auditory Mechanics: Processes and Models. A. L. Nuttall, T. Ren, P. Gillespice, K. Grosh and E. De Boer. New jersey, London, Singapore, Beijing, Shanghai, Hong Kong, Taibei, Chennai, World Scientific: 458-465.

Hubbard, A. E. and D. C. Mountain (1983). "Alternating current delivered into the scala media alters sound pressure at the eardrum." Science 222(4623): 510-2.

Hubbard, A. E., D. C. Mountain and F. Chen (2003). Time-domain responses from a nonlinear sandwich model of the cochlea. Biophysics of the

Cochlea: From Molecules to Models. A. W. Gummer. New Jersey, London, Singapore, Hong Kong., World Scientific: 351-358.

Hubbard, A. E., Z. Yang, L. Shatz and D. C. Mountain (2000). Multi-mode Cochlear models. Recent Developments in Auditory Mechanics. H. Wada. Singapore, New Jersey, London, Hong Kong, World Scientific: 167-173.

Kalluri, R. and C. A. Shera (2001). "Distortion-product source unmixing: a test of the two-mechanism model for DPOAE generation." J Acoust Soc Am 109(2): 622-37.

Karavitaki, K. D. and D. C. Mountain (2007). "Evidence for oscillatory fluid flow in the tunnel of Corti." Biophys J.

Kemp, D. T. (1978). "Stimulated acoustic emissions from within the human auditory system." J Acoust Soc Am 64(5): 1386-91.

Kemp, D. T. (1979). "Evidence of mechanical nonlinearity and frequency selective wave amplification in the cochlea." Arch Otorhinolaryngol 224(1-2): 37-45.

Kemp, D. T. (2002). "Otoacoustic emissions, their origin in cochlear function, and use." Br Med Bull 63: 223-41.

Kemp, D. T., P. Bray, L. Alexander and A. M. Brown (1986). "Acoustic emission cochleography--practical aspects." Scand Audiol Suppl 25: 71-95.

Kim, D. O., C. E. Molnar and J. W. Matthews (1980). "Cochlear mechanics: nonlinear behavior in two-tone responses as reflected in cochlear-nerve-fiber responses and in ear-canal sound pressure." J Acoust Soc Am 67(5): 1704-21.

Kimberley, B. P., D. K. Brown and J. J. Eggermont (1993). "Measuring human cochlear traveling wave delay using distortion product emission phase responses." J Acoust Soc Am 94(3 Pt 1): 1343-50.

Knight, R. D. and D. T. Kemp (2001). "Wave and place fixed DPOAE maps of the human ear." J Acoust Soc Am 109(4): 1513-25.

Lu, S., F. Chen, D. C. Mountain and A. E. Hubbard (Submitted). "Is Longitudinal Fluid Flow in The Organ of Corti Fundamental to Cochlear Function?" Submitted.

Lu, S., J. Spisak, D. C. Mountain and A. E. Hubbard (2006). A New Multicompartments Model of Cochlea. Auditory Mechanics: Processes and

Models. A. L. Nuttall, T. Ren, P. Gillespice, K. Grosh and E. De Boer. New jersey, London, Singapore, Beijing, Shanghai, Hong Kong, Taibei, Chennai, World Scientific: 508-509.

Magnan, P., A. Dancer, R. Probst, J. Smurzynski and P. Avan (1999). "Intracochlear acoustic pressure measurements: transfer functions of the middle ear and cochlear mechanics." Audiol Neurootol 4(3-4): 123-8.

Mills, D. M. (2000). "Frequency responses of two- and three-tone distortion product otoacoustic emissions in Mongolian gerbils." J Acoust Soc Am 107(5 Pt 1): 2586-602.

Mountain, D. C. and A. E. Hubbard (1989). "Rapid force production in the cochlea." Hear Res 42(2-3): 195-202.

Mountain, D. C., H. H. Nakajima, S. Rafee and A. E. Hubbard (2000). Forward and Reverse Traveling Waves in the Gerbil Cochlea. Recent Developments in Auditory Mechanics. H. Wada. Singapore, New Jersey, London, Hong Kong, World Scientific: 102-108.

Murata, K., T. Moriyama, Y. Hosokawa and S. Minami (1991). "Alternating current induced otoacoustic emissions in the guinea pig." Hear Res 55(2): 201-14.

Nakajima, H. H., E. S. Olson, D. C. Mountain and A. E. Hubbard (1994). "Electrically evoked otoacoustic emissions from the apical turns of the gerbil cochlea." J Acoust Soc Am 96(2 Pt 1): 786-94.

Olson, E. S. (1998). "Observing middle and inner ear mechanics with novel intracochlear pressure sensors." J Acoust Soc Am 103(6): 3445-63.

Ren, T. (2002). "Longitudinal pattern of basilar membrane vibration in the sensitive cochlea." Proc Natl Acad Sci U S A 99(26): 17101-6.

Ren, T. (2004). "Reverse propagation of sound in the gerbil cochlea." Nat Neurosci 7(4): 333-4.

Ren, T., W. He, M. Scott and A. L. Nuttall (2006). "Group delay of acoustic emissions in the ear." J Neurophysiol 96(5): 2785-91.

Ren, T. and A. L. Nuttall (1995). "Extracochlear electrically evoked otoacoustic emissions: a model for in vivo assessment of outer hair cell electromotility." Hear Res 92(1-2): 178-83.

Ren, T. and A. L. Nuttall (2001). "Basilar membrane vibration in the basal turn of the sensitive gerbil cochlea." Hear Res 151(1-2): 48-60.

Ruggero, M. A. and A. N. Temchin (2002). "The roles of the external, middle, and inner ears in determining the bandwidth of hearing." Proc Natl Acad Sci U S A 99(20): 13206-10.

Shera, C. A. and J. J. Guinan, Jr. (1999). "Evoked otoacoustic emissions arise by two fundamentally different mechanisms: a taxonomy for mammalian OAEs." J Acoust Soc Am 105(2 Pt 1): 782-98.

Shera, C. A., A. Tubis and C. L. Talmadge (2004). "Do forward- and backward-traveling waves occur within the cochlea? Countering the critique of Nobili et al." J Assoc Res Otolaryngol 5(4): 349-59.

Shera, C. A., A. Tubis, C. L. Talmadge, E. de Boer, P. F. Fahey and J. J. Guinan, Jr. (2007). "Allen-Fahey and related experiments support the predominance of cochlear slow-wave otoacoustic emissions." J Acoust Soc Am 121(3): 1564-75.

Stone, K. A., B. D. Smith, J. M. Lembke, L. A. Clark and M. B. McLellan (2000). "Universal newborn hearing screening." J Fam Pract 49(11): 1012-6.

Vetesnik, A., R. Nobili and A. Gummer (2006). "How does the inner ear generate distortion product otoacoustic emissions?. Results from a realistic model of the human cochlea." ORL J Otorhinolaryngol Relat Spec 68(6): 347-52.

Voss, S. E. and C. A. Shera (2004). "Simultaneous measurement of middle-ear input impedance and forward/reverse transmission in cat." J Acoust Soc Am 116(4 Pt 1): 2187-98.

Wilson, H. K. and M. E. Lutman (2006). "Mechanisms of generation of the 2f2-f1 distortion product otoacoustic emission in humans." J Acoust Soc Am 120(4): 2108-15.

Wilson, J. P. (1980). "Model for cochlear echoes and tinnitus based on an observed electrical correlate." Hear Res 2(3-4): 527-32.

Wilson, J. P. and J. R. Johnstone (1973). "Basilar membrane correlates of the combination tone 2f 1 -f 2." Nature 241(5386): 206-7.

Withnell, R. H., L. A. Shaffer and C. L. Talmadge (2003). "Generation of DPOAEs in the guinea pig." Hear Res 178(1-2): 106-17.

Zweig, G. and C. A. Shera (1995). "The origin of periodicity in the spectrum of evoked otoacoustic emissions." J Acoust Soc Am **98**(4): 2018-47.

Bibliography

List of Abbreviated Journal Titles

Am J Physiol	American Journal of Physiology
Ann Biomed Eng	Annals of Biomedical Engineering
Biophys J	Biophysical Journal
Brain Behav Evo	Brain, Behavior and Evolution
Curr Opin Neurobiol	Current Opinion in Neurobiology
Hear Res	Hearing Research
J Acoust Soc Am	Journal of the Acoustical Society of America
J Assoc Res Otolaryngol	Journal of the Association for Research in Otolaryngology
J Biomech Eng	Journal of Biomechanical Engineering
J Fam Pract	Journal of Family Practice
J Membr Biol	Journal of Membrane Biology
J Morphol	Journal of Morphology
J Neurophysiol	Journal of Neurophysiology
J Physiol	Journal of Physiology
Nat Neurosci	Nature Neuroscience
Neurosci	Neuroscience
ORL J Otorhinolaryngol Relat Spec	ORL; Journal of Oto-Rhino-Laryngology and Its Related Specialties
Otolaryngol Head Neck Surg	Otolaryngology and Head and Neck Surgery
Proc Natl Acad Sci U S A	Proceedings of the National Academy of Sciences of the United States of America
Trans Am Otol Soc	Transactions / American Otological Society

124

Ami, M., A. Abdullah, M. A. Awang, B. Liyab and L. Saim (2008). "Relation of distortion product otoacoustic emission with tinnitus." Laryngoscope **118**(4): 712-7.

Brownell, W. E., C. R. Bader, D. Bertrand and Y. de Ribaupierre (1985). "Evoked mechanical responses of isolated cochlear outer hair cells." Science **227**(4683): 194-6.

Cai, H., B. Shoelson and R. S. Chadwick (2004). "Evidence of tectorial membrane radial motion in a propagating mode of a complex cochlear model." Proc Natl Acad Sci U S A **101**(16): 6243-8.

Chadwick, R. S. (1998). "Compression, gain, and nonlinear distortion in an active cochlear model with subpartitions." Proc Natl Acad Sci U S A **95**(25): 14594-9.

Chadwick, R. S., E. K. Dimitriadis and K. H. Iwasa (1996). "Active control of waves in a cochlear model with subpartitions." Proc Natl Acad Sci U S A **93**(6): 2564-9.

Chan, D. K. and A. J. Hudspeth (2005). "Mechanical responses of the organ of corti to acoustic and electrical stimulation in vitro." Biophys J **89**(6): 4382-95.

Cheatham, M. A. and P. Dallos (1994). "Stimulus biasing: a comparison between cochlear hair cell and organ of Corti response patterns." Hear Res **75**(1-2): 103-13.

Cohen, A. and M. Furst (2004). "Integration of outer hair cell activity in a one-dimensional cochlear model." J Acoust Soc Am **115**(5 Pt 1): 2185-92.

Dallos, P. (1983). "Some electrical circuit properties of the organ of Corti. I. Analysis without reactive elements." Hear Res **12**(1): 89-119.

Dallos, P. (1985). "Response characteristics of mammalian cochlear hair cells." J Neurosci **5**(6): 1591-608.

Dallos, P. (1986). "Neurobiology of cochlear inner and outer hair cells: intracellular recordings." Hear Res **22**: 185-98.

Dallos, P. and B. N. Evans (1995). "High-frequency motility of outer hair cells and the cochlear amplifier." Science **267**(5206): 2006-9.

Davis, H. (1958). "A mechano-electrical theory of cochlear action." Trans Am Otol Soc **46**: 180-96.

de Boer, E. (1983). "Power amplification in an active model of the cochlea--short-wave case." J Acoust Soc Am **73**(2): 577-9.

de Boer, E. (1990). "Can shape deformations of the organ of Corti influence the travelling wave in the cochlea?" Hear Res **44**(1): 83-92.

de Boer, E. (1990). Wave-propagation modes and boundary conditions for the ulfendahl-flock-khanna preparation. The Mechanics and Biophysics of Hearing Proceedings. P. Dallos. Berlin, Springer-Verlag: 333-339.

de Boer, E. (1993). "The sulcus connection. On a mode of participation of outer hair cells in cochlear mechanics." J Acoust Soc Am **93**(5): 2845-59.

Dong, W. and E. S. Olson (2005). "Two-tone distortion in intracochlear pressure." J Acoust Soc Am **117**(5): 2999-3015.

Dong, W. and E. S. Olson (2006). "Middle ear forward and reverse transmission in gerbil." J Neurophysiol **95**(5): 2951-61.

Dong, W. and E. S. Olson (2008). "Supporting evidence for reverse cochlear traveling waves." J Acoust Soc Am **123**(1): 222-40.

Dong, X. X., M. Ospeck and K. H. Iwasa (2002). "Piezoelectric reciprocal relationship of the membrane motor in the cochlear outer hair cell." Biophys J **82**(3): 1254-9.

Edge, R. M., B. N. Evans, M. Pearce, C. P. Richter, X. Hu and P. Dallos (1998). "Morphology of the unfixed cochlea." Hear Res **124**(1-2): 1-16.

Faulstich, M. and M. Kossl (2000). "Evidence for multiple DPOAE components based upon group delay of the 2f(1)-f(2) distortion in the gerbil." Hear Res **140**(1-2): 99-110.

Frank, G., W. Hemmert and A. W. Gummer (1999). "Limiting dynamics of high-frequency electromechanical transduction of outer hair cells." Proc Natl Acad Sci U S A **96**(8): 4420-5.

Geisler, C. D. (1986). "A model of the effect of outer hair cell motility on cochlear vibrations." Hear Res **24**(2): 125-31.

Geisler, C. D. (1991). "A cochlear model using feedback from motile outer hair cells." Hear Res **54**(1): 105-17.

Geisler, C. D. (1993). "A realizable cochlear model using feedback from motile outer hair cells." Hear Res **68**(2): 253-62.

Geisler, C. D. and C. Sang (1995). "A cochlear model using feed-forward outer-hair-cell forces." Hear Res **86**(1-2): 132-46.

Greenwood, D. D. (1990). "A cochlear frequency-position function for several species--29 years later." J Acoust Soc Am **87**(6): 2592-605.

Grosh, K., J. Zheng, Y. Zou, E. de Boer and A. L. Nuttall (2004). "High-frequency electromotile responses in the cochlea." J Acoust Soc Am **115**(5 Pt 1): 2178-84.

Hall, J. W., 3rd, J. E. Baer, P. A. Chase and M. K. Schwaber (1994). "Clinical application of otoacoustic emissions: what do we know about factors influencing measurement and analysis?" Otolaryngol Head Neck Surg **110**(1): 22-38.

He, W., A. Fridberger, E. Porsov, K. Grosh and T. Ren (2008). "Reverse wave propagation in the cochlea." Proc Natl Acad Sci U S A **105**(7): 2729-33.

He, W., A. L. Nuttall and T. Ren (2007). "Two-tone distortion at different longitudinal locations on the basilar membrane." Hear Res **228**(1-2): 112-22.

Holton, T. and A. J. Hudspeth (1986). "The transduction channel of hair cells from the bull-frog characterized by noise analysis." J Physiol **375**: 195-227.

Hubbard, A. (1993). "A traveling-wave amplifier model of the cochlea." Science **259**(5091): 68-71.

Hubbard, A. E. and C. D. Geisler (1972). "A hybrid-computer model of the cochlear partition." J Acoust Soc Am **51**(6): 1895-903.

Hubbard, A. E., S. Lu, J. Spisak and D. C. Mountain (2006). The Evolution of Multicompartment Cochlear Model. Auditory Mechanics: Processes and Models. A. L. Nuttall, T. Ren, P. Gillespice, K. Grosh and E. De Boer. New jersey, London, Singapore, Beijing, Shanghai, Hong Kong, Taibei, Chennai, World Scientific: 458-465.

Hubbard, A. E. and D. C. Mountain (1983). "Alternating current delivered into the scala media alters sound pressure at the eardrum." Science **222**(4623): 510-2.

Hubbard, A. E., D. C. Mountain and F. Chen (2003). Time-domain responses from a nonlinear sandwich model of the cochlea. Biophysics of the Cochlea: From Molecules to Models. A. W. Gummer. New Jersey, London, Singapore, Hong Kong., World Scientific: 351-358.

127

Hubbard, A. E., Z. Yang, L. Shatz and D. C. Mountain (2000). Multi-mode Cochlear models. Recent Developments in Auditory Mechanics. H. Wada. Singapore, New Jersey, London, Hong Kong, World Scientific: 167-173.

Hudspeth, A. (1997). "Mechanical amplification of stimuli by hair cells." Curr Opin Neurobiol 7(4): 480-6.

Iwasa, K. H. (2001). "A two-state piezoelectric model for outer hair cell motility." Biophys J 81(5): 2495-506.

Iwasa, K. H. and R. S. Chadwick (1992). "Elasticity and active force generation of cochlear outer hair cells." J Acoust Soc Am 92(6): 3169-73.

Kalluri, R. and C. A. Shera (2001). "Distortion-product source unmixing: a test of the two-mechanism model for DPOAE generation." J Acoust Soc Am 109(2): 622-37.

Kanis, L. J. and E. de Boer (1993). "Self-suppression in a locally active nonlinear model of the cochlea: a quasilinear approach." J Acoust Soc Am 94(6): 3199-206.

Karavitaki, K. D. and D. C. Mountain (2007). "Evidence for oscillatory fluid flow in the tunnel of Corti." Biophys J.

Kemp, D. T. (1978). "Stimulated acoustic emissions from within the human auditory system." J Acoust Soc Am 64(5): 1386-91.

Kemp, D. T. (1979). "Evidence of mechanical nonlinearity and frequency selective wave amplification in the cochlea." Arch Otorhinolaryngol 224(1-2): 37-45.

Kemp, D. T. (2002). "Otoacoustic emissions, their origin in cochlear function, and use." Br Med Bull 63: 223-41.

Kemp, D. T., P. Bray, L. Alexander and A. M. Brown (1986). "Acoustic emission cochleography--practical aspects." Scand Audiol Suppl 25: 71-95.

Kennedy, H. J., M. G. Evans, A. C. Crawford and R. Fettiplace (2003). "Fast adaptation of mechanoelectrical transducer channels in mammalian cochlear hair cells." Nat Neurosci 6(8): 832-6.

Kiang, N. Y., M. B. Sachs and W. T. Peake (1967). "Shapes of tuning curves for single auditory-nerve fibers." J Acoust Soc Am 42(6): 1341-2.

Kim, D. O., C. E. Molnar and J. W. Matthews (1980). "Cochlear mechanics: nonlinear behavior in two-tone responses as reflected in cochlear-nerve-

fiber responses and in ear-canal sound pressure." <u>J Acoust Soc Am</u> **67**(5): 1704-21.

Kimberley, B. P., D. K. Brown and J. J. Eggermont (1993). "Measuring human cochlear traveling wave delay using distortion product emission phase responses." <u>J Acoust Soc Am</u> **94**(3 Pt 1): 1343-50.

Knight, R. D. and D. T. Kemp (2001). "Wave and place fixed DPOAE maps of the human ear." <u>J Acoust Soc Am</u> **109**(4): 1513-25.

Kolston, P. J., E. de Boer, M. A. Viergever and G. F. Smoorenburg (1990). "What type of force does the cochlear amplifier produce?" <u>J Acoust Soc Am</u> **88**(4): 1794-801.

Lay, D. M. (1972). "The anatomy, physiology, functional significance and evolution of specialized hearing organs of gerbilline rodents." <u>J Morphol</u> **138**(1): 41-120.

Liao, Z., A. S. Popel, W. E. Brownell and A. A. Spector (2005). "High-frequency force generation in the constrained cochlear outer hair cell: a model study." <u>J Assoc Res Otolaryngol</u> **6**(4): 378-89.

Liao, Z., A. S. Popel, W. E. Brownell and A. A. Spector (2005). "Modeling high-frequency electromotility of cochlear outer hair cell in microchamber experiment." <u>J Acoust Soc Am</u> **117**(4 Pt 1): 2147-57.

Liberman, M. C., J. Gao, D. Z. He, X. Wu, S. Jia and J. Zuo (2002). "Prestin is required for electromotility of the outer hair cell and for the cochlear amplifier." <u>Nature</u> **419**(6904): 300-4.

Lim, K. M. and H. Li (2006). "A two-layer outer hair cell model with orthotropic piezoelectric properties: Correlation of cell resonant frequencies with tuning in the cochlea." <u>J Biomech</u>.

Lu, S., F. Chen, D. C. Mountain and A. E. Hubbard (Submitted). "Is Longitudinal Fluid Flow in The Organ of Corti Fundamental to Cochlear Function?" <u>Submitted</u>.

Lu, S., J. Spisak, D. C. Mountain and A. E. Hubbard (2006). A New Multicompartments Model of Cochlea. <u>Auditory Mechanics: Processes and Models</u>. A. L. Nuttall, T. Ren, P. Gillespice, K. Grosh and E. De Boer. New jersey, London, Singapore, Beijing, Shanghai, Hong Kong, Taibei, Chennai, World Scientific: 508-509.

Lu, T. K., S. Zhak, P. Dallos and R. Sarpeshkar (2006). "Fast cochlear amplification with slow outer hair cells." Hear Res **214**(1-2): 45-67.

Magnan, P., A. Dancer, R. Probst, J. Smurzynski and P. Avan (1999). "Intracochlear acoustic pressure measurements: transfer functions of the middle ear and cochlear mechanics." Audiol Neurootol **4**(3-4): 123-8.

Mammano, F. and J. F. Ashmore (1993). "Reverse transduction measured in the isolated cochlea by laser Michelson interferometry." Nature **365**(6449): 838-41.

Markin, V. S. and A. J. Hudspeth (1995). "Modeling the active process of the cochlea: phase relations, amplification, and spontaneous oscillation." Biophys J **69**(1): 138-47.

Martin, P. and A. J. Hudspeth (1999). "Active hair-bundle movements can amplify a hair cell's response to oscillatory mechanical stimuli." Proc Natl Acad Sci U S A **96**(25): 14306-11.

Mills, D. M. (2000). "Frequency responses of two- and three-tone distortion product otoacoustic emissions in Mongolian gerbils." J Acoust Soc Am **107**(5 Pt 1): 2586-602.

Misrahy, G. A., K. M. Hildreth, E. W. Shinabarger and W. J. Gannon (1958). "Electrical properties of wall of endolymphatic space of the cochlea (guinea pig)." Am J Physiol **194**(2): 396-402.

Mountain, D. C. and A. E. Hubbard (1989). "Rapid force production in the cochlea." Hear Res **42**(2-3): 195-202.

Mountain, D. C. and A. E. Hubbard (1994). "A piezoelectric model of outer hair cell function." J Acoust Soc Am **95**(1): 350-4.

Mountain, D. C., H. H. Nakajima, S. Rafee and A. E. Hubbard (2000). Forward and Reverse Traveling Waves in the Gerbil Cochlea. Recent Developments in Auditory Mechanics. H. Wada. Singapore, New Jersey, London, Hong Kong, World Scientific: 102-108.

Muller, M. (1996). "The cochlear place-frequency map of the adult and developing Mongolian gerbil." Hear Res **94**(1-2): 148-56.

Murata, K., T. Moriyama, Y. Hosokawa and S. Minami (1991). "Alternating current induced otoacoustic emissions in the guinea pig." Hear Res **55**(2): 201-14.

130

Naidu, R. C. and D. C. Mountain (1998). "Measurements of the stiffness map challenge a basic tenet of cochlear theories." Hear Res 124(1-2): 124-31.

Naidu, R. C. and D. C. Mountain (2001). "Longitudinal coupling in the basilar membrane." J Assoc Res Otolaryngol 2(3): 257-67.

Nakajima, H. H., E. S. Olson, D. C. Mountain and A. E. Hubbard (1994). "Electrically evoked otoacoustic emissions from the apical turns of the gerbil cochlea." J Acoust Soc Am 96(2 Pt 1): 786-94.

Neely, S. T. (1993). "A model of cochlear mechanics with outer hair cell motility." J Acoust Soc Am 94(1): 137-46.

Neely, S. T. and D. O. Kim (1983). "An active cochlear model showing sharp tuning and high sensitivity." Hear Res 9(2): 123-30.

Neely, S. T. and D. O. Kim (1986). "A model for active elements in cochlear biomechanics." J Acoust Soc Am 79(5): 1472-80.

Nowotny, M. and A. W. Gummer (2006). "Nanomechanics of the subtectorial space caused by electromechanics of cochlear outer hair cells." Proc Natl Acad Sci U S A 103(7): 2120-5.

Olson, E. S. (1998). "Observing middle and inner ear mechanics with novel intracochlear pressure sensors." J Acoust Soc Am 103(6): 3445-63.

Olson, E. S. (1999). "Direct measurement of intra-cochlear pressure waves." Nature 402(6761): 526-9.

Olson, E. S. and D. C. Mountain (1991). "In vivo measurement of basilar membrane stiffness." J Acoust Soc Am 89(3): 1262-75.

Peterson, L. C. and B. P. Bogert (1950). "A Dynamical Theory of Cochlea." J Acoust Soc Am 22(3): 369-381.

Plassmann, W., W. Peetz and M. Schmidt (1987). "The cochlea in gerbilline rodents." Brain Behav Evol 30(1-2): 82-101.

Rabbitt, R. D., H. E. Ayliffe, D. Christensen, K. Pamarthy, C. Durney, S. Clifford and W. E. Brownell (2005). "Evidence of piezoelectric resonance in isolated outer hair cells." Biophys J 88(3): 2257-65.

Rabbitt, R. D., R. Boyle, G. R. Holstein and S. M. Highstein (2005). "Hair-cell versus afferent adaptation in the semicircular canals." J Neurophysiol 93(1): 424-36.

Ramamoorthy, S., N. V. Deo and K. Grosh (2007). "A mechano-electro-acoustical model for the cochlea: response to acoustic stimuli." J Acoust Soc Am **121**(5 Pt1): 2758-73.

Ren, T. (2002). "Longitudinal pattern of basilar membrane vibration in the sensitive cochlea." Proc Natl Acad Sci U S A **99**(26): 17101-6.

Ren, T. (2004). "Reverse propagation of sound in the gerbil cochlea." Nat Neurosci **7**(4): 333-4.

Ren, T., W. He, M. Scott and A. L. Nuttall (2006). "Group delay of acoustic emissions in the ear." J Neurophysiol **96**(5): 2785-91.

Ren, T. and A. L. Nuttall (1995). "Extracochlear electrically evoked otoacoustic emissions: a model for in vivo assessment of outer hair cell electromotility." Hear Res **92**(1-2): 178-83.

Ren, T. and A. L. Nuttall (2001). "Basilar membrane vibration in the basal turn of the sensitive gerbil cochlea." Hear Res **151**(1-2): 48-60.

Rhode, W. S. (1971). "Observations of the vibration of the basilar membrane in squirrel monkeys using the Mossbauer technique." J Acoust Soc Am **49**(4): Suppl 2:1218+.

Ricci, A. J., A. C. Crawford and R. Fettiplace (2000). "Active hair bundle motion linked to fast transducer adaptation in auditory hair cells." J Neurosci **20**(19): 7131-42.

Ruggero, M. A. and A. N. Temchin (2002). "The roles of the external, middle, and inner ears in determining the bandwidth of hearing." Proc Natl Acad Sci U S A **99**(20): 13206-10.

Salt, A. N. and T. Konishi (1986). The cochlear fluids: perilymph and endolymph. Neurobiology of Hearing: The Cochlea. R. A. Altschuler and R. P. Bobbin. New York, Raven Press: 123-137.

Santos-Sacchi, J. (1989). "Asymmetry in voltage-dependent movements of isolated outer hair cells from the organ of Corti." J Neurosci **9**(8): 2954-62.

Scherer, M. P. and A. W. Gummer (2004). "Vibration pattern of the organ of Corti up to 50 kHz: evidence for resonant electromechanical force." Proc Natl Acad Sci U S A **101**(51): 17652-7.

Shera, C. A. and J. J. Guinan, Jr. (1999). "Evoked otoacoustic emissions arise by two fundamentally different mechanisms: a taxonomy for mammalian OAEs." J Acoust Soc Am **105**(2 Pt 1): 782-98.

Shera, C. A., A. Tubis and C. L. Talmadge (2004). "Do forward- and backward-traveling waves occur within the cochlea? Countering the critique of Nobili et al." J Assoc Res Otolaryngol **5**(4): 349-59.

Shera, C. A., A. Tubis, C. L. Talmadge, E. de Boer, P. F. Fahey and J. J. Guinan, Jr. (2007). "Allen-Fahey and related experiments support the predominance of cochlear slow-wave otoacoustic emissions." J Acoust Soc Am **121**(3): 1564-75.

Spector, A. A. (1999). "Nonlinear electroelastic model for the composite outer hair cell wall." ORL J Otorhinolaryngol Relat Spec **61**(5): 287-93.

Spector, A. A., W. E. Brownell and A. S. Popel (2003). "Effect of outer hair cell piezoelectricity on high-frequency receptor potentials." J Acoust Soc Am **113**(1): 453-61.

Spector, A. A., N. Deo, K. Grosh, J. T. Ratnanather and R. M. Raphael (2006). "Electromechanical models of the outer hair cell composite membrane." J Membr Biol **209**(2-3): 135-52.

Spector, A. A. and R. P. Jean (2004). "Modes and balance of energy in the piezoelectric cochlear outer hair cell wall." J Biomech Eng **126**(1): 17-25.

Spector, A. A., A. S. Popel, R. A. Eatock and W. E. Brownell (2005). "Mechanosensitive channels in the lateral wall can enhance the cochlear outer hair cell frequency response." Ann Biomed Eng **33**(8): 991-1002.

Stone, K. A., B. D. Smith, J. M. Lembke, L. A. Clark and M. B. McLellan (2000). "Universal newborn hearing screening." J Fam Pract **49**(11): 1012-6.

Strassmaier, M. and P. G. Gillespie (2003). "Fast adaptation in the mammalian cochlea: a conserved mechanism for cochlear amplification." Nat Neurosci **6**(8): 790-1.

Tolomeo, J. A. and C. R. Steele (1995). "Orthotropic piezoelectric properties of the cochlear outer hair cell wall." J Acoust Soc Am **97**(5 Pt 1): 3006-11.

Vetesnik, A., R. Nobili and A. Gummer (2006). "How does the inner ear generate distortion product otoacoustic emissions?. Results from a realistic model of the human cochlea." ORL J Otorhinolaryngol Relat Spec **68**(6): 347-52.

Viergever, M. A. and E. de Boer (1987). "Matching impedance of a nonuniform transmission line: application to cochlear modeling." J Acoust Soc Am 81(1): 184-6.

von Békésy, G. (1960). Experiments in hearing. New York,, McGraw-Hill.

Voss, S. E. and C. A. Shera (2004). "Simultaneous measurement of middle-ear input impedance and forward/reverse transmission in cat." J Acoust Soc Am 116(4 Pt 1): 2187-98.

Weitzel, E. K., R. Tasker and W. E. Brownell (2003). "Outer hair cell piezoelectricity: frequency response enhancement and resonance behavior." J Acoust Soc Am 114(3): 1462-6.

Wilson, H. K. and M. E. Lutman (2006). "Mechanisms of generation of the 2f2-f1 distortion product otoacoustic emission in humans." J Acoust Soc Am 120(4): 2108-15.

Wilson, J. P. (1980). "Model for cochlear echoes and tinnitus based on an observed electrical correlate." Hear Res 2(3-4): 527-32.

Wilson, J. P. and J. R. Johnstone (1973). "Basilar membrane correlates of the combination tone 2f 1 -f 2." Nature 241(5386): 206-7.

Withnell, R. H., L. A. Shaffer and C. L. Talmadge (2003). "Generation of DPOAEs in the guinea pig." Hear Res 178(1-2): 106-17.

Zweig, G. and C. A. Shera (1995). "The origin of periodicity in the spectrum of evoked otoacoustic emissions." J Acoust Soc Am 98(4): 2018-47.

Zwicker, E. (1986). "A hardware cochlear nonlinear preprocessing model with active feedback." J Acoust Soc Am 80(1): 146-53.

Zwislocki, J. J. (1950). "Theory of the Acoustical Action of the Cochlea." J Acoust Soc Am 22(6): 778-784.

VITA

Name: Shan Lu

Year of Birth: 1969

Address: 14 Westside Dr, Acton, MA 01720

Education

Ph.D. (2009) in Electrical and Computer Engineering, Boston University, Boston MA

Thesis: A Nonlinear Multicompartmental Cochlear Model

M.S. (2001) in Biomedical Engineering, Virginia Commonwealth University, Richmond, VA

Thesis: A System for Real Time Home Health Care through the Internet

B.E. (1991) in Automatic Control, Tsinghua University, Beijing China

PUBLICATIONS

Lu Shan, Spisak, J., Mountain, D. C. and Hubbard, A. E., "A New Multicompartments Model of Cochlea" in Auditory Mechanisms: Processes and Models. A. L. Nuttall, ed., World Scientific, Singapore

Lu Shan, Hubbard, A. E. and Mountain, D. C., "A Multicompartmental Cochlear Model with a Bi-directional Feedback System". BMES Annual Meeting, Chicago, IL 2006

Hubbard, A. E , Lu Shan, Spisak, J. and Mountain, D. C., "The Evolution of Multi-compartment Cochlear Model" in Auditory Mechanisms: Processes and Models. A. L. Nuttall, ed., World Scientific, Singapore

Xiaoming Zhao, Shan Lu, Dingyu Fei and Charles R. Doarn, "The Architecture, Communication and Implement of a Telemedicine System Based on Bluetooth and the Internet" in Biomedical Engineering recent developments. J. Vossoughi ed., Medical and Engineering publishers, Washington DC